Channel Variations in MIMO Wireless Communication Systems: Eigen-Structure Perspectives

Ping-Heng Kuo

A Thesis Submitted in Partial Fulfillment
of the Requirements for the Degree of

Doctor of Philosophy
in
Electrical and Computer Engineering

University of Canterbury
Christchurch, New Zealand
June 12, 2007

Abstract

Many recent research results have concluded that the multiple-input multiple-output (MIMO) wireless communication architecture is a promising approach to achieve high bandwidth efficiencies. MIMO wireless channels can be simply defined as a link for which both the transmitting and receiving ends are equipped with multiple antenna elements. This advanced communication technology has the potential to resolve the bottleneck in traffic capacity for future wireless networks.

Applying MIMO techniques to mobile communication systems, the problem of channel fading between the transmitters and receivers, which results in received signal strength fluctuations, is inevitable. The time-varying nature of the mobile channel affects various aspects of receiver design. This thesis provides some analytical methodologies to investigate the variation of MIMO eigenmodes. Although the scope is largely focussed on the temporal variation in this thesis, our results are also extended to frequency variation.

Accurate analytical approximations for the level crossing rate (LCR) and average fade duration (AFD) of the MIMO eigenmodes in an independent, identically distributed (i.i.d.) flat-fading channel are derived. Furthermore, since several channel metrics (such as the total power gain, eigenvalue spread, capacity and Demmel condition number) are all related to the eigenmodes, we also derive their LCRs and AFDs using a similar approach. The effectiveness of our method lies in the fact that the eigenvalues and corresponding channel

metrics can be well approximated by gamma or Gaussian variables. Our results provide a comprehensive, closed-form analysis for the temporal behavior of MIMO channel metrics that is simple, robust and rapid to compute. An alternative simplified formula for the LCR for MIMO eigenmodes is also presented with applications to different types of autocorrelation functions (ACF). Our analysis has been verified via Monte Carlo computer simulations.

The joint probability density function (PDF) for the eigenvalues of a complex Wishart matrix and a perturbed version of it are also derived in this thesis. The latter version can be used to model channel estimation errors and variations over time or frequency. Using this PDF, the probabilities of adaptation error (PAE) due to feedback delay in some adaptive MIMO schemes are evaluated. In particular, finite state Markov chains (FSMC) have been used to model rate-feedback system and dual-mode antenna selection schemes. The PDF is also applied to investigate MIMO systems that merge singular value decomposition (SVD)-based transceiver structure and adaptive modulation. A FSMC is constructed to investigate the modulation state entering rates (MSER), the average stay duration (ASD), and the effects of feedback delay on the accuracy of modulation state selection in mobile radio systems.

The system performance of SVD-based transceivers is closely related to the quality of the channel information at both ends of the link. Hence, we examine the effect of feedback time delay, which causes the transmitter to use outdated channel information in time-varying fading channels. In this thesis, we derive an analytical expression for the instantaneous signal to interference plus noise ratio (SINR) of eigenmode transmission with a feedback time delay. Moreover, this expression implies some novel metrics that gauge the system performance sensitivity to time-variations of the steering vectors (eigenvectors of the channel correlation matrix) at the transmitter.

Finally, the fluctuation of the channel in the frequency domain is of interest. This is motivated by adaptive orthogonal frequency division multiplexing

(OFDM) systems where the signalling parameters per subcarriers are assigned in accordance with some channel quality metrics. A Gaussian distribution has been suggested to approximate the number of subcarriers using certain signalling modes (such as outage/transmission and diversity/multiplexing), as well as the total data rates, per OFDM realization. Additionally, closed-form LCRs for the channel gains (including the individual eigenmode gains) over frequency are also derived for both single-input single output (SISO) and MIMO-OFDM systems. The corresponding results for the average fade bandwidth (AFB) follow trivially, These results may be useful for system design, for example by calculating the feedback overheads based on subcarrier aggregation.

Acknowledgments

First of all, I owe an extreme debt of gratitude to my supervisor - Assoc. Prof. Peter Smith. Under the excellent guidance that he has provided, this research project progressed smoothly with the aid of his invaluable comments. An equal debt of gratitude is owed to my co-supervisor - Dr. Lee Garth, his assistance and suggestions regarding many of my papers are undoubtedly precious.

I would also like to acknowledge all those who have been involved in the collaboration - Dr. Mansoor Shafi (Telecom New Zealand), Prof. Neil O'Connell (University College Cork, Ireland), Dr. Alan Clark (British Telecom) and Krishna Prasad Kongara (Tait Radio Communications/University of Canterbury). Their knowledge, expertise and experience have significantly enhanced the material in this project. I am indebted to the people in the Communications Research Group at the University of Canterbury; in particular, I wish to thank Prof. Desmond Taylor and Dr. Philippa Martin for sharing tips for oral presentations at conferences.

I am grateful to all my friends, in either New Zealand or Taiwan, who have accompanied me throughout my frustrations during this period. My memories at this university, from the undergraduate study to Ph.D, are absolutely unforgettable because of those nice classmates and great colleagues.

Last but not the least, my deepest gratitude and sincerest love is owed to my family - Mum, Dad and my siblings. I would have never be able to accomplish this arduous work without their love, support and encouragement.

List of Original Papers

The majority of the material present in this thesis is based on the following original papers:

- Journal Papers:

  - P.-H. Kuo, P. J. Smith and L. M. Garth, "Joint density for eigenvalues of two correlated complex Wishart matrices: characterization of MIMO systems," *IEEE Trans. Wireless Commun.*, vol. 6, no. 11, pp. 3902-3906, Nov. 2007.

  - P.-H. Kuo, P. J. Smith, L. M. Garth and N. O'Connell, "Level crossing analysis for MIMO eigenmodes and associated channel metrics," submitted to *IEEE Trans. Info. Theory*, Mar. 2007.

  - K. P. Kongara, P.-H. Kuo, P. J. Smith, L. M. Garth and A. Clark, "Block-based performance measures for MIMO-OFDM beamforming systems," submitted to *EURASIP J. Wireless Commun. and Networking*, May 2007.

  - P.-H. Kuo, P. J. Smith and L. M. Garth, "Simple LCR formulas for MIMO link gain and eigenmodes of channels with arbitrary power azimuth spectrum," submitted to *IEEE Trans. Veh. Technol.*, Dec. 2007.

- Conference Papers:

  - P. J. Smith, P.-H. Kuo and L. M. Garth, "Level crossing rates for MIMO eigenvalues: Implication for adaptive systems," in *Proc. IEEE Int. Conf. on Commun. (ICC)*, Seoul, Korea, May 2005, pp. 2442-2446.

  - P.-H. Kuo and P. J. Smith, "Temporal behavior of MIMO channel metrics," in *Proc. IEEE Int. Conf. on Wireless Networks, Commun. and Mobile Computing (WirelessCom)*, Maui, HI, USA, Jun. 2005, pp. 857-862.

  - P.-H. Kuo, P. J. Smith, L. M. Garth and M. Shafi, "Instantaneous signal and interference power of MIMO eigenmode transmission with feedback time delay," in *Proc. IEEE Int. Conf. on Commun. (ICC)*, Istanbul, Turkey, Jun. 2006, pp. 4143-4148.

  - P.-H. Kuo and P. J. Smith, "On the probability of adaptation error in MIMO systems," in *Proc. IEEE Int. Symp. on Personal Indoor and Mobile Radio Commun. (PIMRC)*, Helsinki, Finland, Sep. 2006.

  - P.-H. Kuo, P. J. Smith and L. M. Garth, "A Markov model for MIMO channel condition number with application to dual-mode antenna selection" in *Proc. IEEE Vehicular Technology Conf. (VTC-Spring)*, Dublin, Ireland, Apr. 2007, pp. 471-475.

  - K. P. Kongara, P.-H. Kuo, P. J. Smith, L. M. Garth and A. Clark, "Performance Analysis of Adaptive MIMO OFDM Beamforming Systems," submitted to *IEEE Int. Conf. on Commun. (ICC) 2008*.

Contents

List of Tables

List of Figures

Chapter 1

Introduction

In this introductory chapter, an overview of multiple-input multiple-output (MIMO) communication systems is presented, which commences with a description of the high capacity demands in future wireless communication networks, and how MIMO systems have the potential to fulfill the demand. Then, the motivation for the research is given, followed by a brief elaboration of the main contributions. The structure of the thesis is summarized in the last section of this chapter.

1.1 An Overview of MIMO Systems

In the last century, the advances in very large scale integration (VLSI) and digital signal processing (DSP) technologies have enabled the implementation of complicated algorithms and coding systems in small devices with low power consumption, as required in modern mobile communications. Such technical breakthroughs have promoted the rapid growth of the global market in wireless communication equipment and services. Furthermore, the demands for higher network capacity and improved performance of wireless communications are continuously growing. With the advent of applications such as multimedia data transmission (audio and video streams) or online gaming networks, a much higher spectral efficiency is needed to provide the services with adequate

quality [1, 2]. As has been envisaged in [3], it is essential to plan and develop new communication technologies, in order to cope with the increasingly high demand for network capacity in the future wireless systems. Hence, the development of faster and more reliable wireless techniques has became one of the most vibrant areas in communications engineering. However, this is a difficult task since wireless systems have to contend with signal fading, multi-path propagation, interference, noise and limited bandwidth.

According to Shannon's information theory, it is well-known that the capacity represents the highest possible data rate that channel can support. Also, his classic formula for channel capacity is a function of bandwidth and signal-to-noise ratio (SNR) [4]. Increasing signal power and expanding channel bandwidth are two intuitive ways to improve capacity. Unfortunately, both of these ideas are impractical, as the power is generally constrained in mobile devices and the channel spectrum is usually limited by certain regulations. Thus, many approaches like advanced modulation and coding schemes have been proposed to offer higher spectral efficiency. The concept of utilizing the degrees of freedom in the spatial domain through antenna arrays, which has emerged in the last few decades, is now being regarded as one of the strongest candidates for the next generation of wireless communications [5]. In particular, researchers have shown that schemes with multiple antennas on both sides (so called MIMO systems) can tremendously enhance the system throughput, reliability and coverage, without the necessity of extra power and bandwidth [6, 7]. MIMO systems have received considerable attention in the last decade due to their potential benefits, and related research has been very active in recent years, in both academia and industry [8, 9]. A testimony to this can be seen from recent standardizations for many commercial radio applications. Table 1.1 summarizes the standards that have adopted MIMO techniques to enhance their performance [10]. More details of current standardizations associated with MIMO techniques can be found in [10] and the references therein.

Standards	Air-Interfaces
WLAN 802.11n	OFDM
WiMAX 802.16 2004	OFDM/OFDMA
WiMAX 802.16e	OFDMA
3GPP Release 7	WCDMA
3GPP Release 8 (LTE)	OFDMA
802.20	OFDM
802.22	OFDM

Table 1.1: MIMO standards and the corresponding air-interface technology.

Interestingly, Table 1.1 indicates that all standards employ orthogonal frequency division multiplexing (OFDM) schemes except for 3GPP Release 7. This implies an expectation for future systems to merge OFDM and MIMO, which is usually referred to as MIMO-OFDM. An excellent overview of this technology is given in [11].

Generally speaking, multiple antenna systems can be classified into two main categories: diversity systems and spatial multiplexing systems [12]. The main goal of a diversity scheme is to improve the error performance and hence the system reliability. The primary structure for spatial diversity consists of an antenna array at the receiver side only [13]. The idea is to provide multiple versions of the transmitted messages with different fading severity. The receiver then implements some combining algorithm. For example, the receiver can simply pick up the signal with the best SNR, this is the so called *selection diversity*. Alternatively, the receiver could use *maximum ratio combining*, which takes the sum of all the received signals weighted according to their SNR values. Such schemes are effective methods in combating multi-path fading problems [14].

Space-time coding (STC) is an extension of traditional spatial diversity, which aims to provide more reliable communication. While conventional methods use multiple antennas at the receiver only to combat fading effects, STC

further enhances the gain by adding the utilization of transmit diversity. The two most well-known techniques in this category are Space-Time Trellis Codes (STTC) proposed in [15], and Space-Time Block Codes (STBC) [16]. STTC can become very complicated as the number of antennas increases. The implementation of STBC (a well-known example being the Alamouti scheme [16]), on the other hand, is relatively simple. Hence, despite its performance loss as compared to STTC, STBC receives a lot of attention in the context of MIMO systems. Such schemes code the message in both space and time. In other words, replicas of the message are transmitted at a delayed time on different antennas. The initial structure proposed in [16] consist of two transmit and one receive antenna, and the idea was further generalized in [17] for systems with arbitrary numbers of antennas by using the theory of orthogonal designs. This type of configuration allows a very simple maximum-likelihood decoding algorithm [18].

While diversity schemes can improve the error performance significantly, spatial multiplexing schemes, on the other hand, are capable of providing very high system throughputs. Such a scheme simply divides the incoming data into sub-streams and transmits them on different antennas. Modulation and coding for each transmit antenna occurs independently. Thus, the overall throughput is raised as multiple data streams are sent simultaneously. In general, spatial multiplexing schemes can be classified into *open-loop* or *closed-loop* configurations, depending on the existence of a feedback mechanism. Bell Lab Space-Time (BLAST) [19] is a typical open-loop spatial multiplexing architecture, as channel state information (CSI) is estimated and used only at the receiver side to separate and extract the transmitted messages. Many researchers have shown that throughput can be increased if both terminals of the link possess CSI [20]. Thus, despite the higher system complexity, there is a strong interest in closed-loop schemes with a feedback link to provide CSI to the transmitter.

By and large, MIMO systems inherit the diversity gain which maintains

performance in terms of bit error rates (BER), while it can also improve the data rate through multiplexing (sending independent data streams over different antennas). However, a trade-off has been found between diversity and multiplexing [21]. Considerable research is now focussed on attempting to develop systems that can enjoy the advantages of both techniques.

1.2 Research Framework

This section describes the main objective of this thesis, including the motivation, and a summary of the contributions.

1.2.1 Motivations

Intensive research into MIMO systems has been carried out in the last few years. However, most results are based on the assumption of a quasi-stationary channel; that is, the channel is time-invariant. In practice, due to the inevitable fading effects in wireless transmission, the received signal strength fluctuates over time and frequency. Therefore, variation in the wireless channels is crucial in several aspects of system design and performance evaluation.

The temporal behavior of traditional wireless communication systems with a single antenna on both sides (SISO channel), has been investigated by many researchers and a large body of results has appeared in the literature. However, for MIMO systems, the related work is very sparse. Most work has been based on either field measurements or computer simulations, rather than analytical derivations. Thus, this thesis aims to present a more systematic study of channel variation with an analytical approach based on the statistical properties of the MIMO channel. In particular, the scope is largely focussed on the dynamic behavior of the MIMO channel eigen-structure.

Many studies have shown the importance of the eigen-structure of the MIMO channel correlation matrix in characterizing the system in its spatial

domain [22]. The importance of the eigen-structure has been revealed by many authors in different applications. In particular, the eigenvalues represent the power gains of the multiple orthogonal spatial links [23] (known as eigenmodes or eigen-channels) that are intrinsic to the MIMO channel. To realize the eigenmodes within the MIMO channel, the singular value decomposition (SVD) is particularly useful. The SVD is a mathematical tool that has been frequently employed in the context of MIMO system analysis. Most importantly, the SVD is the core concept for a beam-forming architecture called eigen-beamforming or eigenmode transmission. The SVD requires both the transmitter and receiver to have CSI. In this scenario, the SVD can be used to compute the steering matrices for the transmitter and receiver based on the channel estimates. This operation has been shown to be the optimum method for MIMO pre-coder design [24, 25]. As CSI is usually estimated at the receiver, the transmitter needs to acquire the estimated CSI via a feedback link, in order to implement SVD transmission. Therefore, a reliable feedback channel is required unless the system is based on time-division duplex (TDD) where reciprocity can be utilized [26].

Furthermore, achieving channel capacity is based on the idea of transmission power being adaptively allocated over the eigenmodes using the "water-filling" algorithm or its variants [27]. Similarly, the overall data rate can be significantly improved through the application of adaptive modulation (or bit allocation) [28]. In these adaptive schemes, the parameters of the physical layer signalling are changed in accordance with the channel status to increase the overall link quality. More details on the SVD and adaptive signalling will be discussed in Chapter 2.

Nevertheless, due to the variation of the mobile channel, the feedback control can be very difficult in practice. It is impossible to estimate the MIMO channel perfectly and frequently enough in a rapidly varying environment.

Hence, various efficient channel tracking strategies [29, 30] and feedback methods [31] have been developed. In addition, many power allocation algorithms have also been devised to achieve near-optimal capacity without (or with minimal) feedback information [32, 33, 34, 35]. Intuitively speaking, the feedback mechanism can be more rigorously designed and hence more feasible in practice, if the dynamic behavior of the eigenvalues is known statistically. For example, crucial parameters in system design such as estimation and feedback/adaptation rates [36, 37] can be judiciously chosen with a knowledge of the channel variation.

1.2.2 Specific Contributions

To investigate the dynamic behavior of the wireless channel and its impact on MIMO communication systems, we consider several different aspects. The level crossing rate (LCR) measures how often the process down-crosses a certain threshold. A Markov chain, on the other hand, partitions the process into multiple discrete states, and the system behavior is assessed by the transition probabilities among the states. In this thesis, both approaches are applied to investigate MIMO eigen-structures. The methods are further adapted to cover the other important MIMO channel metrics based on eigenmodes, such as channel capacity and condition numbers. The transition probabilities between Markov states can be computed via conditional probability theory or approximated via the LCR. In order to use the former technique, the joint density for the eigenvalues of two correlated complex Wishart matrices is also derived.

As the work was mainly motivated by the SVD transmission architecture, the impacts of channel variation on the performance of such a scheme is another interesting issue. In particular, we assess how the feedback delay, which causes the transmitter to obtain outdated CSI, affects the performance of SVD

systems. The main contribution in this area is the derivation of analytical expressions for the instantaneous signal to interference plus noise ratio (SINR). From the expression, the relationship between system sensitivity to feedback delay and the eigenmodes can be revealed.

It has been seen that MIMO systems are frequently proposed in combination with an OFDM air-interface in many wireless standards. This motivates the exploration of how the channel responses vary across the frequency domain within the wideband OFDM channel. Hence, a few issues regarding channel variation in the frequency domain are also examined.

To recapitulate, the main contributions of this thesis are summarized and listed below:

- Derivations of level crossing rates (LCR) and average fade duration (AFD) for:
  - eigenmode gains;
  - the total power gain of the MIMO channel;
  - MIMO channel capacity;
  - MIMO channel condition numbers.
- Constructions of Markov models for MIMO Systems. Related work includes:
  - deriving the joint density for the eigenvalues of two correlated complex Wishart matrices;
  - Markov modeling for MIMO channel capacity with applications to rate-feedback systems;
  - Markov modeling for MIMO channel condition number with applications to dual-mode antenna selection systems;

  - Markov modeling for the joint behavior of eigenmodes with applications to adaptive modulation.

- Investigating the impact of feedback delay on MIMO-SVD systems:

  - derivation of an expression for instantaneous SINR;

  - identification of system sensitivity to feedback delay.

- Characterizing OFDM subcarrier gain variation in the frequency domain:

  - distributions for the number of subcarriers using certain transmission modes in adaptive OFDM systems;

  - LCR results in the frequency domain and the average fade bandwidth (AFB) of the channel gains in SISO/MIMO OFDM systems.

1.3 Thesis Outline

The rest of this thesis is organized as follows:

Chapter 2 introduces the theoretical background of the mobile propagation channel and MIMO systems. Some common statistical channel models such as the Rayleigh channel, the Ricean channel and spatially correlated channels are elaborated. Then, the SVD and the joint statistics of the eigenvalues of a complex Wishart matrix are reviewed in detail. The last section of Chapter 2 presents an overview of some important MIMO channel quality metrics, including the total power gain, channel capacity, and condition number.

Chapter 3 gives the level crossing analysis of MIMO eigenmodes, which is based on a stochastic differential equation (SDE) that was originally derived for a Brownian diffusion process. Then, the method is extended to obtain the LCR of other channel quality metrics. An alternative, simple formula for computation of the eigenmode LCR is also given in the chapter.

Chapter 4 develops Markov models for MIMO channel metrics. The joint density for the eigenvalues of two correlated complex Wishart matrices is derived. This joint density is then invoked to build the Markov models for systems with adaptive signalling. Specifically, it is applied to compute the autocorrelation coefficient of the capacity and condition number processes, as this ACF is required for Markov chain construction. LCR results are also used to approximate the transition probabilities, as an alternative approach. In addition, for MIMO systems that merge SVD and adaptive modulation, the joint behavior of the multiple eigenmodes is also modeled as a vector Markov process.

Chapter 5 scrutinizes the impact of feedback delay on SVD transmission systems. As shown in the literature, the mismatch of real and estimated steering matrices causes self-interference. An expression for the instantaneous SINR in terms of the eigenmodes is derived in this chapter. Hence the systems sensitivity to feedback delay is characterized.

Chapter 6 focuses on adaptive OFDM systems, in which the signalling parameters on each subcarrier are adjusted in accordance with the prevailing link quality. A Gaussian approximation is suggested for the distribution of the number of subcarriers using a certain transmission mode. Furthermore, the LCR and AFB of the channel gains in the frequency domain are considered.

Chapter 7 gives some conclusions, and some future research directions are pointed out.

Chapter 2

Background and Assumptions

Some required background information is provided in this chapter. Firstly, we explain the phenomenon of small-scale fading and give the mathematical formulation of some commonly used statistical channel models. Then, the importance of the singular value decomposition (SVD) in the context of MIMO systems, including its applications, is discussed in detail. Finally, the MIMO eigenmodes and associated channel metrics are elaborated.

2.1 Mobile Radio Propagation

We concentrate on small-scale fading and neglect the effects of large-scale fading and path loss. In the environment of mobile communications, the phenomenon of multipath causes multiple replicas of the signal to arrive at the receiver with different delays and phases. Furthermore, due to the motion of the mobile unit, the signal experiences random frequency modulation caused by the Doppler shifts on each of the multipath components. Hence, the received signal can fluctuate severely, as the combination of multipath components with different phases can be either destructive or constructive.

The effects of multipath are influenced by a few key factors. Most importantly, the presence of reflecting objects and scatterers in the propagation environment creates a constantly varying channel. The energy of some waves

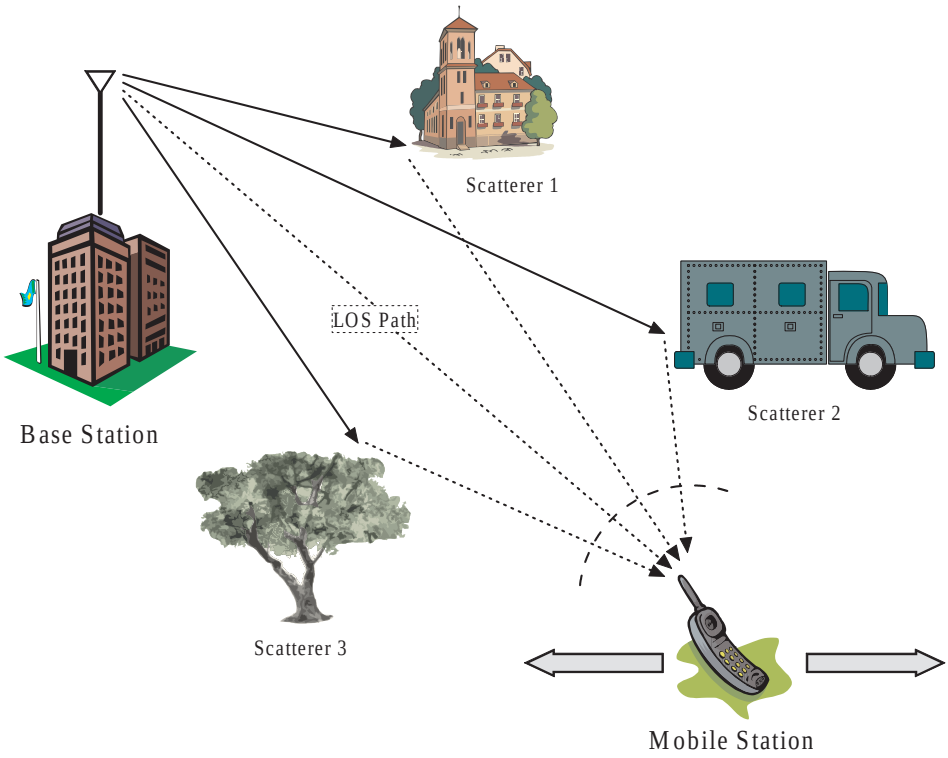

Figure 2.1: An illustration of the multipath phenomenon in a land mobile channel.

are dissipated due to reflections and scattering, while sometimes there exists a line of sight (LOS) component that arrives at at the receiver directly without being obstructed by the environment. Also, the distance (hence the time) traveled by each of the multipath components, as well as their spatial orientation before arriving at the receiver, are displaced with respect to one another. Figure 2.1 illustrates such phenomena.

Consequently, the random phases and amplitudes of the multipath components result in the fluctuation of signal strength. Two critical measures of mobile channel characteristics are *coherence time* and *coherence bandwidth*. The former defines the time interval over which the signal strength maintains a high auto-correlation[1] . The latter, on the other hand, indicates the frequency bandwidth over which the channel response maintains a high auto-correlation.

[1]There is no stipulated value for "high auto-correlation" in the literature. It usually ranges from 0.5 to 0.9 [14].

The channel is considered to be *flat-fading* if the signal bandwidth is smaller than the coherence bandwidth. Otherwise, it is said to be *frequency selective*, which occurs when the arrival times of the multipath components are significantly different (large delay spread). The frequency-selective channel suffers from inter-symbol interference (ISI), and the typical solutions to this problem include equalization and OFDM. We consider a flat-fading channel in most parts of this thesis except for Chapter 6, where the behavior of OFDM systems is of interest. Some common mathematical models for MIMO channels are introduced in the next section.

2.2 Mathematical Models

The characteristics of the propagation channel play a major role in any analysis of a wireless communication system. Usually, channel modeling can be classified into two different types - physical and statistical channel models. The former takes various physical parameters of the propagation environment into account, including the mobilities and exact positions of both terminals, number and location of the surrounding scatterers, and angular spread of emitted/received rays etc. The statistical models, on the other hand, simply assume the channel response is a stationary random process with certain statistical distributions and autocorrelation functions. Although physical models can more precisely imitate the behavior of practical mobile channels, their use leads to intricate analysis methods due to their high complexity. Hence, only statistical models are considered in this thesis as they are simple and yet can catch the essential properties of mobile channels.

2.2.1 Flat-Fading MIMO Signal Model

Consider a (N_t, N_r) MIMO system that employs $N_t \geq 1$ transmit and $N_r \geq 1$ receive antennas as shown in Fig. 2.2, where each of the transmit antennas

sends symbols from a complex symbol alphabet. The transmit symbols are encoded, modulated, up-converted and launched into the radio link. At the receiver, the signals are mixed down to baseband, sampled, and passed on to the decoder to extract the message. For the sake of convenience, it is further postulated that the channel response is independent of frequency and the received symbols are perfectly synchronized, so that inter-symbol interference (ISI) is not a concern; that is, a narrow-band (flat-fading) channel. In such a case, the overall system can be written as [38]

$$\boldsymbol{Y} = \boldsymbol{H}\boldsymbol{X} + \boldsymbol{n}, \tag{2.1}$$

where $\boldsymbol{X}$ and $\boldsymbol{Y}$ are vectors of N_t transmitted and N_r received symbols respectively, and $\boldsymbol{n}$ is circularly symmetrical complex Gaussian noise vector with variance N_0. $\boldsymbol{H}$ is a $N_r \times N_t$ channel matrix:

$$\boldsymbol{H} = \begin{bmatrix} h_{11} & h_{12} & \dots & h_{1N_t} \\ h_{21} & h_{22} & & \vdots \\ \vdots & & \ddots & \vdots \\ h_{N_r1} & \dots & \dots & h_{N_rN_t} \end{bmatrix}. \tag{2.2}$$

The entries, h_{ij}, are the complex baseband equivalents of the channel gains (fade coefficients) between the j^{th} transmit antenna and the i^{th} receive antenna. Each gain consists of the in-phase and quadrature components:

$$h_{ij}(t) = h_{ij,I}(t) + \sqrt{-1}\, h_{ij,Q}(t). \tag{2.3}$$

In fact, the assumptions of flat-fading are usually not practical since future communication systems are mainly wideband and hence have frequency-selective fading channels. Here, the channel response varies significantly across the frequency band and the system suffers from ISI. However, thanks to system air-interfaces based on OFDM, or some other multi-carriers techniques, the wideband response is segmented and converted into several flat fading frequency bins, so each of the bins can be handled separately as a flat fading

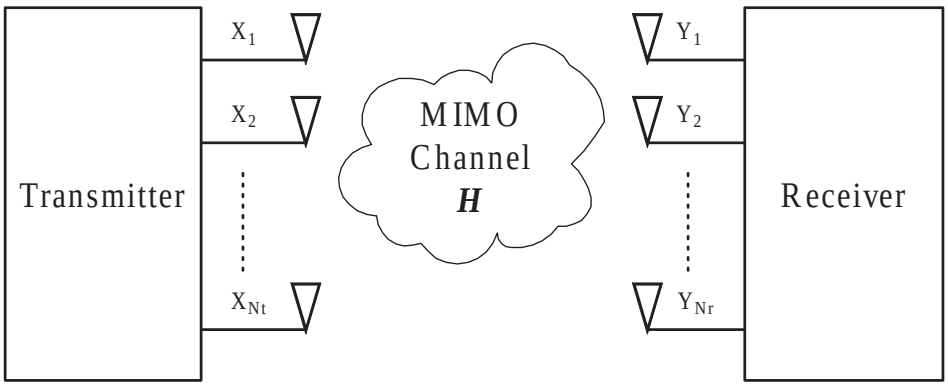

Figure 2.2: Schematic of a general MIMO System

channel. Thus, the assumption of a flat-fading channel can still provide insights into MIMO-OFDM systems. As mentioned previously, such schemes are widely thought to be the core platform for the next generation of wireless communications. We consider OFDM systems in further detail in Chapter 6.

2.2.2 Rayleigh i.i.d Channels

This is the baseline scenario that has been frequently considered in the literature. It is also the case that we will concentrate on in this thesis. In such a model, the entries of $\boldsymbol{H}$ are independent, identically distributed (i.i.d) circular symmetric complex Gaussian. The model is suitable for scenarios with the following conditions. Firstly, the received signal is a combination of a large number of multipath components, which usually occurs when the surrounding environments of both transmitter and receiver arrays possess many scatterers. Secondly, antennas within an array needed to be widely separated and hence there is no spatial correlation among channel responses. Lastly, it should also be assumed that the line-of-sight (LOS) path is absent.

Mathematically, this results in a channel matrix whose entries are zero mean complex Gaussians with unit magnitude variances; that is, $h_{ij} \sim \mathcal{CN}(0,1)$. Under these assumptions, the envelopes of the channel entries have the well-known Rayleigh distribution. It has been shown that Rayleigh i.i.d channels

are more suitable to model indoor and urban environments where many scatterers are often present.

2.2.3 Autocorrelation Function

Throughout this research, the temporal behavior of the mobile channel is assumed to be governed by simple statistical models. In particular, three fading scenarios with different autocorrelation functions (ACFs) are considered: the classic Jakes model, a land mobile channel with Laplacian power azimuth spectrum (PAS), and the mobile-to-mobile (MM) model. These are elaborated below:

- Classic Jakes model: This model assumes that the incoming rays at the moving receiver are isotropic. In other words, the spatial orientation of the received signal power is uniformly distributed between $-\pi$ and π, as illustrated in Fig. 2.3. The ACF for this case is [39]:

$$\rho_{Jakes}(\tau) = J_0(2\pi f_D \tau), \tag{2.4}$$

  where $J_x(\cdot)$ represents the x^{th} order Bessel function of the first kind, f_D is the Doppler frequency (maximum Doppler shift), and τ is the time displacement. Note that

$$f_D = \frac{v_m\, f_c}{c_0}, \tag{2.5}$$

  where v_m, f_c, and c_0 are the velocity of the mobile station, carrier frequency, and the speed of light (3×10^8 m/s) respectively.

- Land mobile channel with Laplacian PAS: Some studies have suggested a Laplacian PAS to describe the distribution of angle of arrival (AoA) at the receiver. Thus, in contrast to the uniform PAS in the classic Jakes model, the incoming multipath components are distributed in a limited range of spatial orientations, as shown in Fig. 2.3. Following the

methods given in [40], we obtain a special case of the ACF:

$$\rho_{Lap}(\tau) \approx J_0(2\pi f_D \tau) + \frac{2}{1+2\,\vartheta^2}\, J_2(2\pi f_D \tau), \tag{2.6}$$

where ϑ indicates the angular spread of the incoming rays. The parameters f_D and τ are the same as in the Jakes model. Note that (2.6) is valid for the special case of an omni-directional antenna pattern, assuming the average AoA is perpendicular to the motion vector of the mobile station (as in [40]). Although we focus on this special case due to its simplicity, we must point out that the main results in this thesis are applicable to other general cases at the expense of more cumbersome expressions.

- Mobile-to-mobile (MM) channel: When both terminals are in motion, as in *ad hoc* or cooperative networks, the ACF is given as [41]

$$\rho_{MM}(\tau) = J_0(2\pi f_{D_1} \tau)\, J_0(2\pi f_{D_2} \tau), \tag{2.7}$$

where f_{D_1} and f_{D_2} are the Doppler frequencies for the two mobile terminals, assuming a uniform PAS at both sides.

For all cases listed above, we assume that the spacings between transmit/receive elements in the antenna arrays are large enough, so the complex Gaussian entries in the channel matrix are i.i.d. We plot these three ACFs, $\rho(\tau)$, against the time-displacement, τ, in Fig. 2.4. It can be seen that the autocorrelation of the MM channel decays most rapidly for small τ, while the channel with a Laplacian PAS varies more slowly than the Jakes model.

2.2.4 Other Common MIMO Channel Models

Although only Rayleigh i.i.d models are considered in our research, some other common channel models are reviewed here for completeness.

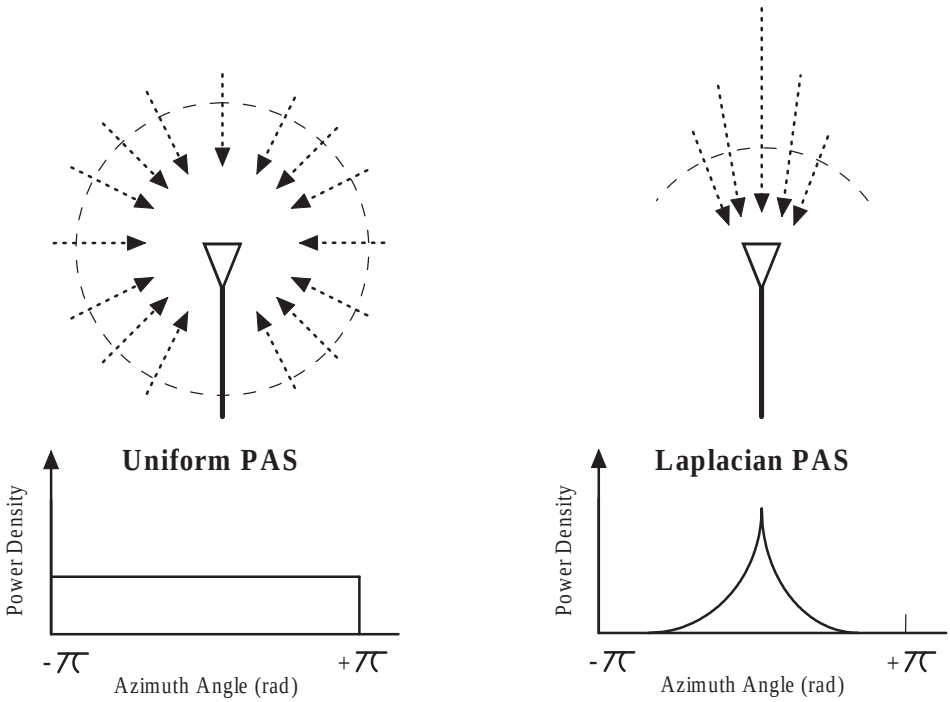

Figure 2.3: Illustrations of a uniform PAS (left) and a Laplacian PAS (right).

Line of Sight (LOS) Ricean Channels

Consider a dominant stationary (nonfading) signal component, for instance, a LOS propagation path between transmitter and receiver without any obstacles. In this case, the resultant signal envelope fading is said to be Ricean distributed. In such cases, the complex entries of the channel matrix $\boldsymbol{H}$ are still Gaussian distributed but no longer zero mean; that is, $h_{ij} \sim \mathcal{CN}(\mu, \sigma^2), \mu > 0$.

The Ricean distribution is characterized by a Ricean Factor $\mathcal{K}$, which is defined as the ratio of the LOS signal power to the variance of the multipath. As the LOS signal power decreases towards zero, the envelope eventually degenerates to Rayleigh fading. The standard MIMO Ricean fading channel model is described as follows.

Typically, the MIMO Ricean channel is composed of a scattered component, $\boldsymbol{H}^{sc}$, and a specular component, $\boldsymbol{H}^{sp}$. The resultant channel is expressed as

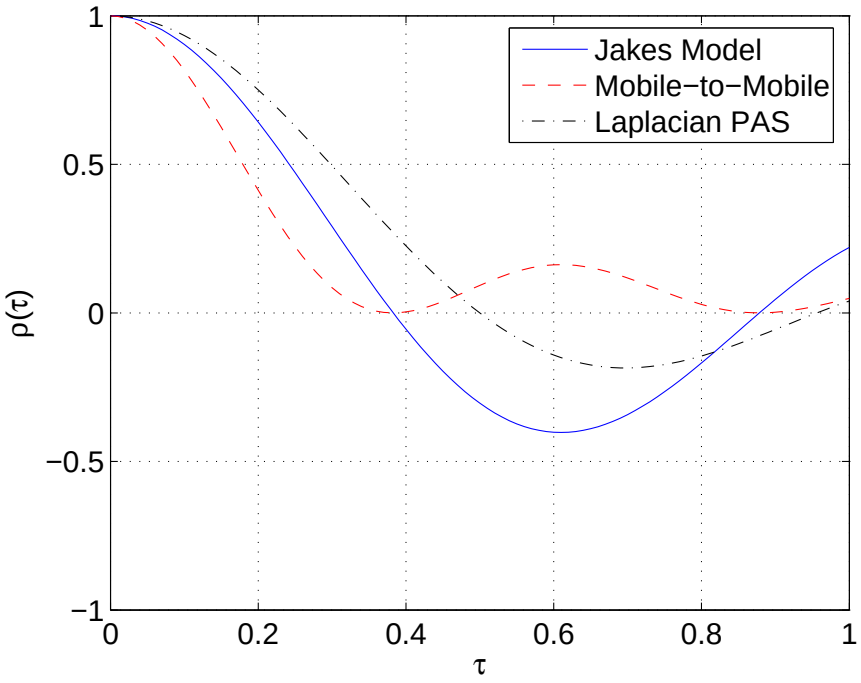

Figure 2.4: The ACFs of three channel models. ($f_D = f_{D_1} = f_{D_2} = 1$Hz and $\vartheta = \pi/3$.)

[42]:

$$\boldsymbol{H}_{ric} = \sqrt{\frac{\mathcal{K}}{\mathcal{K}+1}}\boldsymbol{H}^{sp} + \sqrt{\frac{1}{\mathcal{K}+1}}\boldsymbol{H}^{sc}. \tag{2.8}$$

Note that $\boldsymbol{H}^{sc}$ is equivalent to a Rayleigh i.i.d channel matrix since it corresponds to scattered multipath components. Compared to systems with i.i.d Rayleigh fading, analysis and measurement results have shown that the achievable capacity for spatial multiplexing systems in a Ricean channel is relatively low [43] under the same SNR, especially when the transmission power is uniformly distributed among the transmit antennas. This is due to the reduced rank behavior [43], which leads to fewer effective spatial links. Analytical results on system capacity for a MIMO Ricean channel can be found in [44].

Rayleigh Fading Spatially Correlated Channel

In practice, the assumption of independence among channel entries in the spatial domain may be unrealistic, because signals impinging on different antennas in an array will often have some correlation. The spatial correlation depends on various physical parameters of the antenna arrays and the scatterer characteristics [45]. The correlations between antennas are mainly governed by three parameters [12]: the distances between antennas [46], the angular spread of the arrival incident waves, and the mean angle of arrival of the incident waves.

To model a Rayleigh fading channel with spatial correlations at both transmitter and receiver, the channel matrix can be written as [47]:

$$\boldsymbol{H}_{corr} = \boldsymbol{F}_{RX}^{1/2} \boldsymbol{H}_{iid} \boldsymbol{F}_{TX}^{1/2} \tag{2.9}$$

where $\boldsymbol{H}_{iid}$ is a $N_r \times N_t$ complex Gaussian matrix with zero-mean and unit variance. $\boldsymbol{F}_{TX}$ and $\boldsymbol{F}_{RX}$, on the other hand, are $N_t \times N_t$ and $N_r \times N_r$ covariance matrices at transmitter and receiver sides respectively. Note that (2.9) can be reduced to $\boldsymbol{H}_{iid}$ when both $\boldsymbol{F}_{TX}$ and $\boldsymbol{F}_{RX}$ are identity matrices as in the Rayleigh i.i.d channel. In addition, many researchers have assumed that one of the terminals (transmit or receive array) is located in a rich-scattering environment and hence experiences low spatial correlation. This results in a "semi-correlated" channel, where the covariance matrix at the uncorrelated side ($\boldsymbol{F}_{TX}$ or $\boldsymbol{F}_{RX}$) is an identity matrix in (2.9). The analytical capacity for such a scenario has been derived in [48].

As for the Ricean channel, MIMO systems with spatial correlations are said to be "rank-deficient", as there may be only a few dominant eigenmodes while the other eigenvalues are relatively weak. In spite of the degradation of system throughput due to spatial correlation, the achievable performance is still relatively high in comparison with systems with a single antenna [49].

Key-hole Effects

In the very special case known as a key-hole (also denoted as a "pinhole" in [50]), the channel has only one significant spatial link even when all entries are independent. This happens when the scattered energy travels through a very thin air pipe [50]. The key-hole effect can be imagined as a situation in which the clusters around the transmitter and receiver are separated by a screen with a hole, and the only way for the radio wave to arrive at the desired destination is to pass through the hole. The entries are not complex Gaussian like the other models discussed previously, but the product of two complex Gaussian variables [51]. In physical propagation environments, key-hole effects may occur in hallways (indoor), tunnels, and when the distance between two scatterers is much larger than the radius of scatterer rings. It can also result from certain roof diffractions [8]. However, the experimental results in [52] suggest that the key-hole effect is extremely rare in real-world propagation environments.

2.3 Eigen-Structure of Channel Correlation Matrix

This section gives the fundamentals of the singular value decomposition (SVD) and its relationship to the eigen-structure of the MIMO correlation matrix. As the channel matrix entries are complex Gaussians, the joint statistics of the eigenvalues are governed by the Wishart distribution, which is also discussed in this section.

2.3.1 Singular Value Decomposition

The singular Value Decomposition (SVD) is an elegant tool to analyze MIMO systems. It is capable of identifying the independent spatial excitation modes

that are intrinsic to the channel. Consider a MIMO channel, $\boldsymbol{H}$, with N_t and N_r antennas at transmitter and receiver respectively. Define $m = \min(N_t, N_r)$, $n = \max(N_t, N_r)$ and $l = n - m$. By using the SVD, $\boldsymbol{H}$ can be expressed as [53]

$$\boldsymbol{H} = \boldsymbol{U}\Sigma\boldsymbol{V}^{\dagger}, \tag{2.10}$$

where $\boldsymbol{U} \in \mathcal{C}^{N_r \times N_r}$ and $\boldsymbol{V} \in \mathcal{C}^{N_t \times N_t}$ are unitary matrices, and $[\cdot]^{\dagger}$ represents Hermitian transpose. Σ is a diagonal matrix whose diagonal elements $s_1 \geq s_2 \geq \ldots \geq s_m$ are the positive *singular values* of the channel matrix $\boldsymbol{H}$. The non-diagonal elements of Σ are all zero and m is the rank of $\boldsymbol{H}$. It is easy to show that the squared singular values, s_i^2, are the eigenvalues of the instantaneous correlation matrix $\boldsymbol{H}\boldsymbol{H}^{\dagger}$, since

$$\boldsymbol{H}\boldsymbol{H}^{\dagger} = \boldsymbol{U}\boldsymbol{\Sigma}\boldsymbol{\Sigma}^{\dagger}\boldsymbol{U}^{\dagger}. \tag{2.11}$$

Moreover, the columns of $\boldsymbol{U}$ are eigenvectors of $\boldsymbol{H}\boldsymbol{H}^{\dagger}$ and the columns of $\boldsymbol{V}$ are eigenvectors of $\boldsymbol{H}^{\dagger}\boldsymbol{H}$.

In terms of pure mathematics, the rank of matrix $\boldsymbol{H}$ is said to be m as there are m positive singular values with probability one. In the context of MIMO communication engineering, however, the rank of $\boldsymbol{H}$ is usually defined as the number of significant singular values. In general, the Rayleigh i.i.d channel is anticipated to be "full rank" as the average magnitude of all m singular values are reasonably high.

2.3.2 Realization of Eigenmodes

If both the transmitter and receiver have perfect CSI, $\boldsymbol{U}$ and $\boldsymbol{V}$ can be computed at both sides, so one may simply conceptualize the channel as a bank of m scalar links by defining:

$$\boldsymbol{X'} = \boldsymbol{V}\boldsymbol{X},$$

$$\boldsymbol{Y'} = \boldsymbol{U}^{\dagger}\boldsymbol{Y},$$

$$\boldsymbol{n'} = \boldsymbol{U}^{\dagger}\boldsymbol{n}.$$

Note that the transformation of the noise component does not change its statistical properties, so $\boldsymbol{n'}$ is still additive Gaussian noise and is statistically identical to $\boldsymbol{n}$. So the input-output relationship (2.1) can be re-written as:

$$\boldsymbol{Y'} = \Sigma\boldsymbol{X'} + \boldsymbol{n'}. \tag{2.12}$$

Alternatively, this is equivalent to the bank of scalar links:

$$y'_i = s_i x'_i + n'_i, \quad i = 1, 2, \ldots, m. \tag{2.13}$$

Thus, if we pre-filter the input message symbols $\boldsymbol{X}$ by the matrix $\boldsymbol{V}$ and post-filter the received symbols $\boldsymbol{Y}$ by the matrix $\boldsymbol{U}^{\dagger}$, the ordered eigenvalues of the channel correlation matrix ($\lambda_1 \geq \ldots \geq \lambda_m$) can be realized as the power gains of m independent spatial channels, also known as the eigenmodes. We describe $\boldsymbol{V}$ and $\boldsymbol{U}$ as steering matrices[2] in the rest of the thesis. Such an operation leads to the signalling architecture depicted in Fig. 2.5, which is widely known as *SVD transmission*, *eigenmode transmission* and *eigen-beamforming*. This structure has been proposed in [26, 54, 55] and many other publications.

2.3.3 Joint Eigenvalue Statistics and Wishart Distributions

Since the squared singular values of $\boldsymbol{H}$ are equivalent to the eigenvalues of the correlation matrix $\boldsymbol{H}\boldsymbol{H}^{\dagger}$ as shown in the last section, this section reviews the joint statistics of the eigenvalues. In a Rayleigh i.i.d channel, the corresponding channel correlation matrix is an $m \times m$ matrix known as a *Wishart Matrix*. The Wishart matrix is denoted $\boldsymbol{W}$, and is defined by

$$\boldsymbol{W} = \begin{cases} \boldsymbol{H}\,\boldsymbol{H}^{\dagger}, & \text{for} \quad N_r \leq N_t \\ \boldsymbol{H}^{\dagger}\,\boldsymbol{H}, & \text{for} \quad N_t < N_r \end{cases} \tag{2.14}$$

[2]Some authors call them eigen-beamformers

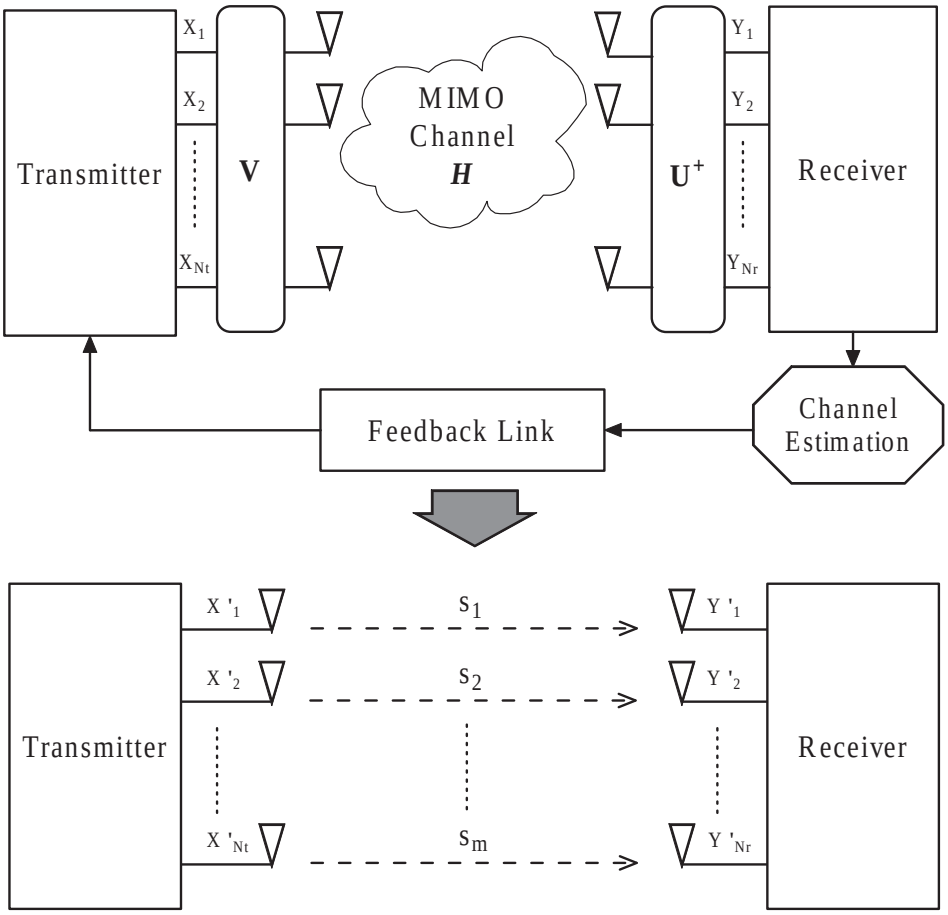

Figure 2.5: The MIMO transceiver architecture based on the SVD, which transforms the channel matrix into a bank of scalar links.

The eigenvalues of $\boldsymbol{W}$, $\lambda_1 \geq \lambda_2 \geq \ldots \geq \lambda_m$ (or $s_1^2 \geq s_2^2 \geq \ldots \geq s_m^2$), have the joint density [56, 57]:

$$f(\lambda_1, \ldots, \lambda_m) = \prod_{i=1}^{m} [(n-i)!(m-i)!]^{-1} \exp\left(-\sum_{i=1}^{m} \lambda_i\right) \times \prod_{i=1}^{m} \lambda_i^l \prod_{i<j} (\lambda_i - \lambda_j)^2. \tag{2.15}$$

The marginal density of any individual eigenvalue can be obtained in closed-form via serial integration, since the joint density is simply a polynomial with exponential terms. Not surprisingly, the marginal densities of individual eigenvalues are also polynomial with exponential terms, so their mean and variance

can be calculated exactly. This is particularly simple with the aid of some symbolic manipulation packages such as MAPLE. Additionally, analytical results on the marginal densities can also be found in [58].

2.4 MIMO Channel Quality Metrics

In the preceding section, the concepts of SVD and eigenmodes have been introduced. As aforementioned, the eigenvalues of the channel correlation matrix reveal some important system characteristics in the spatial domain. In addition, a few important eigenvalue-dependent channel quality metrics have been identified in the literature, and many of them have been employed as the switching criterion in some adaptive MIMO schemes. The general configuration of an adaptive scheme is depicted in Fig. 2.6. As shown in the figure, the channel is estimated at the receiver, then the quality metric is computed based on the estimates and the transmitter is informed through a low-rate feedback link. The transmitter can thereby choose the appropriate signalling parameters or modes for the next transmission, based on the value of the metric. Common signalling parameters or modes in adaptive schemes include data rates (adaptive modulation), antenna selection, code rates in error-correction codes, adaptive interleaving and puncturing for convolutional and turbo codes, or varying block lengths for block codes [59]. This thesis concentrates on rate-adaptation and transmission strategy switching. The objective of this section is to review some important MIMO channel metrics which are functions of the eigenvalues, along with their potential applications in transceiver design.

2.4.1 Eigenmodes

The importance of the eigenmodes has been revealed by many authors in different applications. As discussed before, the eigenvalues give the gains of the virtual links in SVD-transmission architectures [26]. It is also well-known that

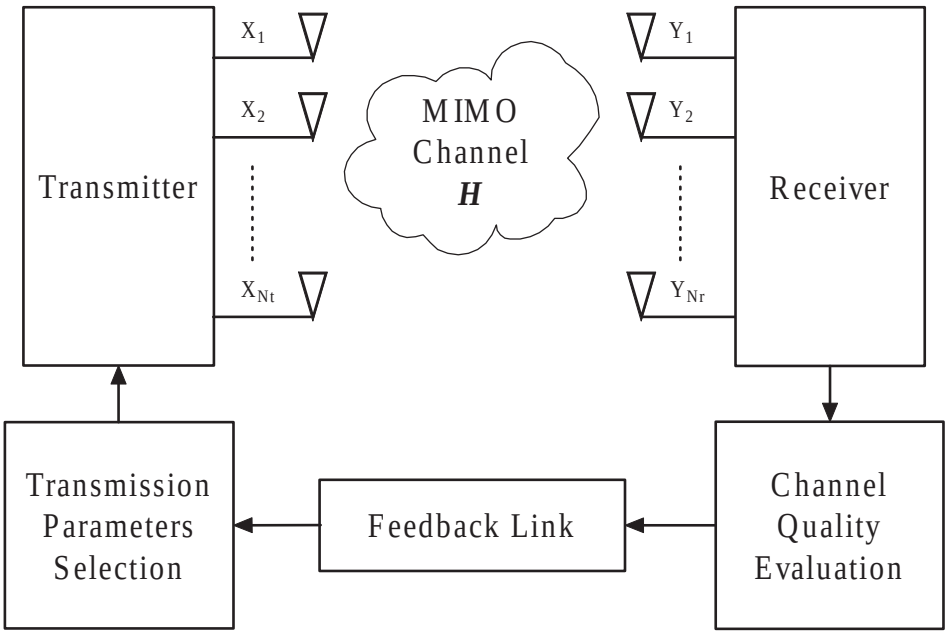

Figure 2.6: The general schematic of an adaptive MIMO system.

the channel capacity can be achieved if the transmission power is adaptively allocated over the eigenmodes using the "water-filling" algorithm. Similarly, applying adaptive modulation (or bit allocation [60]) schemes to the eigenmodes can optimize the data rate [61, 62]. In these adaptive schemes, the parameters of the physical layer signalling are adjusted in accordance with the prevailing channel status to boost the overall performance. In general, such operations require both the transmitter and receiver to know the channel state information (CSI), so that steering matrices ($\boldsymbol{U}$ and $\boldsymbol{V}$) on both sides can be computed and used to diagonalize the channel. Note that although multiple independent data streams are usually considered for transmission over the different eigenmodes, leading to a spatial multiplexing scheme, some researchers have attempted to merge the SVD architecture with STBC [63, 64, 65] to achieve higher diversity gains.

In "water-filling", the basic idea is to inject more power into stronger eigenmodes and less power into weaker links. The power allocated to the eigenmodes

is adjusted in accordance with the prevailing channel status. The power allocated to the i^{th} eigenmode is

$$\mathcal{P}_i = \max(0, \Theta - \tfrac{N_0}{\lambda_i}), \quad i = 1, 2, \ldots, m, \tag{2.16}$$

where Θ is determined to satisfy the constraint:

$$\sum_{i=1}^{m} \mathcal{P}_i = \mathcal{P}, \tag{2.17}$$

and $\mathcal{P}$ is the total available power at the transmitter. Therefore, the received power on the i^{th} eigenmode is

$$\mathcal{P}_{rec,i} = \max(0, \lambda_i \Theta - N_0), \quad i = 1, 2, \ldots, m. \tag{2.18}$$

With the use of the water-filling scheme, the channel capacity of a MIMO system can be expressed as [8]

$$C_{WF} = \textstyle\sum_{i=1}^{m} \log_2(1 + \frac{\mathcal{P}_{rec,i}}{N_0}) \quad \text{bits/s/Hz}. \tag{2.19}$$

The water-filling method can optimize the performance of a MIMO system in terms of capacity. However, its potential gain, as compared to uniform power allocation, diminishes in the high SNR regime.

To implement the water-filling algorithm, a reliable feedback channel is necessary unless the system is time-division duplex based where reciprocity can be utilized [26]. This feedback can be designed to be more efficient, and hence more feasible in practice, if the time-varying characteristics of the eigenvalues are known statistically.

Apart from SVD transmission and water-filling, the eigenvalues are also useful in some other aspects of MIMO systems. For instance, in maximum ratio transmission (MRT) schemes, the maximum signal-to-noise ratio (SNR) is proportional to the largest eigenvalue [66]. On the other hand, the minimum eigenvalue (or its square root, the smallest singular value) plays an important role in the performance of certain MIMO transceiver schemes. It acts as a

metric for the minimum distance between the received vectors [67] and some researchers have proposed the technique of boosting the value of λ_m in order to attain better performance [68]. λ_m has also been used as an antenna selection criterion [69], in which the antenna set with largest λ_m is chosen. Additionally, the channel inversion schemes discussed in [70] suffer from transmission power problems when λ_m drops below a certain threshold [71]. By and large, the eigenvalues play a key role in both the design and analysis of MIMO systems.

2.4.2 Total Power Gain

As the eigenvalues are the power gains for the individual eigenmodes, it is apparent that

$$\gamma = \sum_{i=1}^{m} \lambda_i \tag{2.20}$$

is the total channel gain. This channel gain metric is used in space-time block coding [72]. In addition, because a larger eigenvalue sum generally indicates a better SNR performance, some proposed schemes have used it as a benchmark for adaptive control. For example, an antenna selection algorithm based on the eigenvalue sum is given in [73].

2.4.3 MIMO Channel Capacity

The information theoretic capacity of a MIMO channel gives the maximum possible data rate for error-free transmission. Hence, the channel capacity is an important metric for the "rate feedback" schemes which adapt the transmission rate by monitoring the prevailing channel quality [74]. The dynamic bit-budget of variable data rate schemes (as mentioned in [75]) is also intuitively related to the instantaneous MIMO channel capacity.

Assuming feedback is not available, the water-filling algorithm can not be implemented and the transmitter usually spreads the power equally over the antennas since it does not possess the CSI. For such systems, the MIMO

channel capacity can be written as [57]:

$$C(t) = \sum_{i=1}^{m} \log_2 \left(1 + \frac{\mathcal{P}}{N_t}\lambda_i(t)\right) \quad \text{bits/s/Hz.} \tag{2.21}$$

A survey of environmental factors that affect MIMO channel capacity has been presented in [76].

2.4.4 Condition Numbers

In the absence of CSI at the transmitter, the best strategy for power allocation is to distribute the power evenly over the antennas. In such situations in the high SNR regime, more capacity can be attained if the eigenvalues are less spread out. In the low SNR regime, however, the optimal policy is to inject power into the strongest eigenmode only, so a larger eigenvalue spread is more desirable [77]. Also, the gain of water-filling (compared to uniform power allocation) increases with the difference between the largest and smallest eigenvalue due to lower power wastage [78].

To estimate how many effective spatial links are within the system, the eigenvalue spread is the most widely used indicator of spatial selectivity. One common measure of the eigenvalue spread is the *regular condition number*

$$\kappa = \frac{\lambda_1}{\lambda_m}\,. \tag{2.22}$$

This measure has been proposed as the selection criterion for "dual-mode antenna selection" [79]. Here, κ acts as a metric that indicates whether either multiplexing or diversity is more suitable for the current channel. The ratio of other eigenvalue pairs are also of interest; for example, the receiver of the scheme proposed in [80] computes certain eigenvalue ratios to determine the total number of effective spatial channels.

Alternatively, Heath and Paulraj [81] have proposed another switching criterion between general spatial multiplexing and space-time coding schemes, known as the *Demmel condition number*. The Demmel condition number is

the ratio of the Frobenius Norm and the smallest singular value. Here we are interested in the square of the Demmel condition number, defined as

$$\kappa_D = \frac{\sum_{i=1}^{m} \lambda_i}{\lambda_m} . \tag{2.23}$$

Some field measurements have been carried out to study the statistical properties of κ_D in various propagation environments [82].

2.5 Summary

This chapter gives a review of system models that are frequently used in the area of MIMO wireless communications. In particular, various types of statistical channel models are studied due to their simplicity. A few typical channel ACFs, which govern the time-varition of the channel, are also elaborated.

Under the assumption of flat-fading, the linear relationship between the input and output of a MIMO system is given, where the channel can be written as a random matrix with complex entries. We focus on i.i.d Rayleigh channels where the entries are zero-mean complex Gaussians with unit variance. Through the SVD, the eigen-structure of the channel correlation matrix can be analyzed. Many studies have shown that the eigen-structure possesses information regarding the system characteristics in the spatial domain. The concept of SVD can also be extended to a transceiver architecture known as eigen-beamforming or SVD-transmission, via linear operations on both transmitted and received signals.

The last section provided an overview of some important channel metrics that are related to MIMO eigenmodes, including their potential applications. To be specific, we described eigen-channels, total power gain, channel capacity and condition numbers. One of the major goals of this thesis is to study the time-varying characteristics of these metrics.

Chapter 3

Level Crossing Analysis of MIMO Channel Metrics

For a fading channel, the influence of long but rare fades is totally different to that of short but frequent fades. To gauge how the time-varying nature of the channel affects the system, level crossing rates (LCR) and average fade durations (AFD) are two important second order statistics. LCR is defined as the average number of times that a signal is down-crossing (or up-crossing) a certain threshold, while AFD indicates the average duration that the signal stays below the threshold level [83]. The definitions of level-crossing and fade-duration can be visualized in Fig. 3.1.

These two statistical measures are useful in many aspects of receiver design such as dynamic range, equalization, diversity, modulation schemes, and error control coding [14]. For a more specific example, since the AFD can be translated into the average length of an error burst, the length of a data block and the duration of certain constellations in adaptive modulation can be chosen judiciously.

The analytical LCR and AFD results are well-known for the traditional SISO land mobile channel [39]. However, hitherto only a handful papers have investigated the time-variation characteristics of MIMO fading channels. Much of the previous work on this issue has been carried out by either simulations or

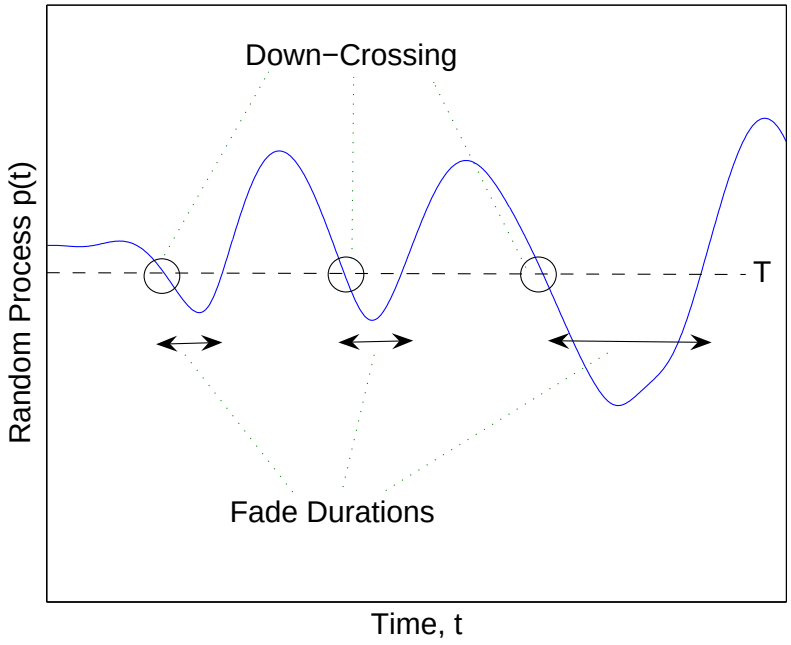

Figure 3.1: An illustration of level-crossings and fade-durations for an arbitrary random process $p(t)$ with a threshold level T.

field measurements, and analytical approaches are relatively sparse. Both [84] and [85] have conducted field experiments to measure the temporal variation of the eigenmode gains, and the LCR and AFD for the eigenmodes have been specifically considered in [85]. The influence of spatial correlation on the LCR and AFD of the MIMO channel capacity have been examined via computer simulations in [86] and [87]. The joint statistics of MIMO channel matrix entries have been analyzed in [88]. The authors in [40] have analyzed the effects of different antenna angles on the LCR of the channel matrix entries. Recently, a LCR result for eigenmodes has been computed analytically [89], but the results are very complicated and hence closed-form calculations are prohibitive for larger MIMO systems. To date, there appears to be no work which addresses the time-variations of eigenmodes in MIMO wireless communication systems with a feasible analytical approach.

The main objective of this chapter is to present a systematic study of the analytical LCR and AFD of MIMO eigenmodes and their associated channel metrics. In particular, the contributions of this chapter include the derivation of closed-form approximations for the LCR and AFD of:

- the individual MIMO eigenmodes,
- the total MIMO channel power gain,
- the regular condition number,
- the Demmel condition number, and
- the MIMO channel capacity (with evenly distributed transmission power).

Here, it has been found that the eigenmodes and the associated metrics can be well approximated by either gamma or Gaussian variables. The gamma distribution can be used to model the distributions of the eigenmodes and the logarithms of the condition numbers, whereas the channel capacity is approximately Gaussian [90]. Hence, the LCRs can be computed by directly applying the standard LCR formulas for gamma [91] and Gaussian [39] processes. Nonetheless, these formulas require the curvatures of the autocorrelation functions of the processes. Hence, the derivation of the corresponding autocorrelation functions (ACF) for the eigenmodes and channel metrics becomes the focus of this work.

The resultant calculation for the ACF, however, is rather complex. Alternatively, a simple LCR formula for the eigenmodes is separately developed and presented, which dispenses with the complicated calculation of ACF. Moreover, in order to show the versatility of this method, it is applied to fading scenarios with different ACFs.

Metrics	Distributions
eigenvalues (small systems)	gamma
eigenvalues (large systems)	gamma mixtures
minimum eigenvalues (symmetric systems)	exponential (exact)
total power gain	chi-square (exact)
channel capacity	Gaussian
logarithm of regular condition number	gamma
logarithm of Demmel condition number	gamma

Table 3.1: Channel metrics and their approximating distributions

3.1 Approximating Distribution Functions and Corresponding LCR Formulas

To analyze the dynamic statistics of random processes, it is also important to characterize the static statistical properties. Instead of finding exact distributions of the MIMO channel metrics of interest, we approximate them with some well-known distribution functions. In particular, the MIMO channel metrics of interest here can be approximated by gamma, exponential, chi-squared or Gaussian processes. Note that the exponential and χ^2 distributions are both special cases of the gamma distribution. The specific details are summarized in Table 3.1.

Note that the smallest eigenvalue of the symmetric channel ($m = n$) is exactly exponentially distributed with probability density function (PDF):

$$f(\lambda_m) = m \exp(-m\lambda_m). \tag{3.1}$$

Accurate approximations of the channel metrics using these statistical distributions, have provided a convenient route to level crossing analysis, because the standard LCR results for these processes are readily available in the literature. The goal of this section is to review these statistical distributions and their corresponding LCR formulas. The accuracy of the approximations to the metrics of interest is also demonstrated.

3.1.1 Gamma and Gamma-Mixture Distributions

To discuss the gamma approximations, the following notation needs to be defined. Let a gamma distribution with shape parameter r and scale parameter θ be denoted $g(r, \theta)$. A gamma random variable has mean μ_g and variance σ_g^2 given by r/θ and r/θ^2 respectively. The gamma PDF is given by

$$f(x) = \Gamma(r)^{-1}\, \theta^r\, x^{r-1}\, \exp(-\theta\, x), \qquad x \geq 0\,. \tag{3.2}$$

A LCR formula for the gamma process has been derived in [91]:

$$\mathrm{LCR}_{\mathrm{gamma}}(T) = \frac{1}{2\,\Gamma(r)} \sqrt{\frac{2\,|\ddot{R}(0)|}{\pi}}\, (\theta T)^{r-0.5} \exp\left(-\theta T\right), \tag{3.3}$$

where T is the threshold level, and $\ddot{R}(0)$ is the second derivative (curvature) of the autocorrelation function, $R(\tau)$, of the process at $\tau = 0$. Both here and later, we use the notation $R(\tau)$ to represent the ACF of the process of interest. For example, for an arbitrary random process, $p(t)$, we have

$$R(\tau) = \frac{\mathrm{E}[p(t)p(t+\tau)] - \mathrm{E}[p(t)]\mathrm{E}[p(t+\tau)]}{\sqrt{\mathrm{Var}[p(t)]\,\mathrm{Var}[p(t+\tau)]}}\,. \tag{3.4}$$

Because we can write $R(\tau)$ as a polynomial in τ, $R(\tau) = \sum_{i=0}^{\infty} \Phi_i\, \tau^i$, we see that the curvature is $\ddot{R}(0) = 2\,\Phi_2$. It is important to note that we reserve the notation $\rho(\tau)$ for the ACF of the channel entry itself, which in our case, assuming a land mobile channel with Jakes fading, has the form $\rho(\tau) = J_0(2\pi f_D \tau)$.

The gamma distribution provides excellent accuracy in approximating eigenvalues in MIMO systems with moderate sizes ($N_t \leq 5$ and $N_r \leq 5$). This has also been noted in [92] and [93]. Figure 3.2 exhibits the gamma approximation for the eigenvalues of a (4,4) MIMO channel.

For MIMO systems of larger size, however, the gamma approximation for the eigenvalues is not as accurate, particularly for highly asymmetrical cases. Instead, we have found that a mixture of gamma variables can model the eigenvalue process very well. Such a mixture model allows us to get better

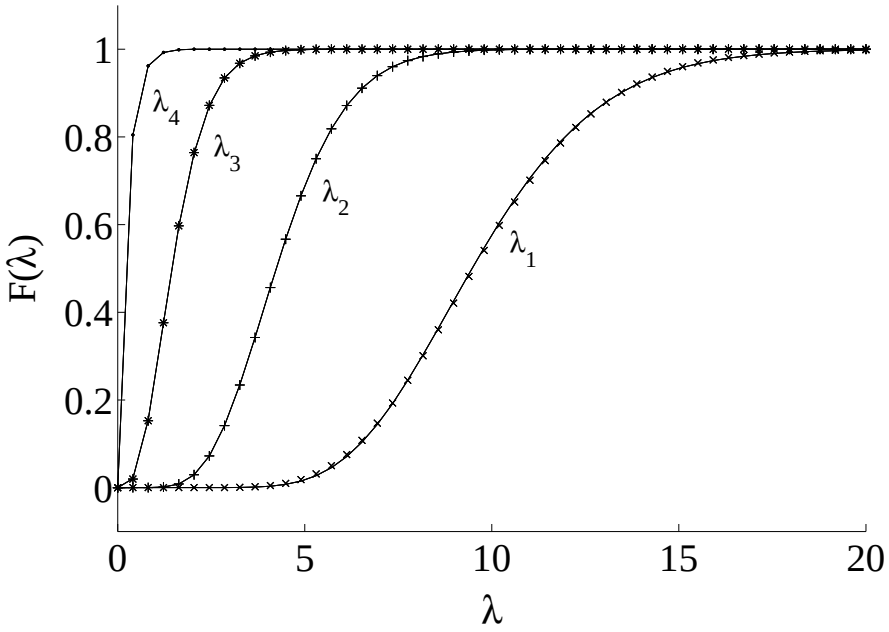

Figure 3.2: CDFs for the eigenvalues of a (4,4) system. Points denote the gamma cumulative distribution function (CDF), while lines denote the exact eigenvalue CDF.

accuracy while utilizing the same LCR results as before. The overall density of a mixture is the sum of the mixing component densities scaled by appropriate weighting factors. Hence, the density of a mixture distribution comprised of k components with densities $f_1(x), \ldots, f_k(x)$ is given by

$$f_{\text{mixture},k}(x) = \phi_1 f_1(x) + \phi_2 f_2(x) + \cdots + \phi_k f_k(x), \tag{3.5}$$

where ϕ_i are the non-negative weighting factors which satisfy $\sum_{i=1}^{k} \phi_i = 1$. In general, for MIMO systems with moderate sizes, we have found that $k = 2$ is sufficient.

In order to find the corresponding parameters of the mixture (r and θ for each gamma component and $\phi_1, \ldots, \phi_k$), we have used numerical optimization routines to minimize the integrated squared error between the exact density of the eigenvalue and the gamma-mixture density. Note that moment methods could be used, but do not appear to give a superior or more convenient numerical approach. Here we give an illustrative example. Consider the maximum

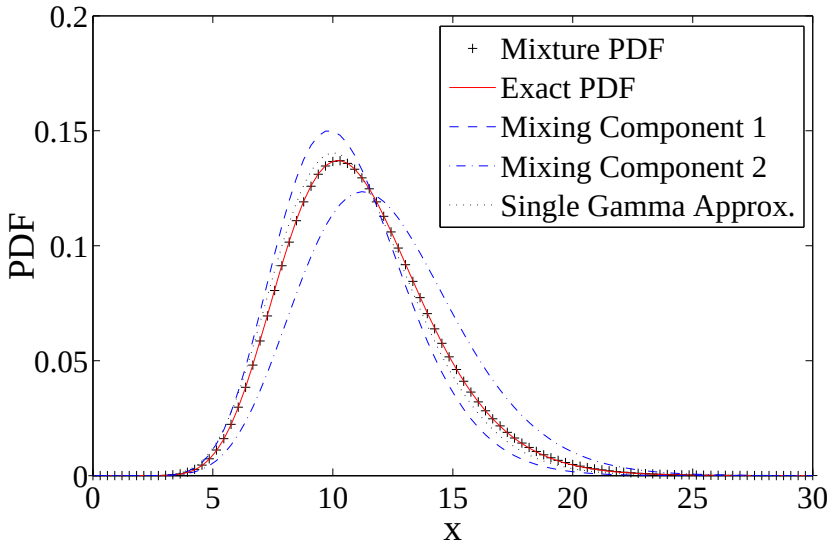

Figure 3.3: A gamma mixture approximation for λ_1 in a (2,8) MIMO channel.

eigenvalue, λ_1, of a (2,8) system approximated using a mixture of two gamma variables. The two mixing components, $f_1(x)$ and $f_2(x)$, are $g(1.4128, 14.9244)$ and $g(1.0928, 13.2911)$ with weighting factors of 0.6322 and 0.3678 respectively. As shown in Fig.3.3, the exact PDF of λ_1 and the resultant mixture distribution are closely aligned with each other.

The resultant LCR is the sum of the LCRs of the mixing components scaled by the corresponding weighting factors:

$$\mathrm{LCR}_{\mathrm{mixture},k}(T) = \phi_1 \,\mathrm{LCR}_1(T) + \phi_2 \,\mathrm{LCR}_2(T) + \cdots + \phi_k \,\mathrm{LCR}_k(T). \qquad (3.6)$$

3.1.2 Gaussian Distribution

The LCR for a Gaussian process has the form [39]:

$$\mathrm{LCR}_{\mathrm{Gaussian}}(T) = \frac{\sqrt{-\ddot{R}(0)}}{2\pi} \exp\left[\frac{-1}{2}\left(\frac{T-\mu}{\sigma}\right)^2\right], \qquad (3.7)$$

where μ and σ are the mean and the standard deviation of the Gaussian process respectively.

3.2 LCR of Total Power Gain

The LCR for the total power gain is considered separately in this section, since γ (defined in Section 2.4.2) is exactly χ^2 distributed with $2N_rN_t$ degrees of freedom [94], and hence this problem is much more straightforward than for the other metrics. It is worth noting that the LCR for γ in the spatially correlated case has been derived in [88], but the results are very complicated. Here we show a very simple closed-form LCR formula that is valid in the case of i.i.d. Rayleigh fading. Following [95], the LCR for a χ^2 random process with $2N_rN_t$ degrees of freedom is given by:

$$\mathrm{LCR}_\gamma(T) = \frac{\pi^{-1/2}\sqrt{-\ddot{\rho}(0)}\,T^{N_rN_t-1/2}\exp(-T)}{\Gamma(N_rN_t)}, \tag{3.8}$$

where T is the threshold level and $\ddot{\rho}(0)$ is the second derivative of the auto-correlation function (ACF) of the underlying Gaussians of the χ^2 process at $\tau = 0$. To obtain $\ddot{\rho}(0)$ for the three channel ACFs described in Section 2.2.3, we first expand the corresponding $\rho(\tau)$ as a polynomial in τ. Then the second order derivative, $\ddot{\rho}(0)$, is simply double the coefficient of the τ^2 term. Thus, the LCR for the total link gain in these three fading scenarios can be derived by substituting the appropriate value for $\ddot{\rho}(0)$ into (3.8). The corresponding results for $\ddot{\rho}(0)$ and LCR_γ for these three scenarios are summarized in Table 3.2.

For SISO channels, where $N_t = N_r = 1$, the results in Table. 3.2 reduce to the LCR formulas that have been derived in [39], [41] and [40]. Hence, we can conclude that (3.8) is a generalized result for the channel gain LCR that includes previous findings as special cases. The AFD for an arbitrary random process $p(t)$, is given by

$$\mathrm{AFD}_p(T) = \frac{\mathrm{Prob}(p < T)}{\mathrm{LCR}_p(T)}. \tag{3.9}$$

Scenarios	$\ddot{\rho}(0)$	$\mathrm{LCR}_\gamma(T)$
Jakes Model	$-2\pi^2 f_D^2$	$\frac{\sqrt{2\pi}\, f_D\, T^{N_r N_t - 0.5} \exp(-T)}{\Gamma(N_r N_t)}$
Laplacian PAS	$\frac{-2\,\pi^2 f_D^2}{1+1/\vartheta^2}$	$\sqrt{\frac{2\,\pi}{1+1/\vartheta^2}}\, \frac{f_D\, T^{N_r N_t - 0.5} \exp(-T)}{\Gamma(N_r N_t)}$
Mobile-to-Mobile	$-2\pi^2(f_{D_1}^2 + f_{D_2}^2)$	$\frac{\sqrt{2\pi}(f_{D_1}^2+f_{D_2}^2)^{0.5}\, T^{N_r N_t - 0.5} \exp(-T)}{\Gamma(N_r N_t)}$

Table 3.2: LCR formulas for the total power gain with different ACFs.

Thus, the AFD for γ can be trivially written as

$$\mathrm{AFD}_\gamma(T) = \frac{\Gamma_{\mathrm{inc}}(T, N_r N_t)}{\mathrm{LCR}_\gamma(T)} \tag{3.10}$$

where the incomplete gamma function, $\Gamma_{\mathrm{inc}}(a, b)$, is defined as

$$\Gamma_{\mathrm{inc}}(a, b) \triangleq \frac{1}{\Gamma(b)} \int_0^a e^{-u} u^{b-1}\, du\,.$$

To verify these formulas, we now compare our calculations with Monte Carlo simulation results. Firstly, for the Jakes model, assuming that $\tau =$ 0.1ms, the receiver is moving with a speed of 5 km/hr and a system carrier frequency of 5.725 GHz (HyperLan 2 standard), we have $f_D = 26.5$Hz from (2.5). We use these parameter values in the other simulations in this chapter, unless otherwise specified. Figures 3.4 and 3.5 illustrate our results for the normalized LCR and the AFD of the eigenvalue sum for MIMO systems with different sizes. They show excellent agreement between the equations in Table 3.2 and the empirical values for the 2×10^5 Monte Carlo simulation points we have generated. Note that the LCR is proportional to the Doppler frequencies. Thus, we can plot the normalized parameter LCR/f_D against the threshold levels in Fig. 3.4. Similarly, as AFD is proportional to $1/f_D$, so we have plotted the normalized parameter AFD $\times\, f_D$ against the threshold levels in Fig. 3.5.

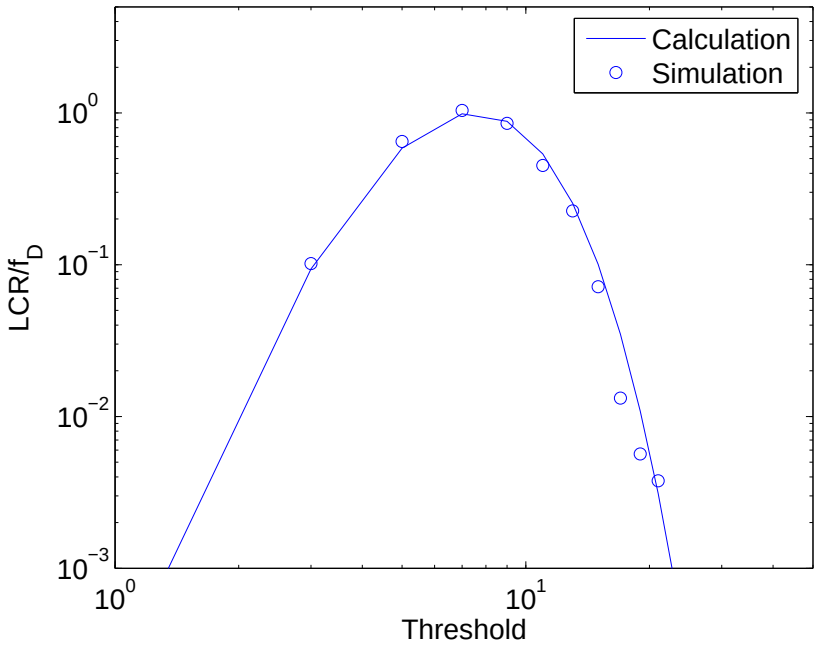

Figure 3.4: A comparison between the calculated and simulated LCR for the total power gain in a (2,4) MIMO system with Jakes fading.

We have also validated the LCR formulas in channels with Laplacian PAS. Figures. 3.6 and 3.7 show the agreement between simulations and calculations, with different angular spreads ϑ. Finally, the simulations for the mobile-to-mobile cases are also carried out with parameters $f_{D_1} = 19.5$Hz and $f_{D_2} = 53$Hz. The results are shown in Figs. 3.8 and 3.9.

3.3 LCR for other Metrics

In the last section, an analytical LCR formula for the MIMO total power gain has been derived. The derivation was straightforward since the ACF for the Gaussian entries are known. Also, it is apparent that the LCR formulas can be computed using the mean, variance and ACF of the processes of interest. Nevertheless, explicit forms for the ACFs of most of the MIMO channel metrics considered in this thesis are not available. Hence, in this section, we derive the

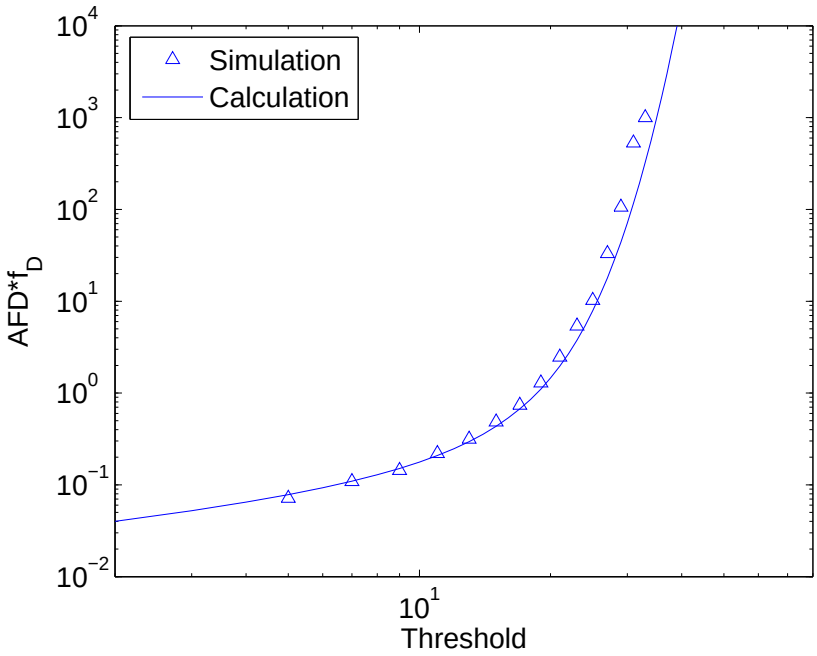

Figure 3.5: A comparison between the calculated and simulated AFD for the total power gain in a (4,4) MIMO system with Jakes fading.

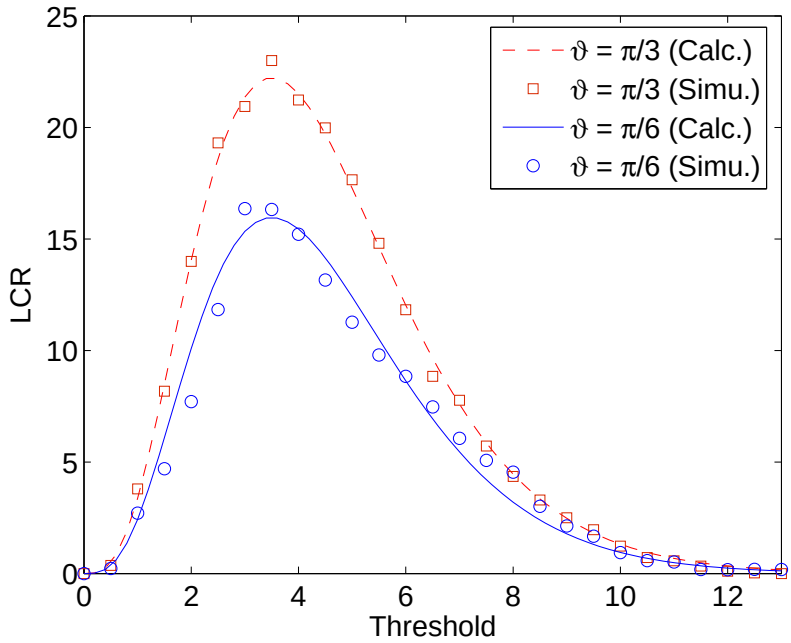

Figure 3.6: A comparison between the calculated and simulated LCR for the total power gain in a (2,2) MIMO system with Laplacian PAS.

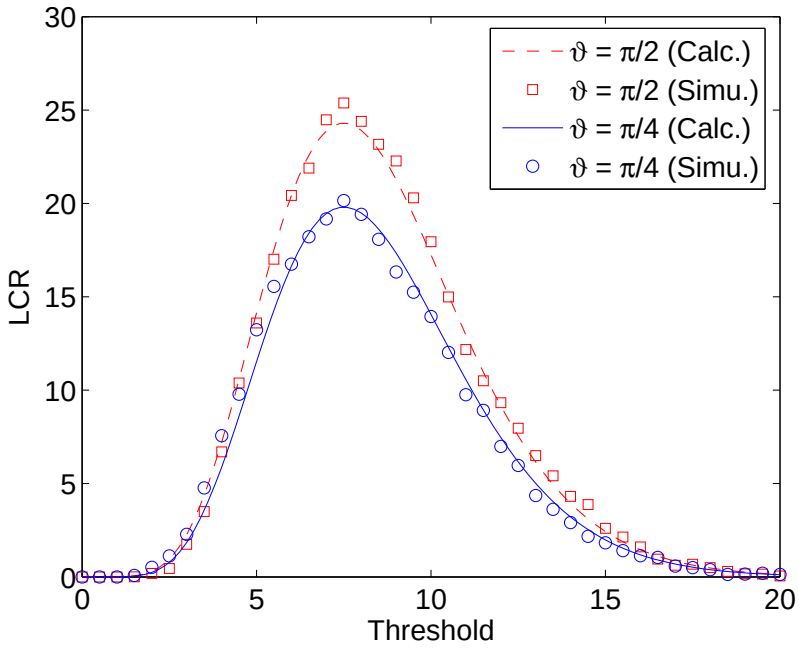

Figure 3.7: A comparison between the calculated and simulated LCR for the total power gain in a (2,4) MIMO system with Laplacian PAS.

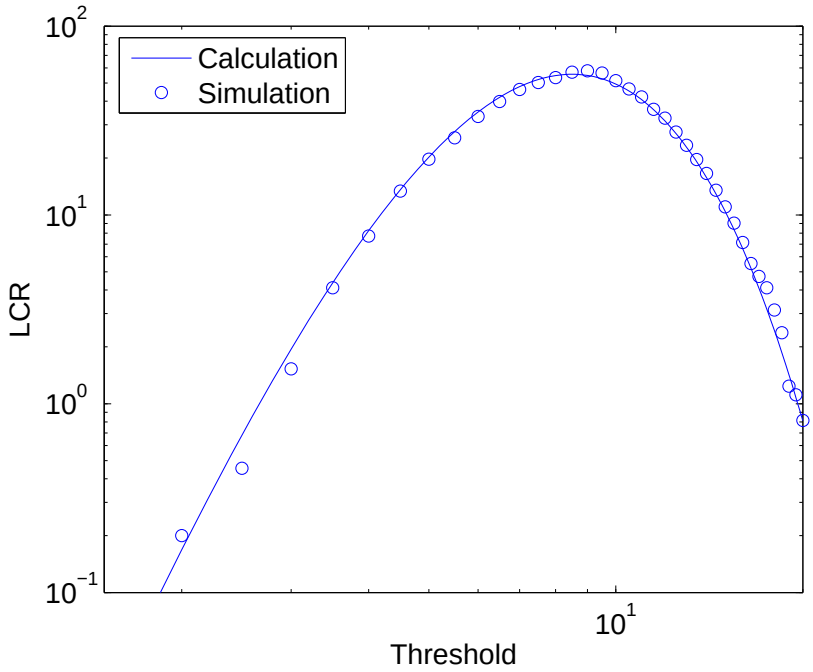

Figure 3.8: A comparison between the calculated and simulated LCR for the total power gain in a (3,3) MIMO system with mobile-to-mobile propagation.

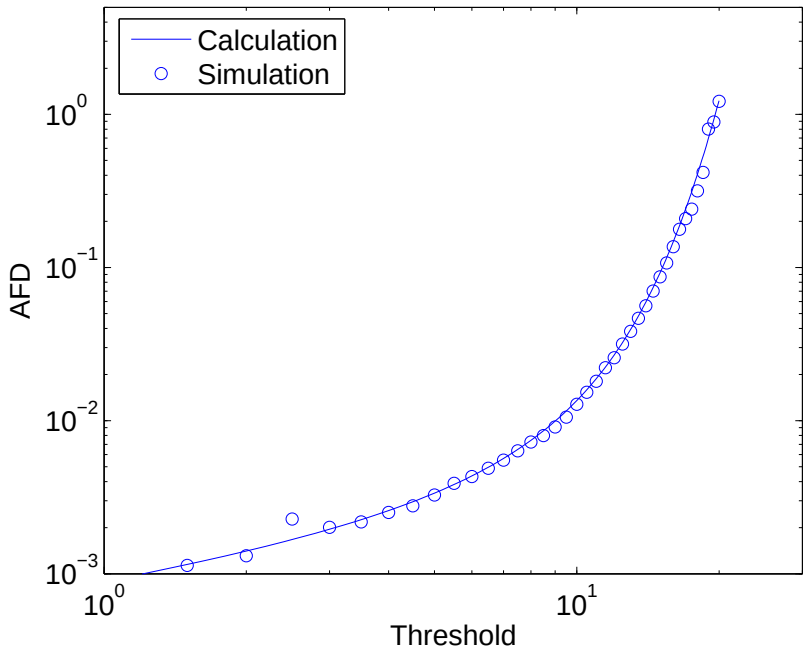

Figure 3.9: A comparison between the calculated and simulated AFD for the total power gain in a (3,3) MIMO system with mobile-to-mobile propagation.

required second order derivatives, $\ddot{R}(0)$, using a stochastic differential equation (SDE)-based approach. The drawback of this approach is that the approximation deteriorates with larger lag τ. However, we only require $R(\tau)$ as $\tau \to 0$. Thus, the general ACF is unavailable, but our technique yields the ACF at lags close to zero, which is sufficient to compute the LCR. Note that analysis using SDE based approaches in the context of communication engineering has gained more visibility in recent years [96, 97].

3.3.1 The Stochastic Differential Equation-Based Approach

In [98], Bru derived a SDE for the eigenvalues $\boldsymbol{w} = (w_1, w_2, \ldots, w_m)$ of $\boldsymbol{B}\boldsymbol{B}^T$ when the elements of $\boldsymbol{B} : m \times n$ follow i.i.d. *real* standard Brownian motion processes and m, n are as defined previously. König and O'Connell [99] found a similar SDE for the case where the elements of $\boldsymbol{B}$ are i.i.d. *complex* standard

Brownian motion processes. This SDE is given by:

$$dw_i(t) = 2\sqrt{w_i(t)}\, d\widetilde{B}_i(t) + 2n\, dt + 2\sum_{k\neq i} \frac{w_i(t) + w_k(t)}{w_i(t) - w_k(t)}\, dt\,. \tag{3.11}$$

In (3.11), $w_i(t)$, $i = 1, \ldots, m$, are the time-varying eigenvalues of $\boldsymbol{B}(t)\boldsymbol{B}^{\dagger}(t)$ and $\widetilde{B}_i(t)$ is the driving Brownian motion process, which is independent of all $w_j(t)$ and $\widetilde{B}_j(t)$ for $i \neq j$. We utilize and modify the results in [99] as follows. By using the standard Euler approximation, $dw_i(t) \approx w_i(t+\tau) - w_i(t)$, we have for small $\tau > 0$

$$w_i(t+\tau) \approx w_i(t) + 2\sqrt{w_i(t)}\,[\widetilde{B}_i(t+\tau) - \widetilde{B}_i(t)] + 2n\,\tau + 2\tau \sum_{k\neq i} \frac{w_i(t) + w_k(t)}{w_i(t) - w_k(t)}. \tag{3.12}$$

The entries of $\boldsymbol{B}(t)$ are complex standard Brownian motion processes, so we have $\mathrm{E}\{[\boldsymbol{B}(t)]_{ij}\} = 0$, $\mathrm{E}\{|[\boldsymbol{B}(t)]_{ij}|^2\} = 2t$ and $\mathrm{E}\{[\boldsymbol{B}(t)]_{ij}[\boldsymbol{B}^{\dagger}(t+\tau)]_{ij}\} = 2t$. Clearly, Brownian motion is not a suitable model in our case, since the power of each link does not increase proportionally with the time elapsed. In our channel model, the $\boldsymbol{H}(t)$ matrix, has elements with zero mean, magnitude variance equal to 1, and ACF equal to $J_0(2\pi f_D \tau)$. To overcome this discrepancy, we transform $\boldsymbol{B}(t)$ so that the resulting statistics match our particular application.

Specifically, we note that at time $t = \tau\,[J_0(2\pi f_D\tau)^{-2} - 1]^{-1}$ the joint distribution of $(\boldsymbol{B}(t)/\sqrt{2t}, \boldsymbol{B}(t+\tau)/\sqrt{2(t+\tau)})$ is identical to that of $(\boldsymbol{H}(t), \boldsymbol{H}(t+\tau))$. Since $(\boldsymbol{B}(t), \boldsymbol{B}(t+\tau))$ are a pair of zero mean Gaussian matrices with i.i.d. entries, this result follows by demonstrating that their elements have the required variance and correlation structure. The variance property is satisfied since

$$\mathrm{E}\left\{\left|\frac{[\boldsymbol{B}(t)]_{ij}}{\sqrt{2t}}\right|^2\right\} = \mathrm{E}\left\{\left|[\boldsymbol{H}(t)]_{ij}\right|^2\right\} = 1\,.$$

The autocorrelation is given by

$$\mathrm{E}\left\{\frac{[\boldsymbol{B}(t)]_{ij}}{\sqrt{2t}}\,\frac{\left[\boldsymbol{B}^{\dagger}(t+\tau)\right]_{ij}}{\sqrt{2(t+\tau)}}\right\} = \frac{2t}{\sqrt{4t(t+\tau)}} = J_0(2\pi f_D\tau), \tag{3.13}$$

where we have used the correlation property for complex Brownian motion

$$\mathrm{E}\left\{\left[\boldsymbol{B}(t)\right]_{ij}\left[\boldsymbol{B}^{\dagger}(t+\tau)\right]_{ij}\right\} = 2\,\min(t, t+\tau)\,.$$

Thus, we rewrite (3.12) using these particular time values and replace $w_i(t)$ by $2t\,\lambda_i(t)$, where $\lambda_i(t)$, $i = 1, \ldots, m$, are the eigenvalues of the channel correlation matrix that we are interested in. Note that the random variable pairs $\{w_i(t), w_i(t+\tau)\}$ and $\{2t\,\lambda_i(t), 2[t+\tau]\,\lambda_i(t+\tau)\}$ are statistically identical at t and $t+\tau$. With some re-arrangement, the modified version of (3.12) becomes

$$\lambda_i(t+\tau) \approx \frac{t}{t+\tau}\,\lambda_i(t) + \frac{\sqrt{2t\tau}}{t+\tau}\,\sqrt{\lambda_i(t)}\,Z_i + \frac{\tau}{t+\tau}\left[n + \sum_{k\neq i}\frac{\lambda_i(t)+\lambda_k(t)}{\lambda_i(t)-\lambda_k(t)}\right], \quad (3.14)$$

where Z_i is a real Gaussian, $Z_i \sim \mathcal{N}(0,1)$, which is independent of $\lambda_1, \ldots, \lambda_m$. By using the time value $t = \tau\,[J_0(2\pi f_D \tau)^{-2} - 1]^{-1}$ as mentioned earlier, we can write $t/(t+\tau) = 1 - 2\pi^2 f_D^2 \tau^2 + o(\tau^3)$ and $\tau/(t+\tau) = 2\pi^2 f_D^2 \tau^2 + o(\tau^3)$, where $o(\tau^3)$ is a remainder term using standard "little o" notation. In other words,

$$\frac{o(\tau^3)}{\tau^3} \to 0 \quad \text{as} \quad \tau \to 0.$$

After some algebra and re-arrangement, we finally obtain the relationship:

$$\lambda_i(t+\tau) = \lambda_i(t) + \alpha_i\,\tau + \beta_i\,\tau^2 + o_i\,\tau^3, \quad (3.15)$$

where

$$\alpha_i = 2\pi f_D \sqrt{\lambda_i(t)}\,Z_i$$
$$\beta_i = 2\pi^2 f_D^2 \left[n + \sum_{k\neq i}\frac{\lambda_i(t)+\lambda_k(t)}{\lambda_i(t)-\lambda_k(t)} - \lambda_i(t)\right].$$

The remainder term, o_i, is a random variable with finite mean $\mathrm{E}[o_i] < \infty$. The remainder term has a finite mean since it is trivial to show that α_i and β_i both have finite means.

The main result here, (3.15), can be used as a unified starting point for the ACF curvature derivations for all of the channel metrics. For ease of notation,

we define

$$\Psi_i(t) \triangleq \sum_{k \neq i} \frac{\lambda_i(t) + \lambda_k(t)}{\lambda_i(t) - \lambda_k(t)} \tag{3.16}$$

in the rest of the paper. In the next few sections, we describe how the ACF curvature can be derived for the various channel metrics.

3.3.2 LCR for Eigenvalues

Using (3.15), it is straightforward to work out the curvature of the ACF at $\tau = 0$, $\ddot{R}(0)$, for the eigenvalue processes. Note that only $\mathrm{E}[\lambda_i(t)\lambda_i(t+\tau)]$ in the ACF expression needs to be examined, because the term $\mathrm{E}[\lambda_i(t)]\mathrm{E}[\lambda_i(t+\tau)]$ is a constant and vanishes due to differentiation. Based on (3.15), the joint moment has the form

$$\mathrm{E}[\lambda_i(t)\lambda_i(t+\tau)] = \mathrm{E}[\lambda_i^2(t) + \lambda_i(t)\,\alpha_i\,\tau + \lambda_i(t)\,\beta_i\,\tau^2 + \lambda_i(t)\,o_i\,\tau^3]\,. \tag{3.17}$$

Using the polynomial expansion $R(\tau) = \sum_{i=0}^{\infty} \Phi_i\,\tau^i$, we have $\ddot{R}(0) = 2\Phi_2$, and for this particular case

$$\ddot{R}_{\lambda_i}(0) = 2\,\frac{\mathrm{E}[\lambda_i(t)\beta_i]}{\mathrm{Var}[\lambda_i(t)]} \tag{3.18}$$

which has the final form

$$\ddot{R}_{\lambda_i}(0) = \frac{4\,\pi^2 f_D^2\,\mathrm{E}\Big[n\lambda_i(t) + \lambda_i(t)\,\Psi_i(t) - \lambda_i^2(t)\Big]}{\mathrm{Var}[\lambda_i(t)]}. \tag{3.19}$$

The remainder term vanishes since $\lambda_i(t)\,o_i$ has a finite mean. A numerical value for (3.19) can be calculated exactly using a symbolic manipulation software package and invoking some of the results in [58]. Note that $\mathrm{E}[\lambda_i(t)]$ and $\mathrm{Var}[\lambda_i(t)]$ are available from [58] or via symbolic integration of the joint density in (2.15). Also, $\mathrm{E}[\lambda_i(t)\,\Psi_i(t)]$ can be obtained in closed form using symbolic integration, since the $\lambda_i(t) - \lambda_k(t)$ terms in the denominator of $\Psi_i(t)$ are canceled by the $[\lambda_i(t) - \lambda_k(t)]^2$ terms in the joint density (2.15). A full analysis and derivation of these moments is beyond the scope of this thesis, but the

structure of the joint PDF ensures that they can be expressed in closed form. Examples of the results from symbolic integration are given in Tables 3.3, 3.4, and 3.5. Here we tabulate the numerical values for the parameters required in (3.19) for some typical system sizes.

System	λ_1	λ_2	λ_3	λ_4
(2,2)	3.5	0.5		
(2,4)	6.1875	1.8125		
(3,3)	6.5208	2.1458	0.3333	
(4,4)	9.7723	4.4086	1.5692	0.25

Table 3.3: Eigenvalue means

System	λ_1	λ_2	λ_3	λ_4
(2,2)	3.25	0.25		
(2,4)	5.4023	1.0273		
(3,3)	5.5135	1.1385	0.1111	
(4,4)	7.6392	2.2442	0.5964	0.0625

Table 3.4: Eigenvalue variances

System	λ_1	λ_2	λ_3	λ_4
(2,2)	5	-1		
(2,4)	25.1250	-1.1250		
(3,3)	21.9514	-2.8403	-1.1111	
(4,4)	54.2754	-0.3631	-4.7871	-1.1250

Table 3.5: Means of $\lambda_i \Psi_i$

Substituting the value of (3.19) into (3.3), we acquire the LCR for the eigenvalue process. The AFD can also be acquired based on (3.9), where the probability, Prob($\lambda_i < T$), can be computed using either the exact marginal density of eigenvalues or the corresponding gamma approximation. All the

LCR and AFD results that have been generated are shown in Figs. 3.10 - 3.19. The simulations were carried out using the parameter values given in the last section. The results provide some valuable insights into the fluctuation behavior of eigenmodes, which may be useful for some schemes that adapt their signalling parameters to the prevailing link quality. For example, by using the LCR results, we can conjecture how often that the message constellation size should be adjusted in schemes that employ adaptive modulation over the eigenmodes [61].

As mentioned before, for MIMO systems that are highly asymmetric, the eigenvalues should be approximated by gamma-mixtures instead of single gamma variables. However, this does not affect $\ddot{R}_{\lambda_i}(0)$ because all of the mixing components are governed by the same ACF. Thus, we use the same value of $\ddot{R}_{\lambda_i}(0)$ in the LCR computation for all of the mixing components, and then scale and combine them to obtain the net LCR, as described before. Our simulation results for a (2,8) system are shown in Fig. 3.14 and 3.19. The excellent agreement between our analytical approximations and the simulation results verify that both the first-order and second-order statistics of the MIMO eigenchannels can be well-approximated by gamma processes (for moderate number of antennas) or gamma-mixtures (for highly asymmetrical systems).

3.3.3 LCR for Channel Capacity

The relationship between $\lambda_i(t)$ and $\lambda_i(t+\tau)$ that we have derived above can also be used to calculate the ACF of the capacity process, $R_C(\tau)$, and its curvature at $\tau = 0$, $\ddot{R}_C(0)$.

From the expression for the MIMO channel capacity (2.21) and using (3.14),

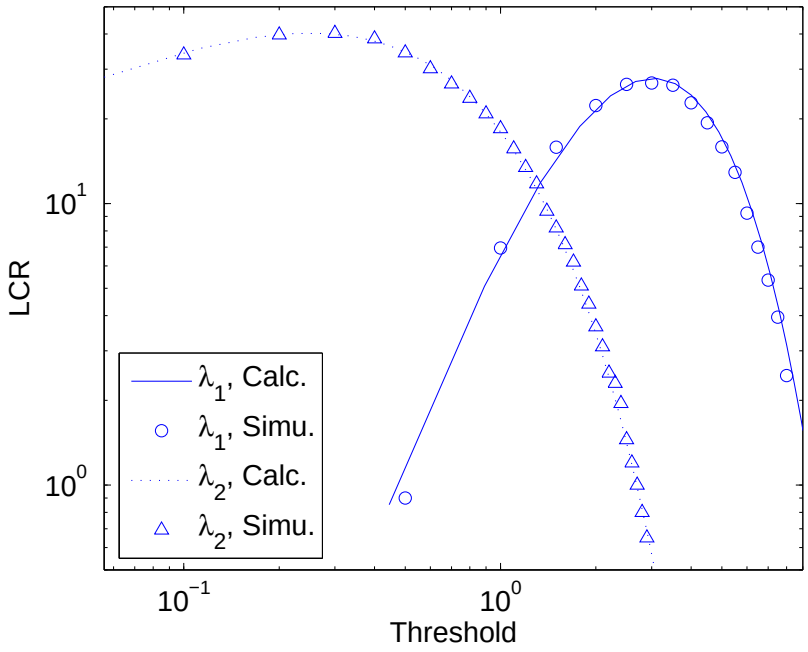

Figure 3.10: A comparison between the calculated and simulated LCR for the eigenvalues in a (2,2) MIMO system, with $f_D\tau = 0.00265$.

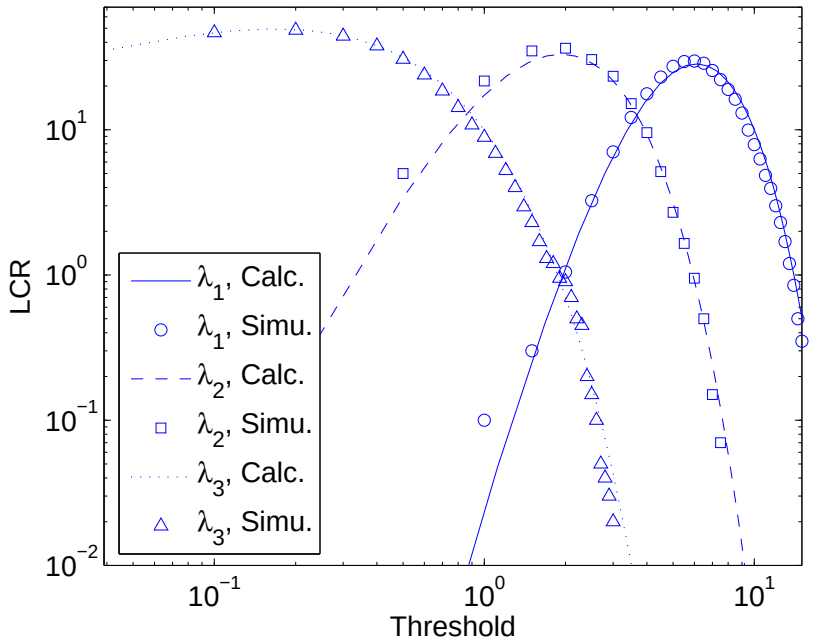

Figure 3.11: A comparison between the calculated and simulated LCR for the eigenvalues in a (3,3) MIMO system, with $f_D\tau = 0.00265$.

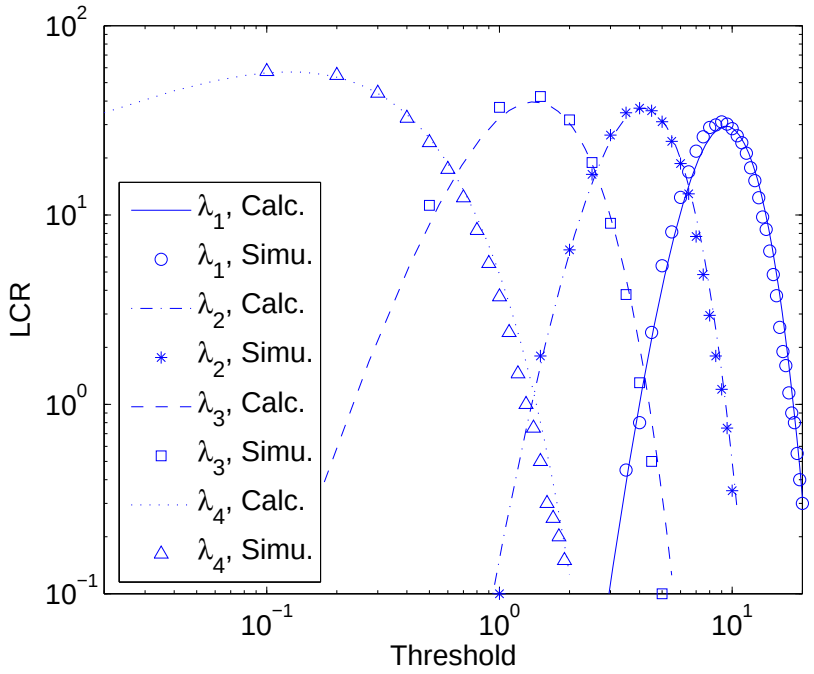

Figure 3.12: A comparison between the calculated and simulated LCR for the eigenvalues in a (4,4) MIMO system, with $f_D\tau = 0.00265$.

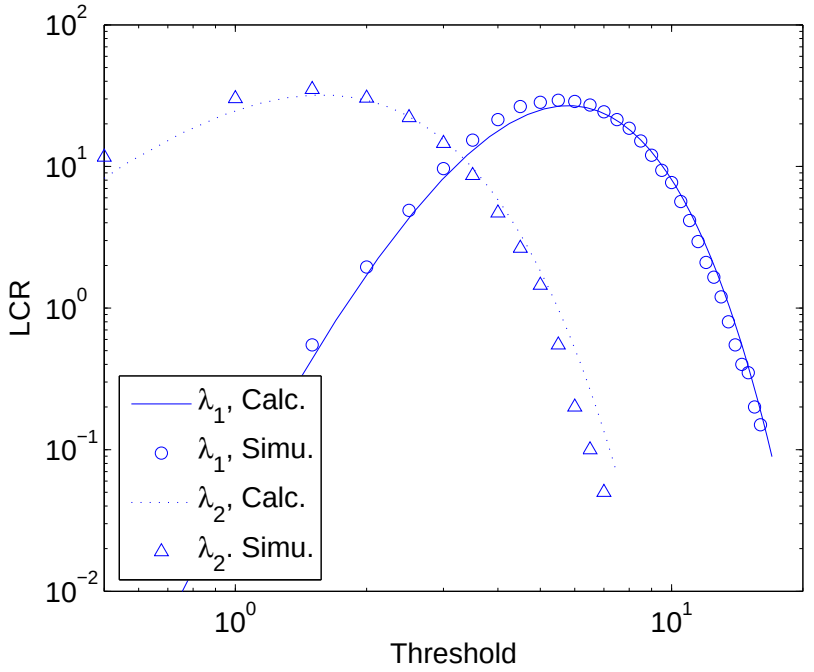

Figure 3.13: A comparison between the calculated and simulated LCR for the eigenvalues in a (2,4) MIMO system, with $f_D\tau = 0.00265$.

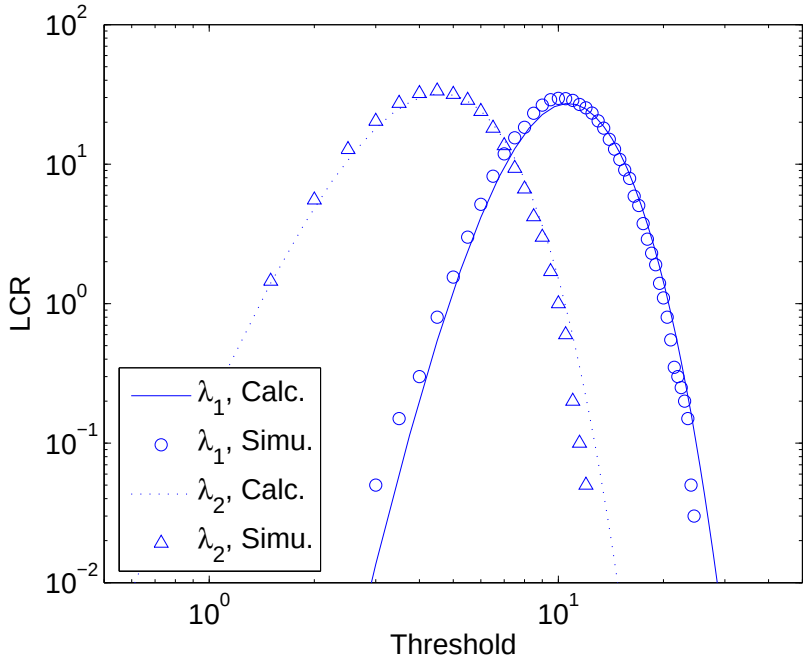

Figure 3.14: A comparison between the calculated and simulated LCR for the eigenvalues in a (2,8) MIMO system, with $f_D\tau = 0.00265$.

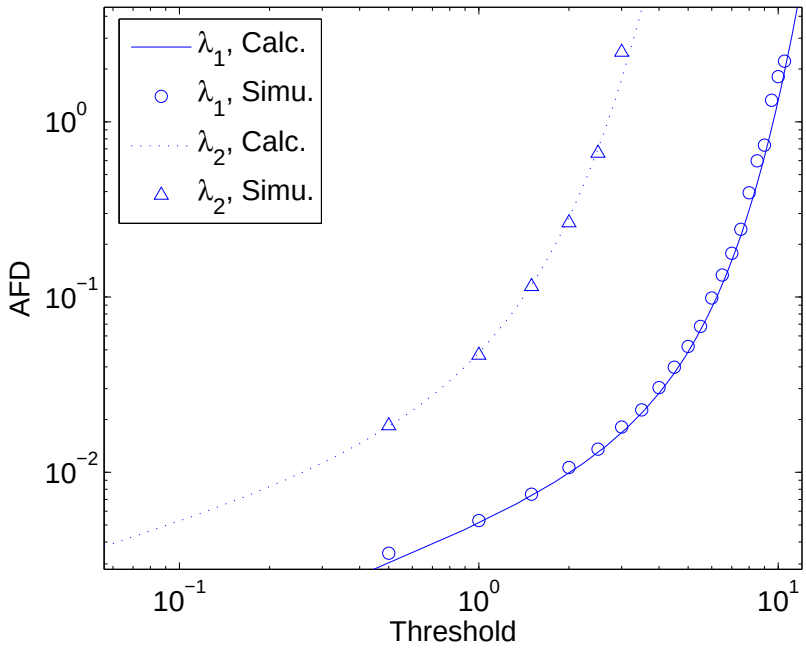

Figure 3.15: A comparison between the calculated and simulated AFD for the eigenvalues in a (2,2) MIMO system, with $f_D\tau = 0.00265$.

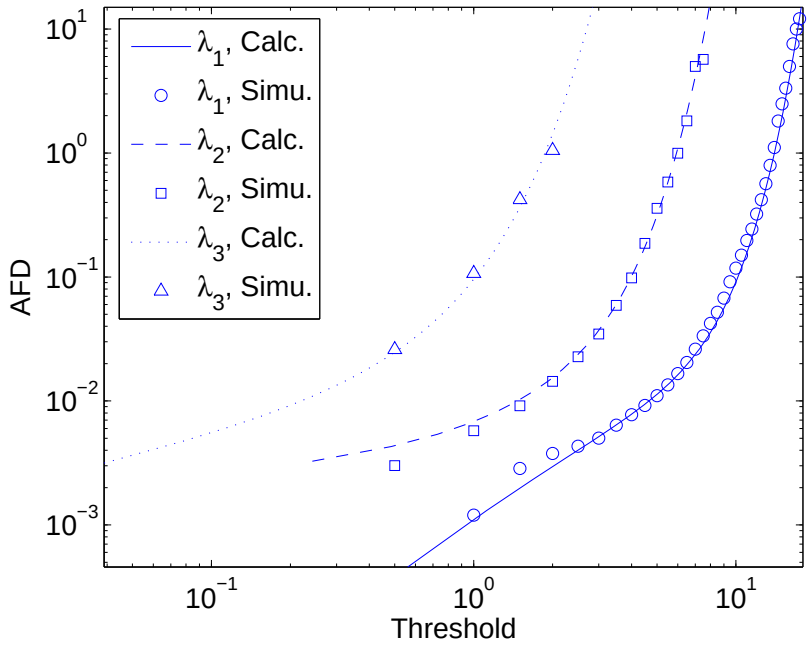

Figure 3.16: A comparison between the calculated and simulated AFD for the eigenvalues in a (3,3) MIMO system, with $f_D\tau = 0.00265$.

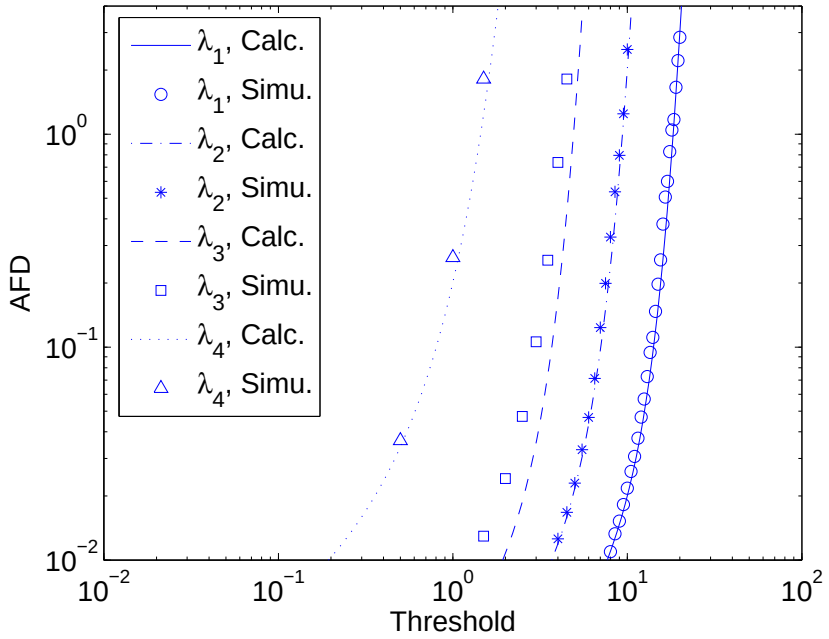

Figure 3.17: A comparison between the calculated and simulated AFD for the eigenvalues in a (4,4) MIMO system, with $f_D\tau = 0.00265$.

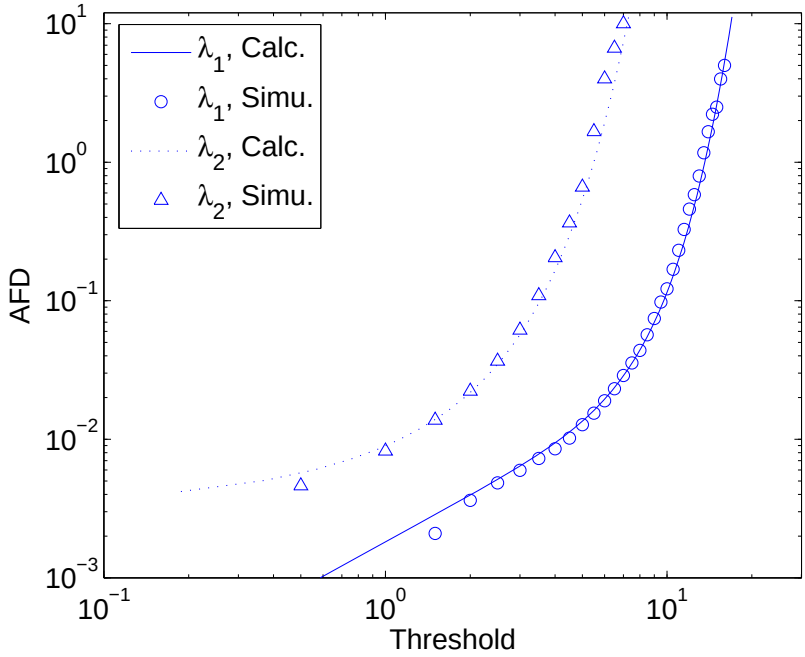

Figure 3.18: A comparison between the calculated and simulated AFD for the eigenvalues in a (2,4) MIMO system, with $f_D\tau = 0.00265$.

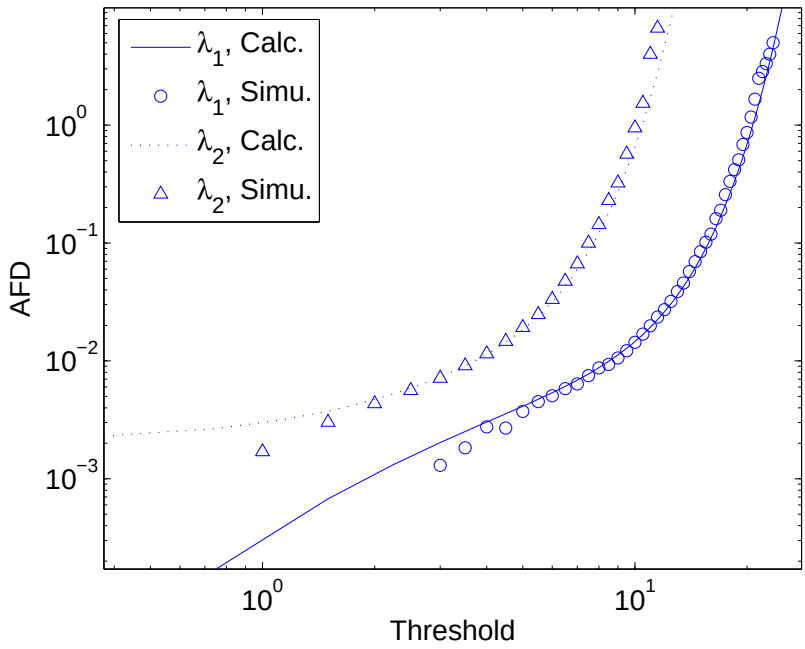

Figure 3.19: A comparison between the calculated and simulated AFD for the eigenvalues in a (2,8) MIMO system, with $f_D\tau = 0.00265$.

the capacity at time $t+\tau$ can be expressed as

$$\begin{aligned} C(t+\tau) &= \sum_{i=1}^{m} \log_2 \left[1 + \frac{\mathcal{P}}{N_t}\lambda_i(t+\tau)\right] \\ &= \sum_{i=1}^{m} \log_2 \left[1 + \frac{\mathcal{P}}{N_t}\lambda_i(t) + \frac{\mathcal{P}}{N_t}\alpha_i\,\tau + \frac{\mathcal{P}}{N_t}\beta_i\,\tau^2 + \frac{\mathcal{P}}{N_t}\,o_i\,\tau^3\right] \\ &= \sum_{i=1}^{m} \left\{ \log_2 \left[1 + \frac{\mathcal{P}}{N_t}\lambda_i(t)\right] + \log_2 \left[1 + \frac{\frac{\mathcal{P}}{N_t}\alpha_i\,\tau + \frac{\mathcal{P}}{N_t}\beta_i\,\tau^2 + \frac{\mathcal{P}}{N_t}\,o_i\,\tau^3}{1 + \frac{\mathcal{P}}{N_t}\lambda_i(t)}\right] \right\}. \end{aligned} \tag{3.20}$$

Since we are only interested in τ^2 terms, we only consider the second term of (3.20). Using the Taylor series expansion about $x = 0$

$$\log_2(1+x) = \frac{1}{\log(2)}\left[x - \frac{x^2}{2} + \frac{x^3}{3} - O(x^4)\right] \tag{3.21}$$

we can re-write the second term of (3.20) and extract the coefficient of the τ^2 term. Note that $O(\cdot)$ is the "big O notation", so that $O(x^4)$ is smaller in magnitude than a constant times $|x|^4$ for small x. We find the second derivative at $\tau = 0$ to be

$$\sum_{i=1}^{m} \frac{1}{\log(2)}\left[\frac{2\,\mathcal{P}\,\beta_i}{N_t + \mathcal{P}\lambda_i(t)} - \frac{\mathcal{P}^2\alpha_i^2}{[N_t + \mathcal{P}\lambda_i(t)]^2}\right].$$

This expression can be used to get $\ddot{R}_C(0)$. We finally have:

$$\begin{aligned} \ddot{R}_C(0) =& \frac{4\,\mathcal{P}\,\pi^2 f_D^2}{\log(2)\,\mathrm{Var}[C]} \\ & \times \sum_{i=1}^{m}\sum_{k=1}^{m} \mathrm{E}\left\{ \log_2\left(1 + \frac{\mathcal{P}\lambda_k}{N_t}\right)\left[\frac{n + \Psi_i - \lambda_i(t)}{N_t + \mathcal{P}\lambda_i(t)} - \frac{\mathcal{P}\lambda_i(t)}{[N_t + \mathcal{P}\lambda_i(t)]^2}\right]\right\}. \end{aligned} \tag{3.22}$$

Again, the remainder terms disappear since they have finite mean.

Direct numerical integration of (3.22) is quite difficult since it involves m variables. However, this complexity can be reduced. Note that the double sum in (3.22) can be written

$$\mathrm{E}\left[\sum_{i=1}^{m}\sum_{k=1}^{m} g(\lambda_k)\,h(\lambda_i)\right] = m\,\mathrm{E}[g(\lambda)\,h(\lambda)] + m(m-1)\,\mathrm{E}[g(\lambda_a)\,h(\lambda_b)]$$

where λ is an arbitrary eigenvalue and (λ_a, λ_b) is an arbitrary pair of distinct eigenvalues. Hence, evaluation of (3.22) can be achieved by only 1-dimensional and 2-dimensional integration using the densities of λ and (λ_a, λ_b) given in [90].

Researchers have shown that the MIMO capacity is approximately Gaussian [74, 90]. In particular, the mean and variance of the MIMO capacity are explicitly given in [57] and [90] respectively. Our level crossing analysis is therefore simplified significantly, since the required first-order statistics are available.

Thus, The LCR for the MIMO channel capacity can then be obtained by substituting (3.22) into (3.7). To verify our analysis, we have simulated (2,2) and (2,4) systems with $\mathcal{P} = 9$ dB. Our results are shown in Figs. 3.20 and 3.21. We observe that increasing the number of antennas on one side decreases the LCR, which matches the conclusions of [86]. Note that the agreement between theory and simulation deteriorates at lower threshold levels. This is caused by the non-ideality of the Gaussian approximation. As shown in [90], the Gaussian approximation for the MIMO capacity is worse for a small number of antennas.

3.3.4 LCR for Condition Numbers

Note that by construction, both κ and κ_D (defined in Section 2.4.4) are long-tailed variables due to the division by λ_m. Since we are unaware of any results on LCRs for long-tailed processes, we have considered simple transformations to pull in the tails. In particular, we have found that $\log(\kappa)$ and $\log(\kappa_D)$ (denoted by K and K_D) can be well approximated by gamma variables (see Figs. 3.22 and 3.23). Hence, we concentrate on the log condition numbers instead of looking at κ and κ_D directly. Additionally, taking the logarithm matches the work in [100] where the eigenvalue spreads are measured on a decibel scale. The accuracy of a gamma approximation for the distributions of K and K_D can be seen in Figs. 3.22 and 3.23 respectively.

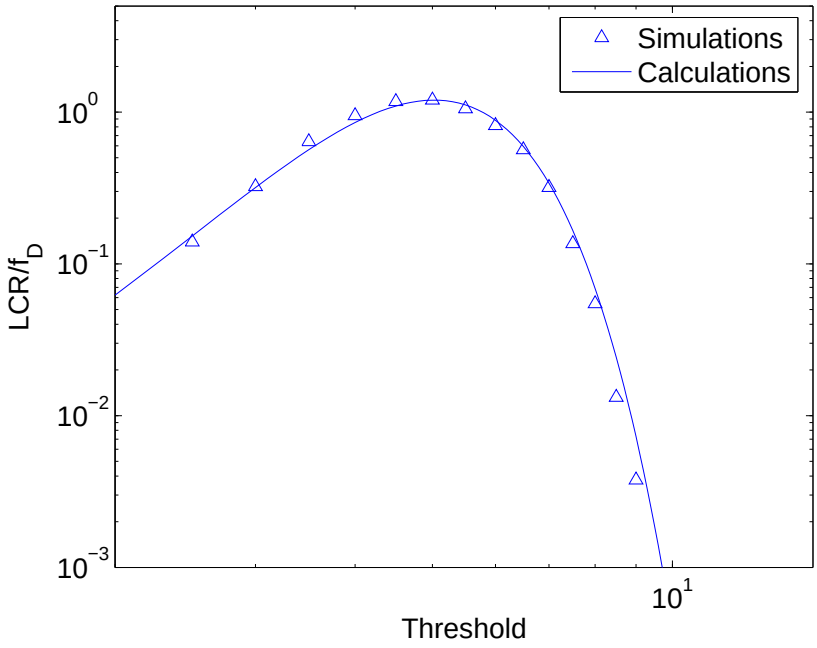

Figure 3.20: A comparison between the calculated and simulated LCR for the capacity in a (2,2) MIMO system, with $f_D\tau = 0.00265$.

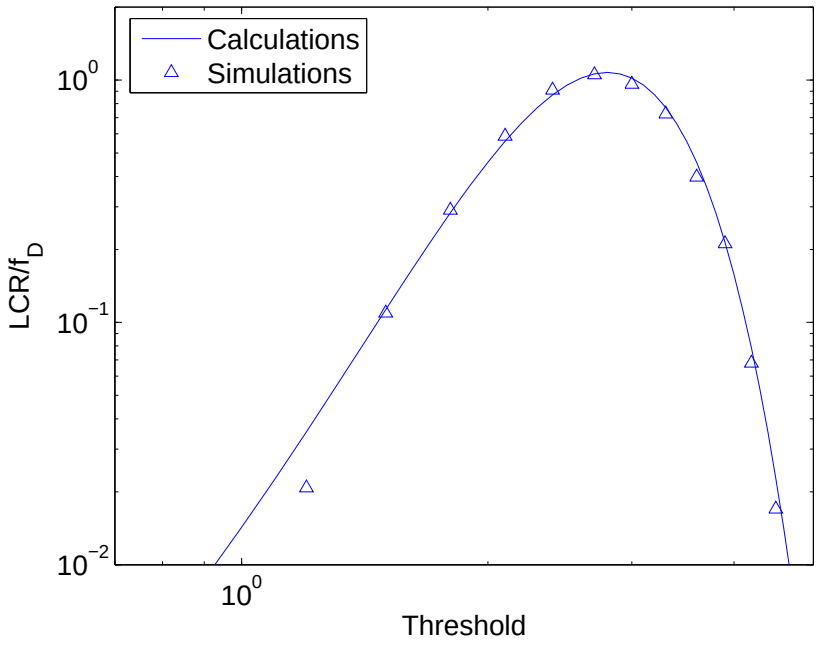

Figure 3.21: A comparison between the calculated and simulated LCR for the capacity in a (2,4) MIMO system, with $f_D\tau = 0.00265$.

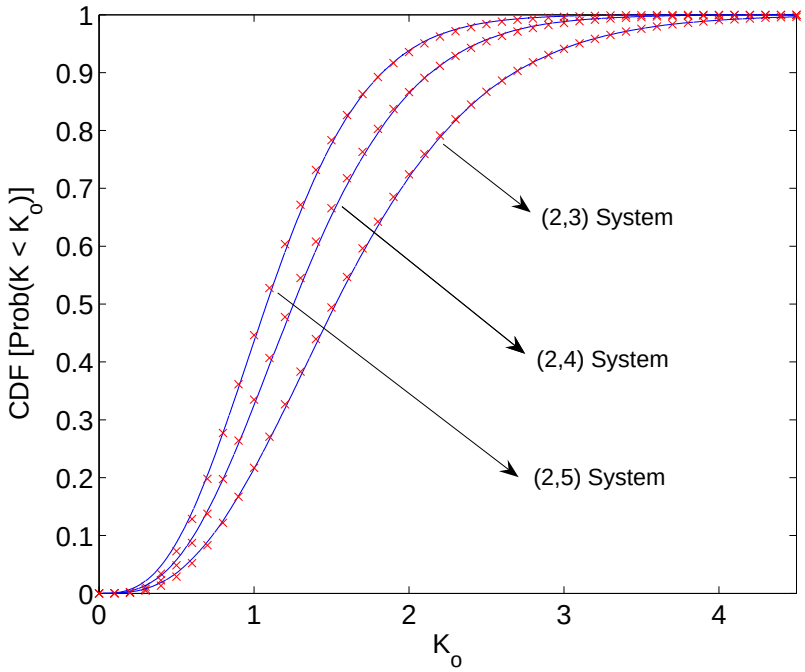

Figure 3.22: A comparison of the exact CDF of K (line) with the gamma approximation (points) for three different cases.

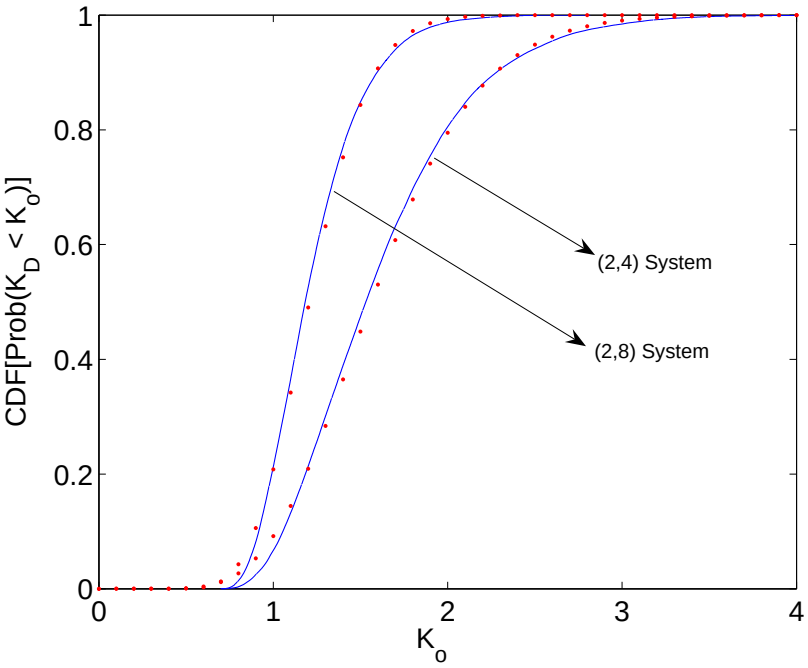

Figure 3.23: A comparison of the exact CDF of K_D (line) with the gamma approximation (points) for two different cases.

Additionally, note that care must be taken when computing the LCRs for the condition numbers. For example, in [101, 102] researchers have shown that

$$\mathrm{E}\left[\frac{1}{\lambda_m}\right] = \frac{1}{N_r - N_t} \tag{3.23}$$

which implies that the mean of the inverse minimum eigenvalue is infinite if the MIMO system is symmetric. As a result, for this case the mean condition number does not exist and the LCR has no meaning. Due to this reason, our scope is focused on the asymmetric system case.

As mentioned before, a direct level crossing analysis for κ and κ_D is not easy due to their long-tailed distributions. Nevertheless, the gamma-like distributions for K and K_D provide an alternative route for our analysis. Note that the expectation and variance of K can be written

$$\begin{aligned}\mathrm{E}[K] &= \mathrm{E}\left[\log\left(\frac{\lambda_1}{\lambda_m}\right)\right] \\ \mathrm{Var}[K] &= \mathrm{Var}\left[\log\left(\frac{\lambda_1}{\lambda_m}\right)\right].\end{aligned}$$

The mean and variance for K require 2-dimensional integration using the joint PDF of (λ_1, λ_m). This joint PDF can be obtained via symbolic integration of (2.15) or by using the results in [58]. Analogous relationships hold for K_D.

By using techniques similar to those for the other metrics, the curvature can be obtained from $\mathrm{E}[K(t)\,K(t+\tau)]$ as follows. The curvature derivations for the regular condition number and the Demmel condition number are very similar, so here we only show the calculation for the regular condition number. It is required to calculate

$$\mathrm{E}\left\{\log\left(\frac{\lambda_1(t)}{\lambda_m(t)}\right)\,\log\left(\frac{\lambda_1(t+\tau)}{\lambda_m(t+\tau)}\right)\right\}. \tag{3.24}$$

For the sake of convenience, we denote $\lambda_i = \lambda_i(t)$ for $i = 1, 2, \ldots, m$ in the rest of the analysis. To compute (3.24) it is convenient to construct the

following expansion:

$$\log\left[\frac{\lambda_1(t+\tau)}{\lambda_m(t+\tau)}\right] = \log\left[\frac{\lambda_1+\Delta\lambda_1}{\lambda_m+\Delta\lambda_m}\right] = \log\left[\frac{\lambda_1+\Delta\lambda_1}{\lambda_m}\left(1-\tfrac{\Delta\lambda_m}{\lambda_m}+\tfrac{\Delta\lambda_m^2}{\lambda_m^2}+\mathcal{D}_1\,\tau^3\right)\right] \tag{3.25}$$

where $\Delta\lambda_i = \lambda_i(t+\tau)-\lambda_i(t)$, $\mathcal{D}_1$ is a remainder term and we have applied the Taylor series expansion about $x=0$

$$\frac{1}{1+x} = 1 - x + x^2 - O(x^3)\,.$$

Using $\Delta\lambda_i = \alpha_i\,\tau+\beta_i\,\tau^2+o_i\,\tau^3$ from (3.15), equation (3.25) can be approximated by

$$\log\left(\frac{\lambda_1}{\lambda_m}\left[1+\frac{\alpha_1\tau^2+\beta_1\tau}{\lambda_1}-\frac{\lambda_1(\alpha_m\tau^2+\beta_m\tau)}{\lambda_m}+\frac{\beta_m^2\tau^2}{\lambda_m^2}-\frac{\beta_1\beta_m\tau^2}{\lambda_1\lambda_m}\right]+\mathcal{D}_2\,\tau^3\right). \tag{3.26}$$

With further expansions and re-arrangements, we finally come to the result:

$$\begin{aligned}&\mathrm{E}\left\{\log\left(\frac{\lambda_1(t)}{\lambda_m(t)}\right)\log\left(\frac{\lambda_1(t+\tau)}{\lambda_m(t+\tau)}\right)\right\}\\ =\;&\mathrm{E}\left\{\left[\log\left(\frac{\lambda_1}{\lambda_m}\right)\right]^2+\log\left(\frac{\lambda_1}{\lambda_m}\right)\left(\frac{\beta_1}{\lambda_1}-\frac{\beta_m}{\lambda_m}\right)\tau\right.\\ &\left.+\log\left(\frac{\lambda_1}{\lambda_m}\right)\left(\frac{\alpha_1}{\lambda_1}-\frac{\alpha_m}{\lambda_m}-\frac{\beta_1^2}{2\lambda_1^2}+\frac{\beta_m^2}{2\lambda_m^2}\right)\tau^2+\mathcal{D}_3\,\tau^3\right\}\end{aligned} \tag{3.27}$$

where $\mathcal{D}_2$ and $\mathcal{D}_3$ are remainder terms. Since only the coefficient of τ^2 term is of interest, we can write the curvature as:

$$\begin{aligned}\ddot{R}_K(0) = \frac{4\,\pi^2 f_D^2}{\mathrm{Var}[K]}\,&\mathrm{E}\left\{\log\left(\frac{\lambda_1(t)}{\lambda_m(t)}\right)\right.\\ &\left.\times\left[(n-1)\left(\frac{1}{\lambda_1(t)}-\frac{1}{\lambda_m(t)}\right)+\left(\frac{\Psi_1}{\lambda_1(t)}-\frac{\Psi_m}{\lambda_m(t)}\right)\right]\right\}.\end{aligned} \tag{3.28}$$

The curvature $\ddot{R}_{\log(\kappa_D)}(0)$ of (3.29) can be found in a similar way, which results in:

$$\begin{aligned}\ddot{R}_{K_D}(0) = \frac{4\,\pi^2 f_D^2}{\mathrm{Var}[K_D]}\,&\mathrm{E}\left\{\log\left(\frac{\sum_{i=1}^m\lambda_i(t)}{\lambda_m(t)}\right)\right.\\ &\left.\times\left[\frac{\sum_{i=1}^m[n+\Psi_i-\lambda_i(t)]-1}{\sum_{i=1}^m\lambda_i(t)}-\frac{n+\Psi_m-\lambda_m(t)+1}{\lambda_m(t)}\right]\right\}.\end{aligned} \tag{3.29}$$

The evaluation of both (3.28) and (3.29) are challenging, and at present the calculation must be performed by multi-dimensional integration over all eigenvalues.

Finally, we can substitute (3.28) and (3.29) into (3.3) and work out the LCRs for K and K_D respectively. The LCRs for both the regular condition number and the Demmel condition number are plotted in Figs. 3.24, 3.25 and 3.26. Comparing the analysis with the simulations, we can see that both formulas are accurate approximations.

It is well known that Rayleigh i.i.d. propagation environments are in general more suitable for spatial multiplexing than Ricean or spatially correlated channels due to a lower eigenvalue spread. However, our results have shown that fluctuations of the eigenvalue spread can be quite severe even in the Rayleigh i.i.d. case. For adaptive systems that exploit condition numbers as the switching criteria [79], a suitable feedback/adaptation rate can be gauged by using the LCR results presented here.

3.4 Alternative LCR for Eigenmodes

An analytical method for calculating the level crossing rate (LCR) of the MIMO eigenmodes has been reported in Section 3.3.2. However, the formula requires the calculation of the curvature of the eigenvalue autocorrelation function (ACF) at $\tau = 0$, which is (3.19). This calculation is awkward, especially when dealing with larger MIMO systems. Thus, here we develop an alternative LCR formula which dispenses with the complicated ACF curvature calculation. This new formula is the based on the LCR of the channel singular values.

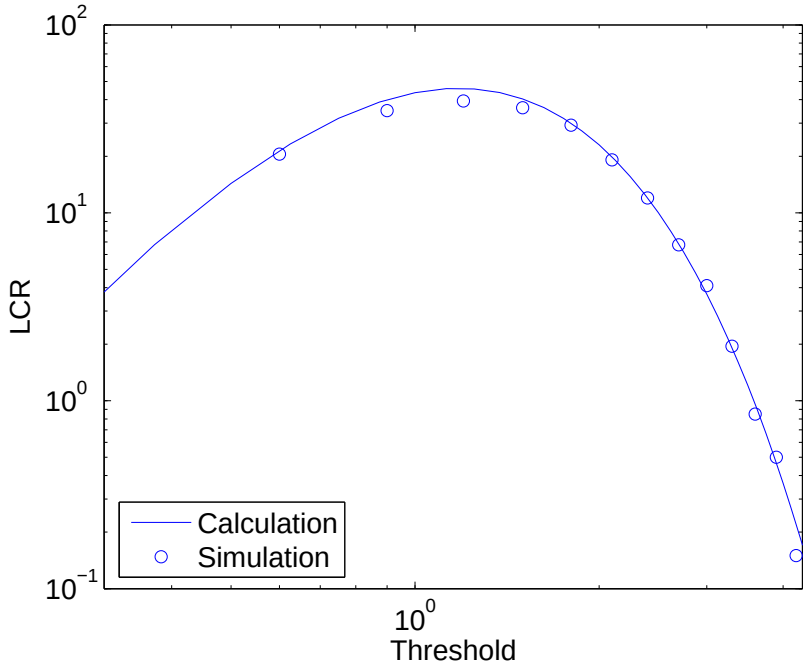

Figure 3.24: A comparison between the calculated and simulated LCR for K in a (2,4) MIMO system, with $f_D\tau = 0.00265$.

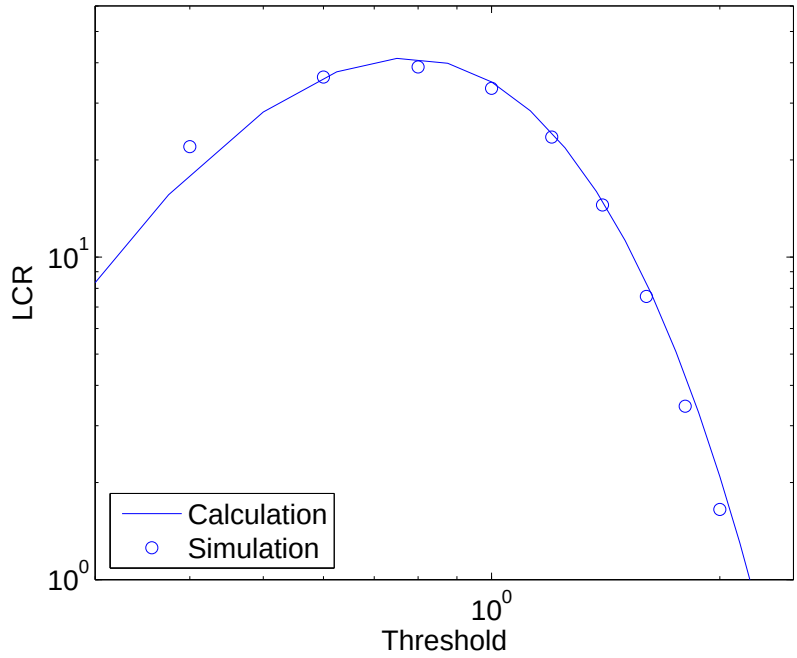

Figure 3.25: A comparison between the calculated and simulated LCR for K in a (2,8) MIMO system, with $f_D\tau = 0.00265$.

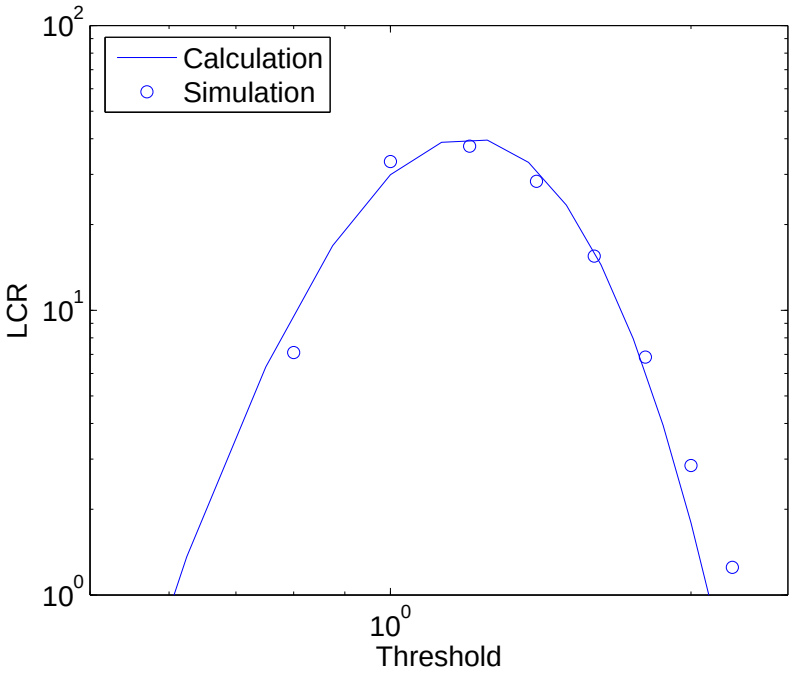

Figure 3.26: A comparison between the calculated and simulated LCR for K_D in a (2,8) MIMO system, with $f_D\tau = 0.00265$.

3.4.1 Derivation

In Section 3.1, we have identified that MIMO eigenvalues are accurately approximated by gamma processes. It is known that a range of power transforms including the square root of a gamma variable may also be approximately gamma [103]. This motivates a gamma approximation to the channel singular values, $s_1 > s_2 > \ldots > s_m$, where $s_i = \sqrt{\lambda_i}$. By fitting the first two moments and modeling s_i as a gamma variable, we can compare the exact distribution function of s_i with the corresponding gamma approximation. Excellent agreements have been observed, as shown by the example in Fig. 3.27. Recall that the gamma approximation is characterized by its shape parameter $r = \mathrm{E}(s)^2/\mathrm{Var}(s)$ and scale factor $\theta = \mathrm{E}(s)/\mathrm{Var}(s)$. To compute the distribution function and moments of the singular values we can work either with the eigenvalues or the singular values since $\mathrm{E}(s_i^q) = \mathrm{E}(\lambda_i^{q/2})$ and

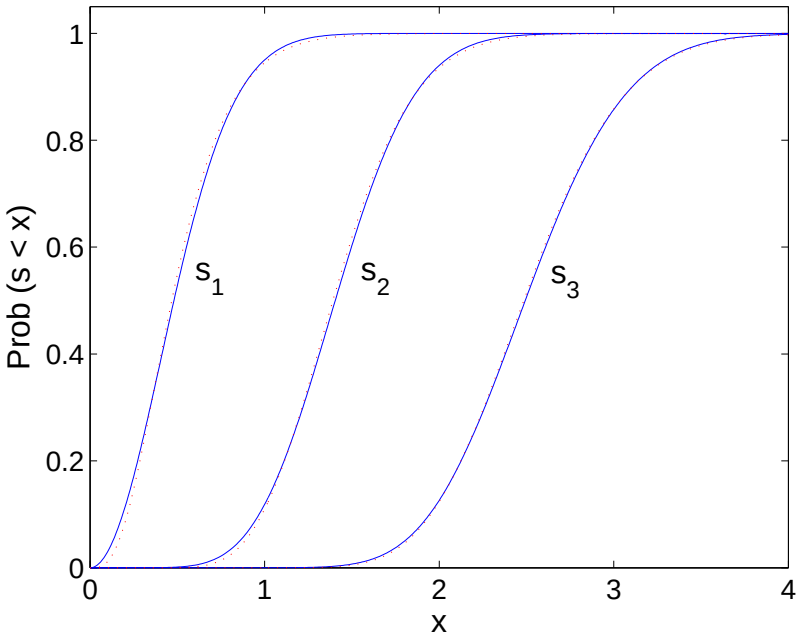

Figure 3.27: A comparison between the analytical distribution (line) of the singular values of a (3,3) MIMO channel matrix with the corresponding gamma approximation (dots).

$\text{Prob}(s_i \leq x) = \text{Prob}(\lambda_i \leq x^2)$. Closed form results for the eigenvalues are reported in [58]. Alternatively the well-known joint PDF for $\lambda_1 > \lambda_2 > \ldots > \lambda_m$ [57] can be transformed into the PDF for $s_1 > s_2 > \ldots > s_m$ as below:

$$f(s_1, \ldots, s_m) = \frac{2^m \exp\left(-\sum_{i=1}^{m} s_i^2\right) \prod_{i=1}^{m} s_i^{2l+1} \prod_{i<j} (s_i^2 - s_j^2)^2}{\prod_{i=1}^{m} [(n-i)!(m-i)!]}, \qquad (3.30)$$

where $l = n - m$. Due to the simple form of (3.30), involving only odd powers of s_i and exponentials, serial integration can be performed with an algebraic software package to obtain the desired results in closed form. This approach was used here.

As the singular values are approximately gamma, we can therefore approximate the LCR of the singular values by a direct application of (3.3) with r, θ derived as above and only $\ddot{R}(0)$ required.

To find the ACF, $R(\tau)$, we exploit a certain stochastic differential equation (SDE) that has been derived in [104]. This SDE is for the case where the

matrix entries are complex Brownian processes:

$$dz_i(t) = d\widetilde{B}_i(t) + \left[\frac{2l+1}{2z_i(t)} + \sum_{i\neq j}\left(\frac{1}{z_i(t)-z_j(t)} + \frac{1}{z_i(t)+z_j(t)}\right)\right]dt, \quad (3.31)$$

where $z_i(t)$ is the i^{th} singular value process of a Brownian diffusion and $d\widetilde{B}_i(t)$ is a real zero-mean Gaussian variable with variance dt, independent of the singular values. As aforementioned, a complex Brownian process is tantamount to the zero-mean complex Gaussian process with variance $2t$, so the SDE does not fit our case as the variance of the wireless channel entry does not increase with elapsed time. However, as argued previously, we can modify (3.31) to accommodate our case of interest.

Following the same arguments as in Section 3.3.1, we replace all $z_i(t)$ in (3.31) by $\sqrt{2t}\, s_i(t)$ (since $s_i = \sqrt{\lambda_i}$). Then, with Euler's approximation and a little algebra, we have the expression:

$$s_i(t+\tau) = \sqrt{\frac{t}{t+\tau}}s_i(t) + \sqrt{\frac{\tau}{t+\tau}}Z_i + \frac{\tau}{\sqrt{t(t+\tau)}}\left(\frac{2l+1}{4s_i} + \frac{\psi_i}{2}\right), \quad (3.32)$$

where

$$\psi_i(t) = \sum_{i\neq j}\left(\frac{1}{s_i(t)-s_j(t)} + \frac{1}{s_i(t)+s_j(t)}\right).$$

Recall that $Z_i \sim \mathcal{N}(0,1)$. In order to match the auto-covariance of the complex Brownian diffusion with the MIMO channel entries, we must look at a particular time point. By setting $t = \tau\left[\rho(\tau)^{-2} - 1\right]^{-1}$ as before, we can re-arrange (3.32) to obtain

$$R(\tau) \approx \frac{1}{\mathrm{Var}(s_i)}\left[\mathrm{E}(\lambda_i) - \mathrm{E}(s_i)^2 + \sqrt{2\xi}\,\mathrm{E}[s_i\, Z_i]\,\tau + \xi\,\mathrm{E}\left(l + \frac{1}{2} + \psi_i s_i - \lambda_i\right)\tau^2\right], \quad (3.33)$$

where ξ depends on the ACF of the underlying Gaussians in the MIMO channel entries. Specifically, ξ is given by

$$\xi = \frac{-1}{2}\,\ddot{\rho}(0). \quad (3.34)$$

Scenarios	ξ
Jakes fading	$\pi^2 f_D^2$
Laplacian PAS	$\frac{\pi^2 f_D^2}{1+1/\vartheta^2}$
Mobile-to-mobile	$\pi^2(f_{D_1}^2 + f_{D_2}^2)$

Table 3.6: Expressions for ξ with different ACFs.

Expressions of ξ for the ACFs we have considered are tabulated in Table 3.6. To compute $\ddot{R}(0)$, note that its value is simply double the τ^2 coefficient in $R(\tau)$. Hence,

$$\ddot{R}(0) = \frac{\xi}{\mathrm{Var}(s_i)} \mathrm{E}\left[\,2\,(l + \psi_i\, s_i - \lambda_i) + 1\,\right]. \tag{3.35}$$

At first glance, the computation of the expectation term in (3.35) appears to be difficult. However, we now show that such a computation is not required. After some algebra, we find that

$$\psi_i\, s_i - \lambda_i = \sum_{i \neq j} \frac{\lambda_i + \lambda_j}{\lambda_i - \lambda_j} + (m-1) - \lambda_i. \tag{3.36}$$

Then, according to (3.15), we know the following statement is true:

$$\lambda_i(t+\tau) \approx \lambda_i(t) + \alpha_i \sqrt{\lambda_i(t)}\, Z_i\, \tau + \beta_i \left(n + \sum_{i \neq j} \frac{\lambda_i + \lambda_j}{\lambda_i - \lambda_j} - \lambda_i \right) \tau^2, \tag{3.37}$$

where α_i and β_i are both constants which depend on the ACF of the channel matrix entries[1] . As the eigenvalue $\lambda_i(t)$ is a stationary process, the means of $\lambda_i(t+\tau)$ and $\lambda_i(t)$ are the same. Thus, if we take the expectation of both sides

[1]The expressions for α_i and β_i are dependent on $\rho(\tau)$. The pair given in (3.15) are only valid for the channel with a Jakes fading process.

of (3.37), it is clear that

$$\mathrm{E}\Big(\sum_{i\neq j}\frac{\lambda_i+\lambda_j}{\lambda_i-\lambda_j}-\lambda_i\Big)=-n. \tag{3.38}$$

By comparing (3.38) with (3.36), we see that

$$\mathrm{E}(\psi_i\, s_i-\lambda_i)=m-n-1=-l-1. \tag{3.39}$$

Hence, (3.35) can be simplified significantly to become

$$\ddot{R}(0)=-\frac{\xi}{\mathrm{Var}(s_i)} \tag{3.40}$$

as the term $\mathrm{E}\left[\,2\,(l+\psi_i\, s_i-\lambda_i)+1\,\right]$ in (3.35) is always -1 for all cases.

Hence, $\ddot{R}(0)$ is simply a constant whose value is solely dependent on ξ (which is governed by the ACF of the underlying Gaussian $\rho(\tau)$) and the variance of s_i. The closed form expression for the LCR of s_i can be obtained by substituting $\ddot{R}(0)$ into (3.3). Moreover, it can easily be extended to obtain the LCR for the eigenvalues λ_i, since $\lambda_i=s_i^2$ and we have $\mathrm{LCR}_{\lambda_i}(T)=\mathrm{LCR}_{s_i}(\sqrt{T})$. Hence

$$\mathrm{LCR}_{\lambda_i}(T)=\sqrt{\frac{|\xi|}{2\pi r}}\,\frac{\theta}{\Gamma(r)}\big(\theta\sqrt{T}\big)^{r-0.5}\exp\big(-\theta\sqrt{T}\big). \tag{3.41}$$

In (3.41) the first two moments of s_i (needed for ξ, r and θ) are the only parameters that are needed to calculate the LCR for λ_i. This has significantly reduced the computational complexity relative to previous results.

3.4.2 Simulation Results

In order to verify our analysis, a number of simulations have been performed. We compare the LCR calculated using our formula with the simulations. A sample size of 2×10^6 and a time displacement $\tau=0.1$ms are used in all simulations. Also, a system carrier frequency of 5.725GHz (HyperLan 2 standard) is chosen. For the Jakes fading case, we assume the mobile terminal is moving at a speed of 5 km/hr, which results in $f_D=26.5$Hz. For the MM

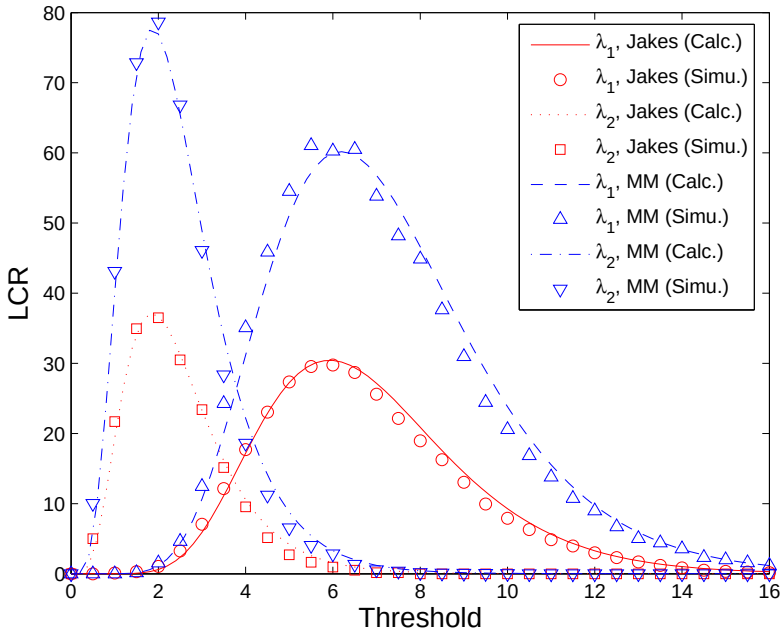

Figure 3.28: A comparison between the calculated and simulated LCR for λ_1 and λ_2 in a (3,3) MIMO system in both MM and Jakes fading scenarios.

case, we assume that the speeds of terminal 1 and terminal 2 are 3km/hr and 10km/hr respectively, giving Doppler frequencies of $f_{D_1} = 15.9$Hz and $f_{D_2} = 53$Hz. Some selected results are plotted in Fig. 3.28 and 3.29. In all cases, mobile-to-mobile channel experiences higher variation as both terminals are in motion. For channels with Laplacian PAS, on the other hand, LCR decreases with angular spread ϑ. All of the figures illustrate the accuracy of our simple formulas.

3.5 Summary

In this chapter, we have investigated the level-crossing statistics of MIMO eigenmodes and their associated channel metrics in i.i.d. Rayleigh fading channels.

As the total power gain (or the sum of eigenvalues) is exactly chi-square

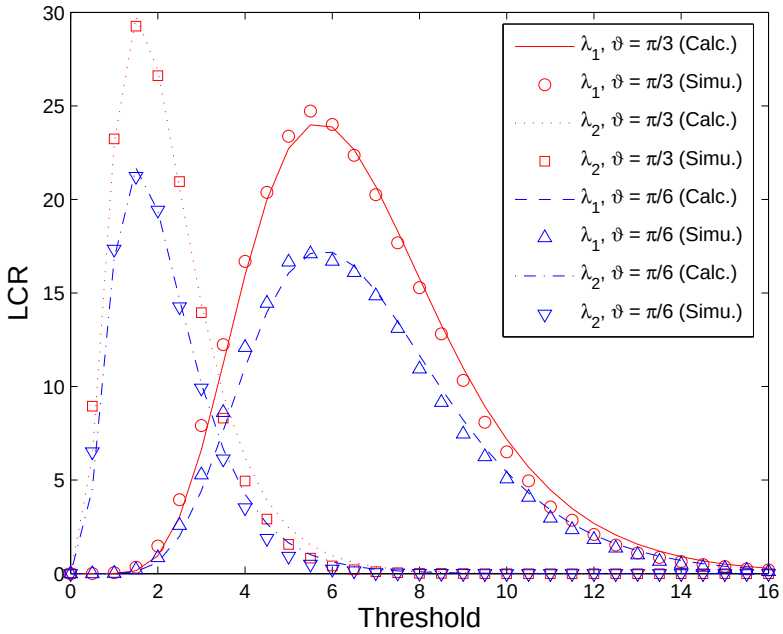

Figure 3.29: A comparison between the calculated and simulated LCR for λ_1 and λ_2 in a (2,4) MIMO systems assuming Laplacian PAS with different angular spreads.

distributed, its LCR merely requires the ACF curvature of the underlying Gaussian. The LCR for the total power gain was derived expediently for three types of ACF mentioned in Chapter 2.

The level crossing analysis for the eigenmodes and other metrics, on the other hand, exploited the fact that the distributions of the eigenvalues and the logarithms of the condition numbers can be well approximated by gamma variables, and the MIMO channel capacity can be approximated by a Gaussian variable. Since LCR formulas for both gamma and Gaussian variables are available in the literature, we have calculated the required curvature of the ACFs for the eigenvalue-dependent metrics. A SDE has been employed to model the changes in the eigenvalue processes over time, hence obtaining a general relationship between $\lambda_i(t)$ and $\lambda_i(t+\tau)$. This serves as a unified starting point for our ACF curvature derivations for the various channel metrics. Although this part of the analysis was carried out under the assumption of

Jakes fading, our analytical method can be easily extended to an arbitrary ACF.

An alternative analytical formula for the LCR of the MIMO eigenmode gains is also given. The computation of the LCR is much less complex than that required in previous work, since the requirement of the ACF curvature calculation is reduced to computing the first two moments of the corresponding singular value. These moments can be obtained conveniently using the joint densities of either the singular values or the eigenvalues. We have applied this technique to three different propagation scenarios.

Through the simulations results, we have verified that all our methods provide very accurate approximations for the LCRs and AFD of the MIMO eigenmodes and other channel metrics. Our approximations can be used to predict the time-varying characteristics of MIMO systems and their associated channel metrics, so that an appropriate feedback/adaptation rate can be chosen in a more judicious manner.

Chapter 4

FSMC with Applications in Adaptive MIMO Schemes

Markov chain modeling is a commonly used approach to study the behavior of random processes. In such a model, the process is partitioned into multiple discrete states, and the dynamic behavior is captured by the transitions among the states. Figure 4.1 shows an illustrative example of a three-state Markov model, where the labels on the arrows between states indicate the transition probabilities.

In contrast to physical models for mobile channels, a finite state Markov chain (FSMC) is relatively simple, and has been widely adopted in the category of SISO channel modeling [105, 106]. Nonetheless, only a handful of papers have attempted to model the behavior of MIMO channels by a FSMC [107]. Along with their simplicity, FSMCs are advantageous for evaluating the performance of practical adaptive communication systems, where there maybe a list of finite options for transmission strategies or parameters at the physical layer (such as data rates and modulation formats). In such systems, the selection from the list of options is made accordance with the current status of the system. For such adaptive systems the discrete state nature of a FSMC is applicable. In addition, FSMC-based channel models can be used in designs of feedback schemes for adaptive modulation systems [108].

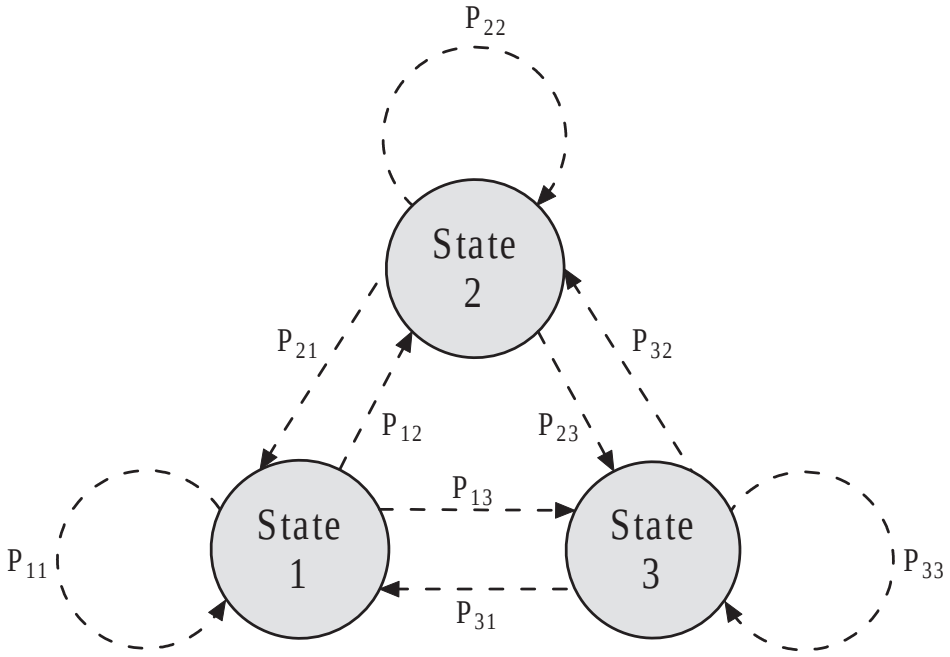

Figure 4.1: An illustration of a simple, first-order Markov model with three states, where P_{ij} denotes the transition probability from state i to j.

In this chapter, only first-order Markov modeling is invoked to study the temporal behavior of MIMO systems due to its simplicity. That is, we assume that the current state is entirely determined by the state at the very last step. This is usually an approximation since the wireless channel is a continuous process with a certain ACF that may not precisely result from a Markov structure. However, our results show that first-order models are sufficient to provide good approximations to the transition probabilities of the MIMO channel metrics considered in this chapter. The scope of the chapter is focussed on three aspects: MIMO channel capacity, condition number, and joint eigenvalue behavior. In all cases the FSMC is applied to explore the practical issues in proposed adaptive MIMO schemes with feedback delay. To be specific, FSMC can be employed to measure how likely it is that the choice made at the receiver of an adaptive system becomes inappropriate during the

feedback interval. As a tool for analysis, the the joint density for the eigenvalues of two complex Wishart matrices is also derived at the beginning of this chapter. This density is employed to characterize the correlations between MIMO channels at two successive time points in this thesis, but its possible applications in other scenarios are also outlined. Additionally, LCR results obtained in the preceding chapter can also be employed to approximate the transition probabilities of the FSMC with slow-varying channels.

4.1 Joint Density for the Eigenvalues of Two Correlated Complex Wishart Matrices

The theory of random matrices has been widely applied in many different areas in science and engineering. As mentioned in the previous chapters, a key application in wireless communications is the area of MIMO systems. As discussed in the preceding chapters, the eigenvalues of a complex Wishart matrix (channel correlation matrix) play a very important role in this field, since these eigenvalues are the power gains of the virtual parallel links (eigenmodes) intrinsic to the baseline MIMO channel with i.i.d. Rayleigh fading. The goal of this section is to derive the joint density for the eigenvalues of two correlated complex Wishart matrices. The potential applications in MIMO systems are also reviewed.

4.1.1 Applications in MIMO Systems

In the context of MIMO system analysis, the channel is usually written as a $N_r \times N_t$ matrix. In order to model the channel variation, the channel matrix is often perturbed by the addition of some other complex Gaussian matrix, mathematically expressed as

$$\widehat{\boldsymbol{H}} = \Upsilon \boldsymbol{H} + \Omega \boldsymbol{\Xi} \tag{4.1}$$

where $\widehat{\boldsymbol{H}}$, $\boldsymbol{H}$ and $\boldsymbol{\Xi}$ are all matrices of the same dimensions $(N_r \times N_t)$ with i.i.d. complex zero-mean Gaussian entries. We also assume that the entries of both $\boldsymbol{H}$ and $\boldsymbol{\Xi}$ have unit variances so that the entries are $\mathcal{CN}(0,1)$. The real constants Υ and Ω determine the variance of $\widehat{\boldsymbol{H}}$.[1] As discussed before, there are m non-zero eigenvalues in each of the Wishart matrices $\boldsymbol{H}\boldsymbol{H}^\dagger$ and $\widehat{\boldsymbol{H}}\widehat{\boldsymbol{H}}^\dagger$. The main interest of this section lies in the joint density function of these $2m$ non-zero eigenvalues.

Some cases where the perturbation in (4.1) is encountered in the field of MIMO research are enumerated below:

- *Additive channel estimation error:* A very common model for channel estimation error is expressed as the additive noise [110]:

$$\widehat{\boldsymbol{H}} = \boldsymbol{H} + \sqrt{\delta^2}\boldsymbol{\Xi} \tag{4.2}$$

  where δ^2 is the variance of the additive error matrix. The exact value of δ^2 depends on the estimation method used. For example, if maximum-likelihood channel estimation is used, we have [110]:

$$\delta^2 = \frac{N_t}{\mathcal{P}\, L_{ts}}$$

  where L_{ts} is the length of training sequence. The authors in [111] have also derived another expression for δ^2 with the Doppler frequency taken into account.

- *Imperfectly estimated and outdated CSI:* In a realistic system model with channel state information (CSI), imperfect CSI is fed back to the transmitter. Hence, the CSI is imperfectly estimated as (4.2) at the receiver, and is also outdated when it is used at the transmitter due to feedback

[1] Here we restrict Υ and Ω to be real valued to keep the notation simple. However, to accommodate complex correlation coefficients that arise, for example, in OFDM, we can allow Υ and Ω to be complex valued, replacing ρ in (4.3) by $|\rho|$ without any effect on the resulting analysis (as shown in [109]).

delay. As shown in [112] and [113], the estimated/outdated channel (estimated at $t-\tau$) in such a scenario can be written as

$$\widehat{\boldsymbol{H}}_{t-\tau} = \rho\,\boldsymbol{H}_t + \sqrt{\delta_e^2}\,\boldsymbol{\Xi} \tag{4.3}$$

where ρ is the correlation coefficient between two channel realizations, time τ apart. Also, $\delta_e^2 \approx 1 - |\rho|^2 + |\rho|^2\,\delta^2$, where δ^2 is the measure of the estimation error as in (4.2). Note that the errors are assumed to be small enough so that second-order terms can be neglected. This model has been frequently applied in the literature (for example, in [113]).

- *Single-tap channel model:* The channel time-variation is often modeled by using a "single-tap" filter (for example, in [114]), which is expressed as

$$\boldsymbol{H}_t = \rho\boldsymbol{H}_{t-\tau} + \sqrt{1-\rho^2}\boldsymbol{\Xi}. \tag{4.4}$$

  In addition, (4.4) can be used to model the channel variation in the frequency domain, which is applicable in the research on OFDM systems. In this case, ρ would be the modulus value of the complex correlation coefficient between the OFDM subcarriers. Also, some channel estimation error models are also realized using (4.4), where the power is scaled to maintain the variance in contrast to the models with additive errors described in (4.2) and (4.3).

Unfortunately, very little previous work has addressed the joint statistics of the eigenvalues of $\boldsymbol{H}\boldsymbol{H}^\dagger$ and $\widehat{\boldsymbol{H}}\widehat{\boldsymbol{H}}^\dagger$. In [115], the joint density of the eigenvalues of realizations at two successive time points, t and $t+\tau$, has been derived. This scenario is the same as in (4.4). Here we aim to derive a more general joint PDF, which caters for any cases that can be expressed in the form of (4.1) and hence is more versatile. Furthermore, the derivation of this PDF is much simpler than that found in [115].

4.1.2 Derivation of the Joint Density

Denoting the eigenvalues of $\boldsymbol{H}\boldsymbol{H}^{\dagger}$ and $\widehat{\boldsymbol{H}}\widehat{\boldsymbol{H}}^{\dagger}$ by $\lambda_1, \ldots, \lambda_m$ and $\widehat{\lambda}_1, \ldots, \widehat{\lambda}_m$ respectively, using Bayes' Rule, the required joint density is:

$$f(\lambda_1, \ldots, \lambda_m, \widehat{\lambda}_1, \ldots, \widehat{\lambda}_m) = f(\widehat{\lambda}_1, \ldots, \widehat{\lambda}_m | \lambda_1, \ldots, \lambda_m) \times f(\lambda_1, \ldots, \lambda_m)\,. \quad (4.5)$$

Since the entries of $\boldsymbol{H}$ are i.i.d. $\mathcal{CN}(0,1)$, $\boldsymbol{H}\boldsymbol{H}^{\dagger}$ is Wishart and the joint density of the ordered eigenvalues is (2.15) in Chapter 2, which is repeated here for convenience:

$$\begin{aligned} f(\lambda_1, \ldots, \lambda_m) = & \prod_{i=1}^{m} [(n-i)!(m-i)!]^{-1} \exp\left(-\sum_{i=1}^{m} \lambda_i\right) \\ & \times \prod_{i=1}^{m} \lambda_i^{l} \prod_{i<j} (\lambda_i - \lambda_j)^2. \end{aligned} \quad (4.6)$$

Rewriting (4.1) as:

$$\frac{\widehat{\boldsymbol{H}}}{\Upsilon} = \boldsymbol{H} + \frac{\Omega}{\Upsilon}\,\boldsymbol{\Xi}, \quad (4.7)$$

we see that (4.7) is the sum of two scaled random matrices. This has a similar form to a complex Brownian matrix diffusion process, the structure of which can be expressed as

$$\boldsymbol{B}(t+\tau) = \boldsymbol{B}(t) + \mathcal{CN}(\boldsymbol{0}, 2\tau\boldsymbol{I}) = \boldsymbol{B}(t) + \sqrt{2\tau}\;\mathcal{CN}(\boldsymbol{0}, \boldsymbol{I}) \quad (4.8)$$

with $\tau \geq 0$. In (4.8) $\boldsymbol{B}(t)$ represents the $N_r \times N_t$ complex Brownian matrix at time point t, and $\mathcal{CN}(\boldsymbol{0}, \sigma^2\boldsymbol{I})$ denotes an i.i.d. complex Gaussian matrix with entries which have zero mean and magnitude variance σ^2. Note that $\boldsymbol{B}(t)$ and $\mathcal{CN}(\boldsymbol{0}, \sigma^2\boldsymbol{I})$ are independent. The underlying eigenvalue process of $\boldsymbol{B}(t)$ has been studied in [99]. Most importantly, it was shown in [99] that the m eigenvalues of $\boldsymbol{B}(t)\boldsymbol{B}^{\dagger}(t)$ evolve as m independent Squared Bessel Processes (BESQ) conditioned never to collide. For this system, define one eigenvalue at time t as w and a second, possibly different eigenvalue, at time $t+\tau$ as $\widehat{w}$. The conditional density of $\widehat{w}$ given w is denoted the transition density and is

given by [116]:

$$f(\widehat{w}|w) = \frac{1}{2\tau}\left(\frac{\widehat{w}}{w}\right)^{\frac{l}{2}} \exp\left[\frac{-w-\widehat{w}}{2\tau}\right] I_l\left(\frac{\sqrt{w\widehat{w}}}{\tau}\right), \tag{4.9}$$

where $l = n - m$ and I_l is the l^{th}-order modified Bessel function.

Since the multiple eigenvalues processes are conditioned never to collide, the ordering $w_1 > w_2 > \ldots > w_m$ is preserved, and the corresponding joint transition density of the eigenvalues is given as [117, 118]:

$$f(\widehat{w}_1, \ldots, \widehat{w}_m|w_1, \ldots, w_m) = \frac{\prod_{i<j}(\widehat{w}_i - \widehat{w}_j)}{\prod_{i<j}(w_i - w_j)} \times \mathcal{G}(\boldsymbol{w}), \tag{4.10}$$

where the operator $\mathcal{G}(\cdot)$ is the determinant defined as

$$\mathcal{G}(\boldsymbol{x}) = \det \begin{bmatrix} f(\widehat{x}_1|x_1) & f(\widehat{x}_2|x_1) & \cdots & f(\widehat{x}_m|x_1) \\ f(\widehat{x}_1|x_2) & f(\widehat{x}_2|x_2) & & \vdots \\ \vdots & & \ddots & \vdots \\ f(\widehat{x}_1|x_m) & \cdots & \cdots & f(\widehat{x}_m|x_m) \end{bmatrix} \tag{4.11}$$

for multiple ordered processes x_1, x_2, …, x_m.

In order to apply the results for the Brownian model, we replace w, $\widehat{w}$ and 2τ in (4.9) with λ, $\widehat{\lambda}$ and $(\Omega/\Upsilon)^2$ respectively. Then, we multiply (4.10) with (4.6) to obtain the joint PDF of the eigenvalues of $\boldsymbol{H}\boldsymbol{H}^\dagger$ and $(\widehat{\boldsymbol{H}}\widehat{\boldsymbol{H}}^\dagger)/\Upsilon^2$. Since the eigenvalues of $\widehat{\boldsymbol{H}}\widehat{\boldsymbol{H}}^\dagger$ have been scaled by Υ^2, we make a simple transformation to obtain the desired results. To recapitulate, we have obtained

$$f(\widehat{\lambda}|\lambda) = \frac{\Upsilon^2}{\Omega^2}\left(\frac{\widehat{\lambda}}{\Upsilon^2\lambda}\right)^{\frac{l}{2}} \exp\left[\frac{-\Upsilon^2\lambda - \widehat{\lambda}}{\Omega^2}\right] I_l\left(2\frac{\Upsilon}{\Omega^2}\sqrt{\lambda\widehat{\lambda}}\right) \tag{4.12}$$

and

$$\begin{aligned} f(\lambda_1, \ldots, \lambda_m, \widehat{\lambda}_1, \ldots, \widehat{\lambda}_m) &= \frac{\prod_{i<j}[\frac{1}{\Upsilon^2}(\widehat{\lambda}_i - \widehat{\lambda}_j)]}{\Upsilon^{2m}\prod_{i<j}(\lambda_i - \lambda_j)} \times \mathcal{G}(\boldsymbol{\lambda}) \times f(\lambda_1, \ldots, \lambda_m) \\ &= \frac{\prod_{i<j}[\frac{1}{\Upsilon^2}(\widehat{\lambda}_i - \widehat{\lambda}_j)]\ \prod_{i<j}(\lambda_i - \lambda_j)}{\Upsilon^{2m}\prod_{i=1}^{m}[(n-i)!(m-i)!]} \\ &\quad \times \prod_{i=1}^{m}\lambda_i^l \times \exp\left(-\sum_{i=1}^{m}\lambda_i\right) \times \mathcal{G}(\boldsymbol{\lambda}), \end{aligned} \tag{4.13}$$

where $\mathcal{G}(\boldsymbol{\lambda})$ can be calculated based on (4.11) and (4.12).

For a numerical example, consider a (2,4) MIMO channel in the scenario of (4.4). The joint density density for the eigenvalues of the two correlated systems can be written as

$$\begin{aligned} f(\widehat{\lambda}_1, \widehat{\lambda}_2, \lambda_1, \lambda_2) = & \frac{\widehat{\lambda}_1 \widehat{\lambda}_2 \lambda_1 \lambda_2 \left(\widehat{\lambda}_1 - \widehat{\lambda}_2\right)(\lambda_1 - \lambda_2)}{12\left(\rho^6 + \rho^{10} - 2\rho^8\right)} \\ & \times \exp\left(\frac{-\lambda_1 - \lambda_2 - \widehat{\lambda}_1 - \widehat{\lambda}_2}{1-\rho^2}\right) \\ & \times \left[I_2\left(\frac{2\rho}{1-\rho^2}\sqrt{\lambda_1 \widehat{\lambda}_1}\right) I_2\left(\frac{2\rho}{1-\rho^2}\sqrt{\lambda_2 \widehat{\lambda}_2}\right) \right. \\ & \left. - I_2\left(\frac{2\rho}{1-\rho^2}\sqrt{\lambda_1 \widehat{\lambda}_2}\right) I_2\left(\frac{2\rho}{1-\rho^2}\sqrt{\lambda_2 \widehat{\lambda}_1}\right) \right]. \end{aligned} \tag{4.14}$$

Similarly, for a SISO channel where $n = m = 1$, the joint density becomes

$$f(\widehat{\lambda}, \lambda) = \frac{1}{1-\rho^2} \exp\left(\frac{-(\lambda + \widehat{\lambda})}{1-\rho^2}\right) I_0\left(\frac{2\rho\sqrt{\lambda\widehat{\lambda}}}{1-\rho^2}\right). \tag{4.15}$$

Note that (4.15) is the density function for the bivariate exponential distribution [119], which is frequently encountered in the context of SISO channel characterization. Thus, we can remark that the bivariate exponential distribution is a special case of the joint density derived here.

In the next two sections, we will show how the joint density (4.13) can be applied in the FSMC modeling of different MIMO channel metrics.

4.2 FSMC for Scalar MIMO Channel Metrics: Capacity and Condition Number

This section constructs FSMCs for two scalar MIMO channel metrics: capacity and condition number. These metrics are considered since they are important switching criteria for certain adaptive MIMO systems [74, 79].

The construction of a FSMC for the MIMO capacity process was motivated by the rate-feedback scheme proposed in [74]. Since the capacity, $C(t)$, represents the maximum rate that a channel can support at time t, the rate-feedback

scheme computes the present channel capacity at the receiver, and sends this information to the transmitter via a feedback link. Thus, the transmitter is able to choose an appropriate data rate for the next signalling interval. For such a system, the probability of adaptation error (PAE) is the probability of rate-assignment error (PORAE), due to feedback delay or/and channel estimation error. For efficient feedback purposes [74], the capacity is partitioned into several discrete quantities as a finite list of states, each corresponding to a specific transmission rate. Through the construction of a FSMC for the capacity, the probability that the capacity process transits to a different state during the feedback period can be evaluated. Recently, we have became aware that FSMC modeling for MIMO capacity has also appeared in [120] with a similar motivation. However, the approach used in [120] to evaluate the transition probabilities is different to the methods present here.

As mentioned in Chapter 2, the channel condition number, defined as $\kappa = \lambda_1/\lambda_m$, is a well-known indicator of spatial selectivity for MIMO channel. Many adaptive MIMO systems have proposed to employ the condition number as a criterion for choosing among multiple signalling strategies. In [79], a "dual-mode" antenna selection scheme is outlined, which uses κ to choose between multiplexing and general diversity techniques. In addition to κ, sometimes the ratios of other eigenvalue pairs are also of interest. For example, in [80] researchers have used the ratio of the largest channel eigenvalue to each of the other eigenvalues in order to estimate the number of effective spatial links. These systems require a feedback mechanism. The scheme in [79] quantizes the condition number into two discrete states, and each state corresponds to a specific transmission strategy. Thus, the evolution of the condition number over time can be conveniently approximated as a two-state FSMC, which can be used to investigate the impacts of feedback delay. Note that the i.i.d. Rayleigh fading MIMO channel is often said to be "well-conditioned", as the average condition number is much lower than for channels with a line-of-sight

path or spatial correlation. In fact, however, the magnitude of the condition number can vary significantly even for an i.i.d. Rayleigh MIMO channel, and we will focus on this baseline case in this chapter.

This section commences with the elaboration of two general analytical approaches that can be used to compute the transition probabilities between states for these two important MIMO channel metrics of interest.

4.2.1 General Methods for Computing Transition Probabilities

To construct a FSMC for both of these metrics, two simple methods are considered: the *conditional probability method* and the *level crossing rate method*. In general, the former can compute transition probabilities between any two states, while the latter is only valid when the channel variation is slow enough, so that only the transitions between adjacent states are possible.

Conditional Probability Method

The transition probabilities can be calculated using conditional probability theory based on Bayes' Rule. Consider a random process $p(t)$, which has been partitioned into N discrete states denoted as $\mathcal{S}_1, \mathcal{S}_2, \ldots, \mathcal{S}_N$. The transition probability, that the process $p(t)$ transits from $\mathcal{S}_i$ to state $\mathcal{S}_j$ during the time displacement τ, is P_{ij}. For simplicity, $p(t)$ and $p(t+\tau)$ are denoted as p and $\widehat{p}$ respectively with PDFs denoted by $f(p)$ and $f(p,\widehat{p})$. The transition probability can therefore be written as:

$$P_{ij} = \frac{\text{Prob}(p \in \mathcal{S}_i, \widehat{p} \in \mathcal{S}_j)}{\text{Prob}(p \in \mathcal{S}_i)}\,. \tag{4.16}$$

Thus, if both the stationary probability density functions, $f(p)$, and the joint density, $f(p,\widehat{p})$, are known, (4.16) can by computed by

$$P_{ij} = \frac{\int_{\mathcal{S}_i}\int_{\mathcal{S}_j} f(p,\widehat{p})\,d\widehat{p}\,dp}{\int_{\mathcal{S}_i} f(p)\,dp}. \tag{4.17}$$

When $i = j$, P_{ij} (or P_{ii}) is simply the probability that the process stays in the same state after the lag τ. It is important to note that

$$\sum_{j=1}^{N} P_{ij} = 1. \tag{4.18}$$

Level Crossing Rate Method

If the process $p(t)$ is slow enough, it is reasonable to assume that only the transitions between neighboring states are possible. To construct a FSMC with N states in such a case, only the transition probabilities between any state and its neighboring states need to be determined. Both [105] and [106] have modeled the SISO Rayleigh fading channel in this way using a FSMC and approximating the transition probabilities using the LCR. Define the transition probabilities from state $\mathcal{S}_i$ to $\mathcal{S}_{i+1}$ and $\mathcal{S}_{i-1}$ as $P_{i,i+1}$ and $P_{i,i-1}$ respectively, then we have:

$$P_{i,i+1} \approx \frac{\mathrm{LCR}(T_{i+1})\,\tau}{\mathrm{Prob}(p \in \mathcal{S}_i)}, i = 1, 2, \ldots, N-1. \tag{4.19}$$

$$P_{i,i-1} \approx \frac{\mathrm{LCR}(T_i)\,\tau}{\mathrm{Prob}(p \in \mathcal{S}_i)}, i = 2, 3, \ldots, N. \tag{4.20}$$

Note that threshold level T_{i+1} represents the boundary between $\mathcal{S}_i$ and $\mathcal{S}_{i+1}$. In addition, as only transitions between adjacent states are possible, it can be deduced easily that:

$$P_{ii} = 1 - (P_{i,i+1} + P_{i,i-1}) \tag{4.21}$$

4.2.2 Rate Feedback Scheme

A rate-feedback scheme has been discussed in [74] where the capacity is quantized into several discrete values that are known by both transmitter and receiver. These quantized values can represent states, and we model the capacity over time as a FSMC over these states. We assume that the receiver possesses

perfect knowledge of the channel, so perfect selection of rate is made at the receiver and the transmitter is informed via a feedback link. Hence, the time-varying nature of the mobile channel may cause the selected rate to become obsolete when applied at the transmitter. The goal here is to find the probability that the current rate selection becomes inappropriate (either too high or too low) during the feedback time period.

To partition the capacity process into a finite list of states, we employ the quantization method proposed in [74]. If η is any non-negative integer, a list of $2\eta + 1$ possible rates, $\mathcal{L}$, can be generated as:

$$\begin{aligned} \mathcal{L} &= \{0, \mu_C(1-\eta\epsilon), \ldots, \mu_C(1-\epsilon), \mu_C, \\ &\quad \mu_C(1+\epsilon), \ldots, \mu_C(1+(\eta-1)\epsilon)\}, \end{aligned} \tag{4.22}$$

where μ_C is the mean rate (the expected value of $C(t)$), and ϵ is an arbitrary proportion of μ_C, known as granularity. Thus, the rate $\mu_C(1+i\epsilon)$ is selected whenever the capacity lies between $\mu_C(1+i\epsilon)$ and $\mu_C(1+(i+1)\epsilon)$. Hence, the states can be denoted $\mathcal{S}_1, \mathcal{S}_2, \ldots \mathcal{S}_{2\eta+1}$ where $\mathcal{S}_1$ occurs when $C < \mu_C(1-\eta\,\epsilon)$, $\mathcal{S}_j$ occurs when $\mu_C(1-(\eta-j+2)\epsilon) \leq C < \mu_C(1+(\eta-j+1)\epsilon)$ for $2 \leq j \leq 2\eta$ and $\mathcal{S}_{2\eta+1}$ occurs when $\mu(1+(\eta-1)\epsilon) \leq C$. In a slight divergence from [74], we have an extra state, "0", to indicate channel outage, when the channel is too weak to support transmission.

As a simple example, consider a (2,2) MIMO system with transmission power $\mathcal{P} = 8\,(9dB)$. For this example, mean capacity, μ_C, is approximately 5 bits per second per Hz (bps/Hz). Thus, if one arbitrarily choose $\eta = 2$ and $\epsilon = 0.4$, a list of possible rates in five states can be generated using (4.22), as shown in Table 4.1.

We first calculate the transition probabilities by the conditional probability method. For the sake of convenience, $C(t)$ and $C(t+\tau)$ are denoted by C and $\widehat{C}$ respectively in the rest of the analysis. As noted in [90] and [74], MIMO channel capacity can be accurately approximated by Gaussian process. Hence, C and

State	Capacity Region (bps/Hz)	Rate Selection (bps/Hz)
$\mathcal{S}_1$	$0 \leq C < 1$	Outage
$\mathcal{S}_2$	$1 \leq C < 3$	1
$\mathcal{S}_3$	$3 \leq C < 5$	3
$\mathcal{S}_4$	$5 \leq C < 7$	5
$\mathcal{S}_5$	$7 \leq C$	7

Table 4.1: Markov states for the capacity process in a (2,2) MIMO system with $\mathcal{P} = 8$, $\eta = 2$ and $\epsilon = 0.4$.

$\widehat{C}$ can be seen as two mutually correlated Gaussian processes with common mean and variance. Thus, the joint density of C and $\widehat{C}$ can be approximated by the bivariate Gaussian distribution, which is written as

$$\begin{aligned} f(C,\widehat{C}) &= \frac{1}{2\pi\sigma_C^2\sqrt{1-R_C^2}} \times \\ &\quad \exp\left(-\frac{(C-\mu_C)^2 - 2R_C(C-\mu_C)(\widehat{C}-\mu_C) + (\widehat{C}-\mu_C)^2}{2\sigma^2(1-R_C^2)} \right), \end{aligned} \tag{4.23}$$

where σ_C^2 and R_C are the variance and autocorrelation coefficient of the capacity process, respectively.

Recall that for an arbitrary stationary random process $p(t)$, the autocorrelation coefficient R_p can be calculated by

$$\begin{aligned} R_p &= \frac{\mathrm{E}[p(t)p(t+\tau)] - \mathrm{E}[p(t)]\,\mathrm{E}[p(t+\tau)]}{\sqrt{\mathrm{Var}[p(t)]\,\mathrm{Var}[p(t+\tau)]}} \\ &= \frac{\mathrm{E}[p\widehat{p}] - \mathrm{E}[p]^2}{\mathrm{Var}[p]}\,. \end{aligned} \tag{4.24}$$

The first two moments of p and the joint moment of p and $\widehat{p}$ are required to obtain the autocorrelation coefficient. The mean and variance of the capacity can be evaluated using the results in [57] and [90] respectively. The joint moment of the capacity process, $\mathrm{E}(C\widehat{C})$, can be calculated by serial integration over the product:

$$\sum_{i=1}^{m} \log_2\left(1+\tfrac{\mathcal{P}}{N_t}\lambda_i\right) \sum_{i=1}^{m} \log_2\left(1+\tfrac{\mathcal{P}}{N_t}\widehat{\lambda}_i\right) \times f(\lambda_1,\ldots,\lambda_m,\widehat{\lambda}_1,\ldots,\widehat{\lambda}_m),$$

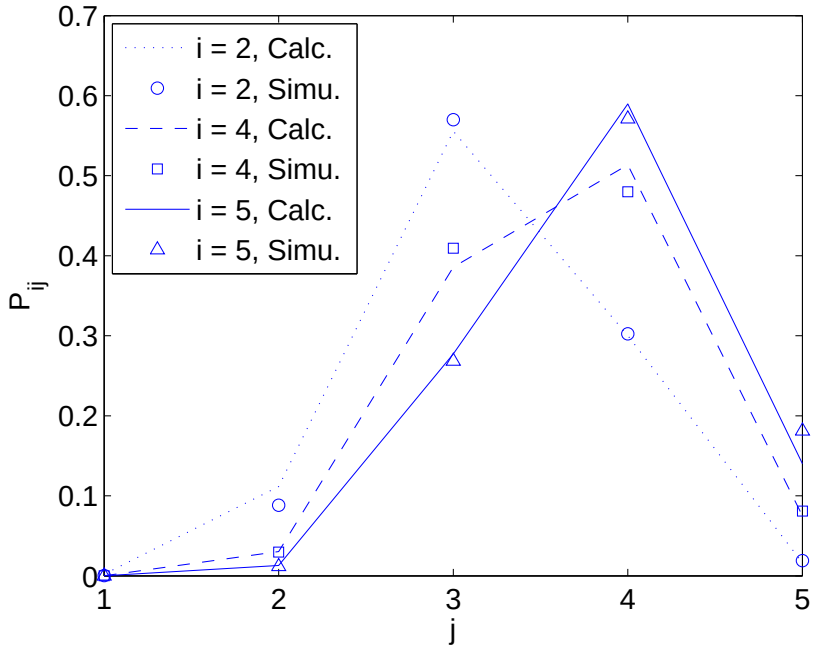

Figure 4.2: Transition probabilities from state i to j (P_{ij}) for C in a (2,2) MIMO system with $f_D\tau = 0.2250$, calculated using the conditional probability method.

where $f(\lambda_1, \ldots, \lambda_m, \widehat{\lambda}_1, \ldots, \widehat{\lambda}_m)$ has been derived in the Section 4.1. Note that $\mathrm{E}(C\widehat{C})$ has been computed following this approach in [115] and [109]. Hence, the value of R_C can be calculated analytically using (4.24).

Thus, all the parameters required by (4.23) are available, and the transition probabilities P_{ij} can be computed by applying (4.17). Note that such a method (as well as the LCR method) also requires the steady state probabilities that the capacity occupies certain regions, and these can be obtained using the Gaussian distribution as it accurately approximates the capacity process.

Some selected simulation results for P_{ij} in (2,2) and (2,4) systems are shown in Figs. 4.2 and 4.3. These simulations are carried out under a very high mobility level ($f_D\tau = 0.2250$). Therefore, transitions between any two states (not just adjacent states) are possible. For example, in Fig. 4.2, there is a probability of at least 0.25 for the capacity to transit from state 5 to 3.

In the scenarios with low mobility, on the other hand, it is reasonable

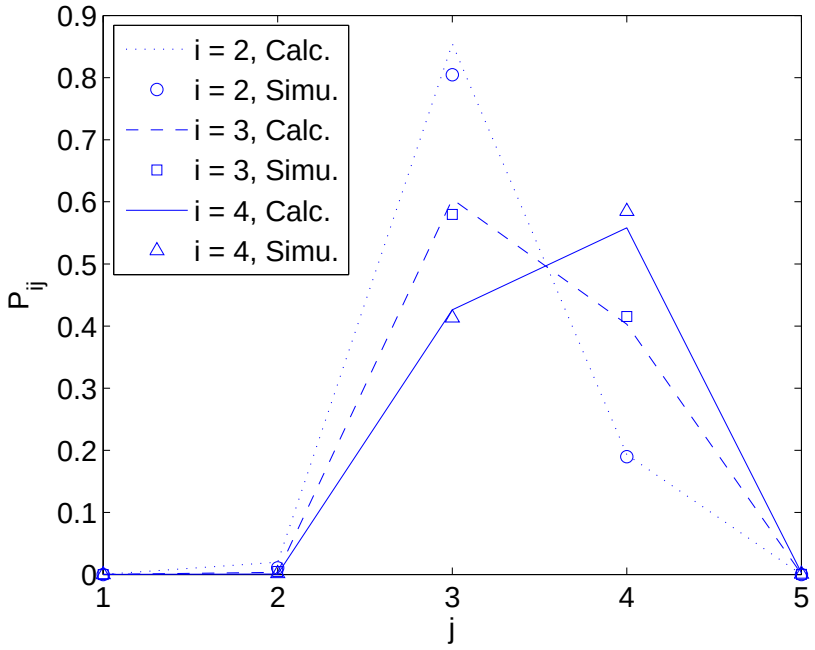

Figure 4.3: Transition probabilities from state i to j (P_{ij}) for C in a (2,4) MIMO system with $f_D\tau = 0.2250$, calculated using the conditional probability method.

to assume that the capacity process is slow enough so that only transitions between adjacent states are possible. In such a case, the LCR method discussed earlier, can be employed. The LCR results for MIMO capacity processes can be found in Chapter 3. The probabilities of transitions to the adjacent higher and lower states in a (2,4) MIMO system with $f_D\tau = 0.0265$, are plotted in Figs. 4.4 and 4.5 respectively. The agreement between analytical and simulation results is shown clearly.

With the FSMC for MIMO capacity available, the impact of feedback delay on rate-selection can be explored. In particular, PORAE represents the probability that the process does not stay in the same state during the feedback interval. Thus, it can be expressed as

$$PORAE_i = \sum_{j \neq i}^{N} P_{ij} = 1 - P_{ii}. \tag{4.25}$$

The PORAE results for both high and low mobilities are plotted in Figs.

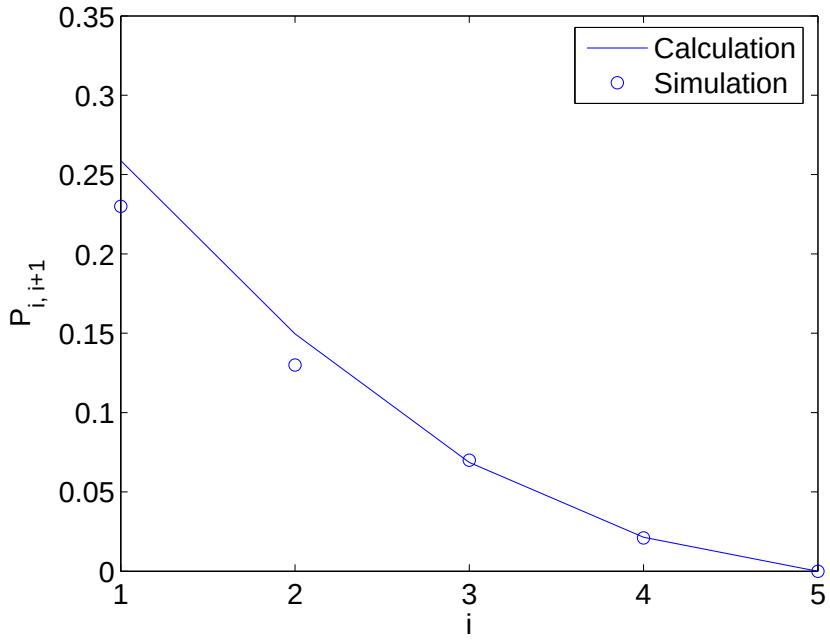

Figure 4.4: Transition probabilities from state i to $i+1$ ($P_{i,i+1}$) for C in a (2,4) MIMO system with $f_D\tau = 0.0265$, calculated using the LCR method.

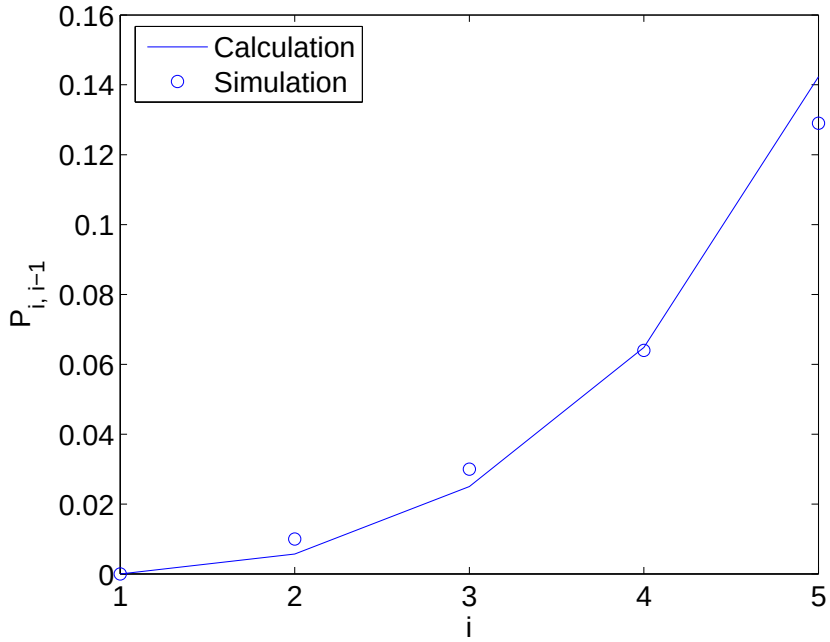

Figure 4.5: Transition probabilities from state i to $i-1$ ($P_{i,i-1}$) for C in a (2,4) MIMO system with $f_D\tau = 0.0265$, calculated using the LCR method.

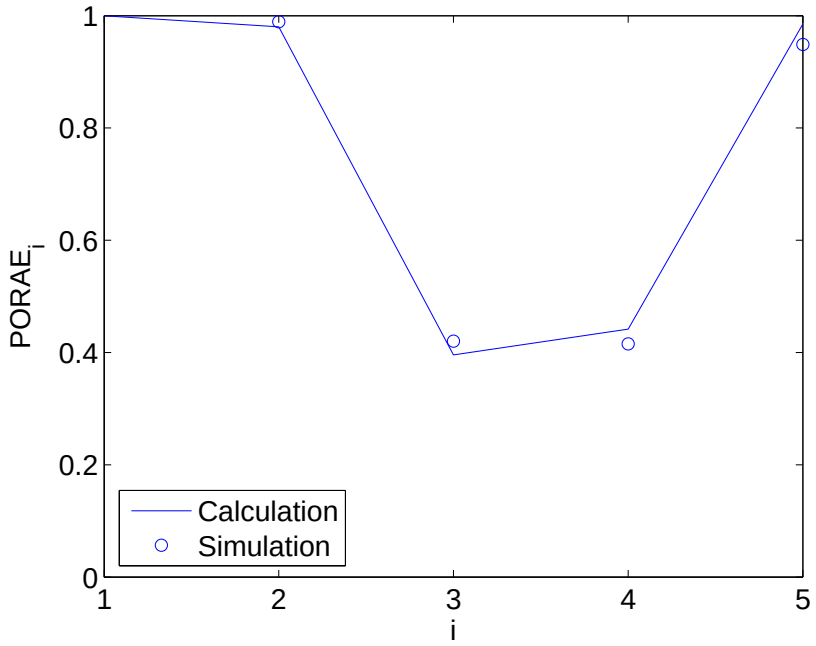

Figure 4.6: The probability of rate-assignment error (PORAE) due to feedback delay, in a (2,4) MIMO system with a high mobility ($f_D\tau = 0.2250$). The calculated results are computed using (4.25).

4.6 and 4.7. The curves are calculated by the conditional probability method and the LCR method, respectively. Good agreement between simulated and analytical results are exhibited in both cases. We observe that feedback delay has a substantial impact on the adaptation performance of rate-feedback schemes. The probability of rate-assignment error is at least 10 percent even for the low mobility case (Fig. 4.7). Interestingly, in the high mobility scenario, it is almost guaranteed that an inappropriate choice will be made, if the transmitter has been informed that the capacity occupies states 1, 2 and 5.

4.2.3 Dual-Mode Antenna Selection Scheme

We now move our scope to the dual-mode antenna selection scheme. The scheme employs the condition number as the switching criterion for choosing between multiplexing and diversity. When multiplexing is selected, multiple

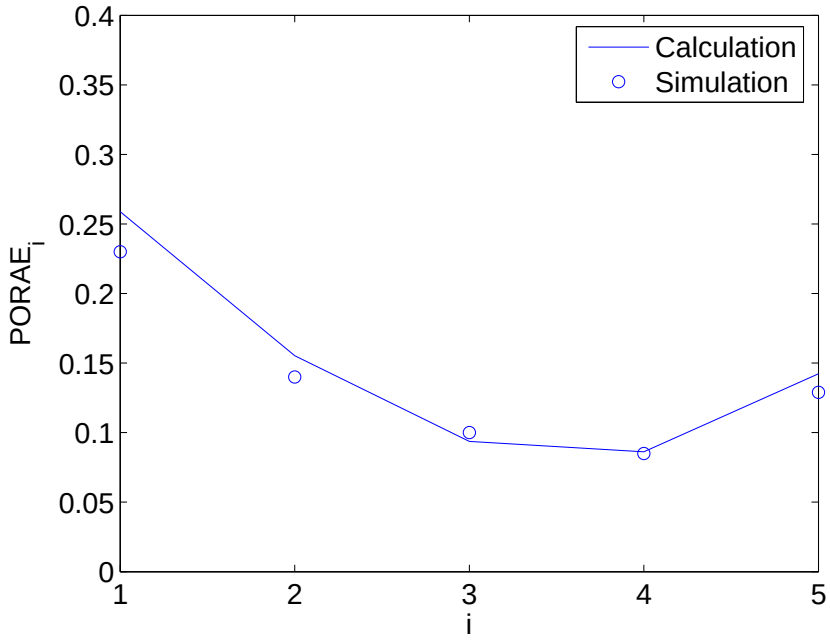

Figure 4.7: The probability of rate-assignment error (PORAE) due to feedback delay, in a (2,4) MIMO system with a low mobility ($f_D\tau = 0.00265$). The calculated results are computed using (4.25).

independent data streams are sent simultaneously from the multiple transmit antennas. For transmit diversity, on the other hand, the data stream is transmitted from the single antenna that has the best link quality.

As discussed in the previous chapters, the statistical distribution of κ is long-tailed, which often complicates any analytical approach. Therefore, we look at the logarithm of κ (denoted $K = \log \kappa$) instead, which appears to be well-approximated by a gamma variable, as has been shown in Chapter 3.

Following [79], multiplexing is chosen if K is less than or equal to the threshold

$$T = \log \left[\frac{d^2_{\min}(N_t, D)}{d^2_{\min}(1, D)} \right], \tag{4.26}$$

where $d_{\min}(N_t, D)$ and $d_{\min}(1, D)$ are the minimum Euclidean distances between points in the modulation constellations for multiplexing and diversity with rate D, respectively. Note that $N_t = 1$ for the diversity scheme since

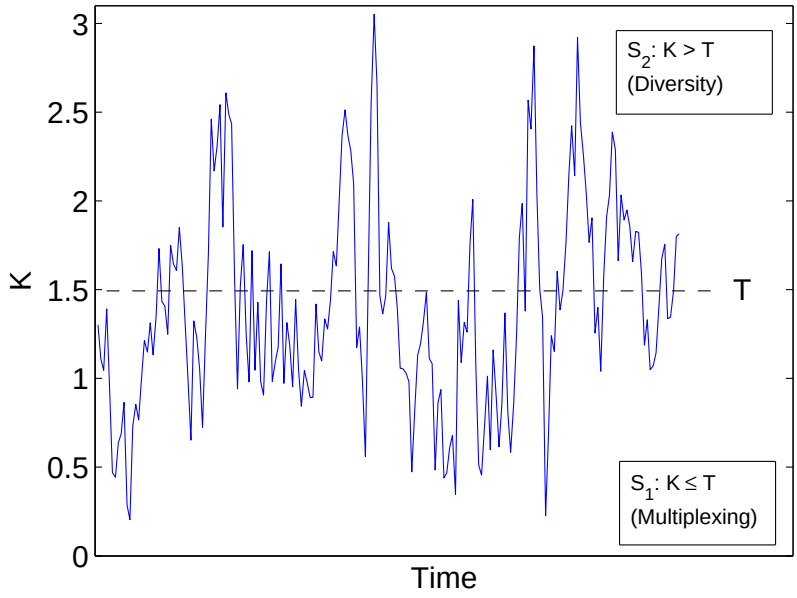

Figure 4.8: A typical condition number trajectory for a (2,4) i.i.d. Rayleigh channel with Jakes fading. For a dual-mode antenna selection scheme, the condition number is quantized into two states: multiplexing ($K \leq T$) and diversity ($K > T$).

only one transmit antenna is used. The system is designed assuming the total data rate D is fixed, regardless of whether multiplexing or diversity is selected. Assuming that QAM is employed, $d^2_{\min}$ can be calculated as [79]:

$$d^2_{\min}(N_t, D) = \frac{6}{N_t(2^{D/N_t} - 1)} \,. \tag{4.27}$$

Hence, the condition number can be modeled by a FSMC with two states: multiplexing ($\mathcal{S}_1$) and diversity ($\mathcal{S}_2$), as illustrated in Fig. 4.8. Although we concentrate on a two-state model, we must point out that our proposed analytical method is also extendable to cases with more than two states. For example, the system proposed in [121] has used the condition number to identify the current propagation environment and then to pick the best transmission method among multiple (more than two) choices accordingly.

As in Section 4.2.2, both the methods for calculating transition probabilities described in Section 4.2.1 are attempted here.

For the conditional probability method, let K and $\widehat{K}$ be $\log\kappa$ at times t and $t+\tau$ respectively. Based on the previous discussion, the condition number is assumed to be a stationary gamma process. Therefore, it can be extrapolated that K and $\widehat{K}$ are approximately two mutually correlated gamma variables. Hence, the joint density of K and $\widehat{K}$ can be written as a bivariate gamma distribution with common shape and scale factors: $r = \mathrm{E}(K)^2/\mathrm{Var}(K)$ and $\theta = \mathrm{E}(K)/\mathrm{Var}(K)$. By modifying the bivariate gamma density function in [122], the joint density $f(K,\widehat{K})$ can be written as:

$$f(K,\widehat{K}) = \frac{(K\widehat{K})^{\frac{r-1}{2}}\theta^{r+1}}{\Gamma(r)(1-R_K)R_K^{\frac{r-1}{2}}}\exp\left\{\frac{-(K+\widehat{K})\theta}{1-R_K}\right\} \times I_{r-1}\left(\frac{2\theta}{1-R_K}\sqrt{R_K K\widehat{K}}\right). \tag{4.28}$$

Akin to the notation in Section 4.2.2, R_K is the correlation coefficient between K and $\widehat{K}$ (or the autocorrelation coefficient of $K(t)$) and can be calculated by using (4.24), which requires $\mathrm{E}(K)$, $\mathrm{Var}(K)$ and $\mathrm{E}(K\widehat{K})$. By using (4.6), $f(\lambda_1,\lambda_m)$, $\mathrm{E}(K)$ and $\mathrm{Var}(K)$ can be acquired. Note that $\mathrm{E}(K)$ can be shown to be infinite when $l=0$ ($N_t=N_r$), so R_K does not exist in this case. Therefore, we concentrate on asymmetrical MIMO systems. The joint moment $\mathrm{E}(K\widehat{K})$, on the other hand, must be computed using the joint density of the eigenvalues at two adjacent time points, which is (4.13). The numerical value of $\mathrm{E}(K\widehat{K})$ can be found by integrating the product

$$\left(\log\frac{\lambda_1}{\lambda_m}\right)\left(\log\frac{\widehat{\lambda}_1}{\widehat{\lambda}_m}\right) \times f(\lambda_1,\ldots,\lambda_m,\widehat{\lambda}_1,\ldots,\widehat{\lambda}_m)$$

with respect to $\lambda_1,\ldots\lambda_m$ and $\widehat{\lambda}_1,\ldots,\widehat{\lambda}_m$ ($2m$-dimensional integration). Note that λ_i and $\widehat{\lambda}_i$ are the eigenvalues at times t and $t+\tau$, respectively. To simplify the approach, we could acquire $\mathrm{E}(K\widehat{K})$ using (3.27). However, (3.27) was derived from a SDE so it may not be accurate when ρ is low. It is possible to analytically obtain $f(\lambda_1,\lambda_m,\widehat{\lambda}_1,\widehat{\lambda}_m)$ which reduces the problem to 4-dimensional integration. However, this is beyond the scope of this thesis.

As all of the parameters required by the bivariate gamma density (4.28) are now available, each transition probability defined by (4.17) can be evaluated using:

$$P_{ij} = \frac{\int_{\mathcal{S}_i} \int_{\mathcal{S}_j} f(K, \widehat{K})\, d\widehat{K}\, dK}{\int_{\mathcal{S}_i} f(K)\, dK} \tag{4.29}$$

where the PDF of K, $f(K)$, is approximated by the gamma density function with parameters r and θ.

Even for the simplest MIMO systems with $m = 2$, the conditional probability method requires quadruple integration to find R_K. Hence, we propose to compute the transition probabilities using an LCR approximation in this section, which substantially reduces the number of integrations required. Besides, the restriction to transitions to neighboring states only is not a problem as we are dealing with a model with only two states. Note that for a two-state model, the transition probability formulas, (4.19) and (4.20), for this particular case can be simplified to

$$P_{ij} \approx \frac{\mathrm{LCR}_K(T)\, \tau}{\mathrm{Prob}(K \in \mathcal{S}_i)} \tag{4.30}$$

$$P_{ii} = 1 - P_{ij}, \qquad i \neq j, \tag{4.31}$$

where $i, j \in \{1, 2\}$, and LCR_K is available in Section 3.3.4.

To verify that these two methods can be used to compute the transition probabilities, we compare our analytically calculated transition probabilities for K with simulation results as a function of the threshold T. For the simulated data, we generated 2×10^6 Monte Carlo samples with parameters $f_D = 26.5$Hz and $\tau = 2.5$ms. Some selected results obtained using the conditional probability method and the LCR method are plotted in Figs. 4.9 and 4.10. By inspection, we can see that although $K(t)$ itself is not a Markov process, the Markov approximation is surprisingly accurate and both methods provide good predictions of the transition probabilities.

We now use these methods to investigate the impact of feedback delay on

the dual-mode antenna selection schemes. As before, we are interested in PAE due to feedback delay. The notion of using a Markov model here is similar to Section 4.2.2, where P_{ij} $(i \neq j)$ represents the probability that an inappropriate mode choice is made due to the channel variation during the feedback period. For simplicity, we only consider MIMO systems using two transmit antennas with data rates $D = 4$ or 8 bits per signalling interval. When $D = 4$, QPSK is used on both antennas for multiplexing, and 16-QAM is used on the single antenna for diversity. In this case, using the formulas (4.26) and (4.27), we find that $T = 0.9163$. Similarly, when $D = 8$, 16-QAM is used on both antennas for multiplexing, while 256-QAM is used on the single antenna for diversity, and $T = 2.1413$ in this case. Note that T increases with D [79].

We investigate the effects of adding receive antennas and increasing Doppler frequency on the transition probabilities. In Fig. 4.11, we plot the transition probabilities as a function of N_r. It can be observed that P_{21} increases with N_r while P_{12} decreases with N_r. Thus, for systems with more receive antennas, we need to be more cautious if diversity is chosen, because it is more likely to become a multiplexing-preferred channel during the feedback delay. In Fig. 4.12, we see that all the transition probabilities increase with f_D, as expected.

Finally, we are interested in the overall probability of adaptation error, which can be computed as

$$P_e = 1 - \sum_{i=1}^{2} \text{Prob}(K \in \mathcal{S}_i, \widehat{K} \in \mathcal{S}_i)\,. \tag{4.32}$$

Figure 4.13 shows that the error probability, P_e, is higher when T is low for systems with more receive antennas. Conversely, performance gets better for systems with fewer antennas if T is sufficiently high. So, when D (and hence T) is high, systems with more receive antennas are preferred. Figure 4.14 shows that P_e increases with f_D for both values of D.

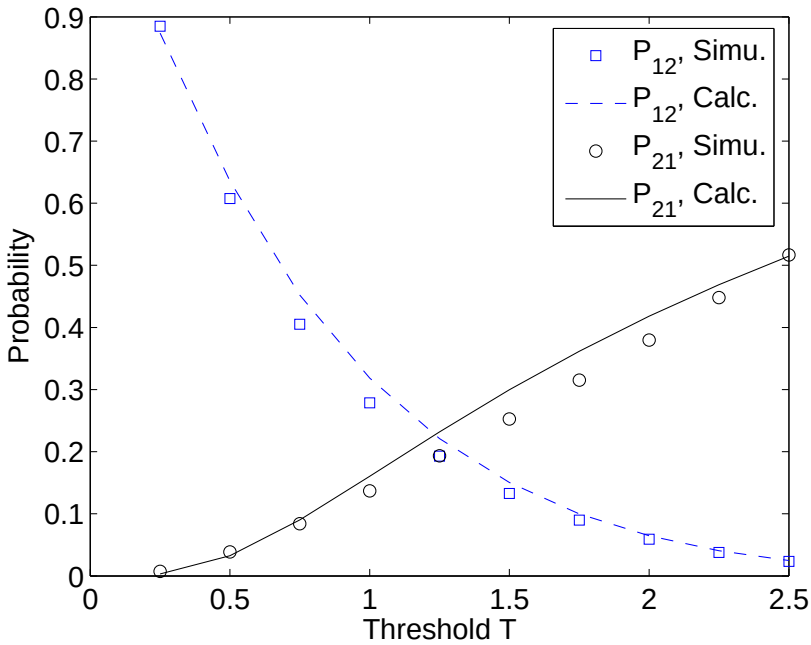

Figure 4.9: Transition probabilities for K in a (2,4) MIMO system, calculated using the conditional probability method.

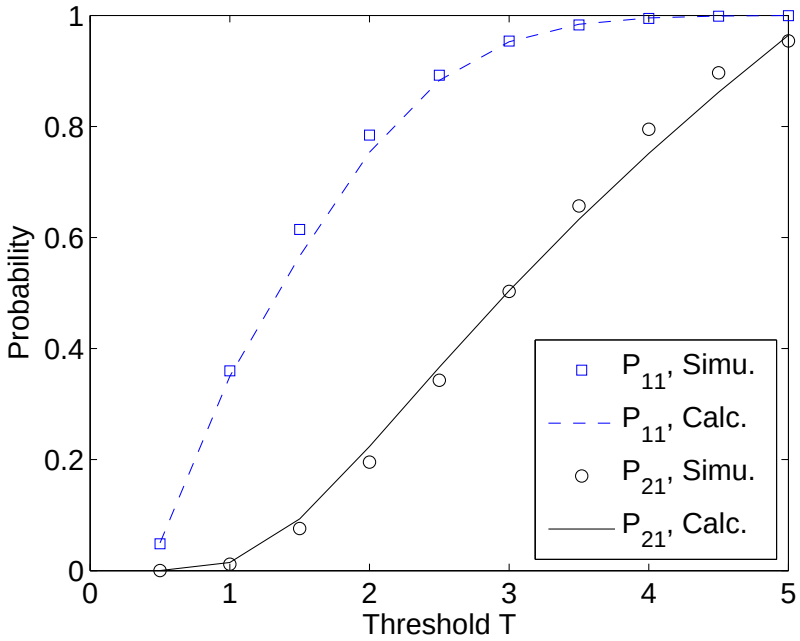

Figure 4.10: Transition probabilities for K in a (3,5) MIMO system, calculated using the LCR method.

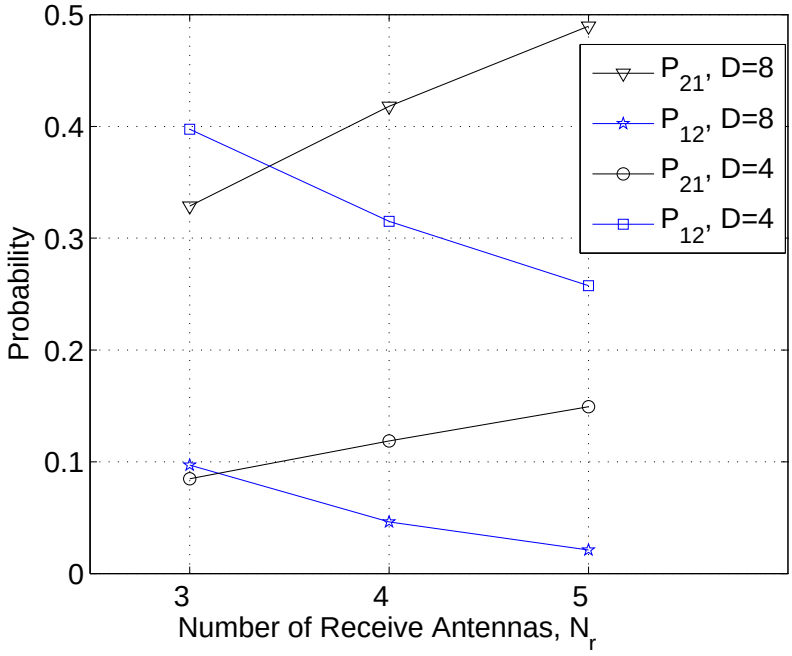

Figure 4.11: Transition probabilities for K in $(2,N_r)$ MIMO systems with different data rates.

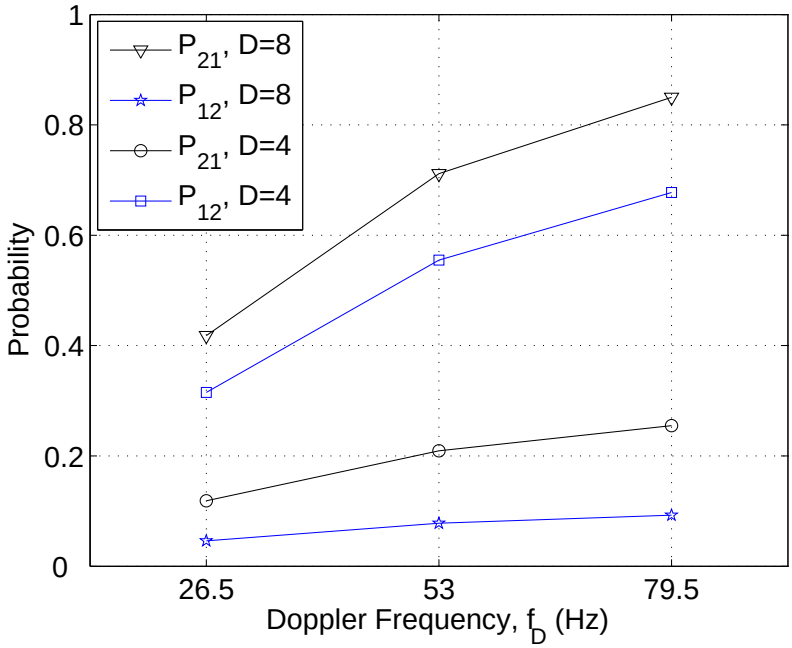

Figure 4.12: Transition probabilities for K in (2,4) MIMO systems with different Doppler frequencies f_D and data rates D.

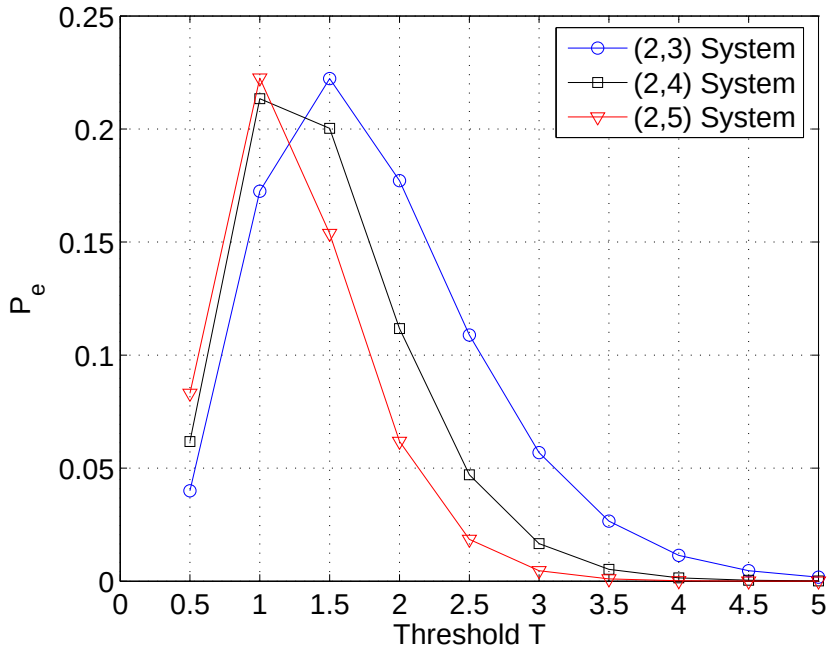

Figure 4.13: Overall probability of adaptation error (P_e) for (2,N_r) MIMO systems with different switching threshold levels T.

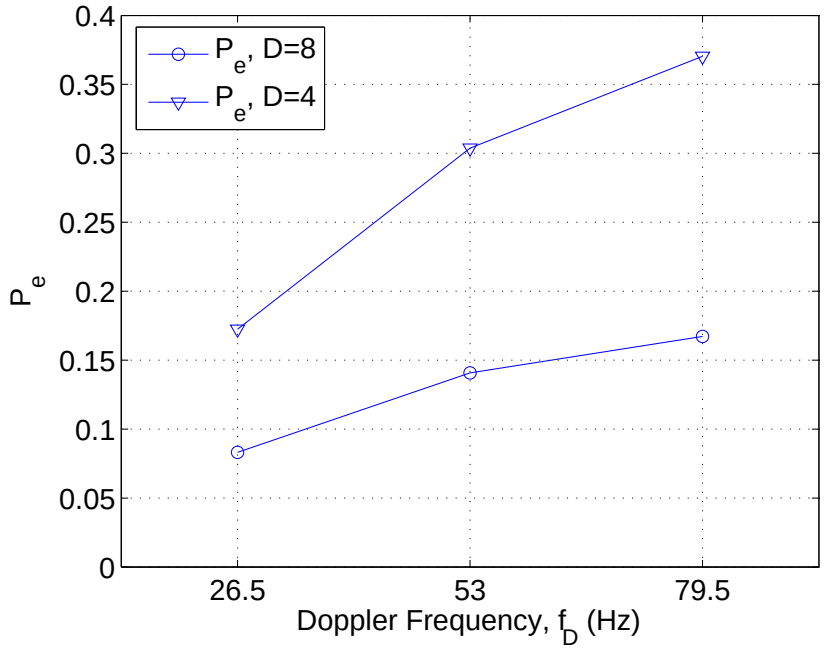

Figure 4.14: Overall probability of adaptation error (P_e) for (2,4) MIMO systems with different different Doppler frequencies f_D and data rates D.

4.3 FSMC for Vector MIMO Metrics: Joint Eigenvalue Behavior

The main interest of this section lies in the joint behavior of multiple eigenmodes. Hence, instead of the scalar processes considered in the last section, FSMC construction for a vector process is carried out here. For SVD-based MIMO systems, adaptive modulation over multiple eigenmodes can be applied to further improve the MIMO system throughput [62]. The service process for an adaptive modulation system is simply the modulation selection over time [123]. Here, we construct a FSMC for the service process by using the joint PDF (4.13) to compute the transition probabilities between states. Using (4.4), we set $\Upsilon = \rho$ and $\Omega = \sqrt{1-\rho^2}$ for the time-varying channel model and assume that the time variation is governed by the ACF $\rho = J_0(2\pi f_D \tau)$. Additionally, λ_i and $\widehat{\lambda}_i$ are the eigenmode gains at time t and $t+\tau$ respectively. We consider a MIMO channel with two antennas at the transmitter and four antennas at the receiver in an i.i.d. Rayleigh flat fading environment ($m = 2$ and $n = 4$). The joint PDF (4.13) for this particular case is simply (4.14) shown at the end of Section 4.1.2.

Assuming five modulation options: BPSK, QPSK, 8-PSK, 16-QAM or outage (no transmission), there are 15 possible modulation pairs over the two eigenmodes, as tabulated in Table 4.2.

We use particular SNR levels as modulation switching thresholds. These thresholds are the minimum SNR levels required for each modulation scheme to achieve a target BER, p_e, of 10^{-3}. Assuming that the transmission power is evenly distributed and the SNR on both eigenmodes is 9dB (normalized noise level), the minimum eigenmode gains required for these modulation types can be calculated by the approximate method for $\mathcal{M}$-PSK in [124]:

$$\lambda_{MPSK} \approx -\frac{1}{8} \ln\left(4\, p_e\right) 2^{1.94 \frac{\ln(\mathcal{M})}{\ln(2)}}. \tag{4.33}$$

State	λ_1	λ_2
1	Outage	Outage
2	BPSK	Outage
3	BPSK	BPSK
4	QPSK	Outage
5	QPSK	BPSK
6	QPSK	QPSK
7	8-PSK	Outage
8	8-PSK	BPSK
9	8-PSK	QPSK
10	8-PSK	8-PSK
11	16-QAM	Outage
12	16-QAM	BPSK
13	16-QAM	QPSK
14	16-QAM	8-PSK
15	16-QAM	16-QAM

Table 4.2: Possible modulation scheme pairs for adaptive MIMO systems with two eigenmodes

Modulation	Corresponding Eigenmode Gain Regions
Outage	$0 \leq \lambda < 0.3310$
BPSK	$0.3310 \leq \lambda < 1.2702$
QPSK	$1.2702 \leq \lambda < 4.8738$
8-PSK	$4.8738 \leq \lambda < 6.6229$
16-QAM	$6.6229 \leq \lambda$

Table 4.3: Corresponding eigenmode gain regions for different modulation methods

Also, for square $\mathcal{M}$-QAM [125]:

$$\lambda_{MQAM} \approx -\frac{2\,(\mathcal{M}-1)\ln(5\,p_e)}{3}. \tag{4.34}$$

The regions are calculated and summarized in Table 4.3.

To compute the probability, P_{ij}, that state i transits to j after time τ, serial integration of the joint PDF (4.13) is required. For example, if $a \leq \lambda_1 < b$, $c \leq \lambda_2 < d$ holds for state i, and $e \leq \widehat{\lambda}_1 < f$, $g \leq \widehat{\lambda}_2 < h$ holds for state j, then

$$P_{ij} = \frac{P(i,j)}{P(i)} = \frac{\int_g^h \int_c^d \int_e^f \int_a^b f(\widehat{\lambda}_1, \widehat{\lambda}_2, \lambda_1, \lambda_2)\, d\lambda_1\, d\widehat{\lambda}_1\, d\lambda_2\, d\widehat{\lambda}_2}{\int_c^d \int_a^b f(\lambda_1, \lambda_2)\, d\lambda_1\, d\lambda_2}\,. \tag{4.35}$$

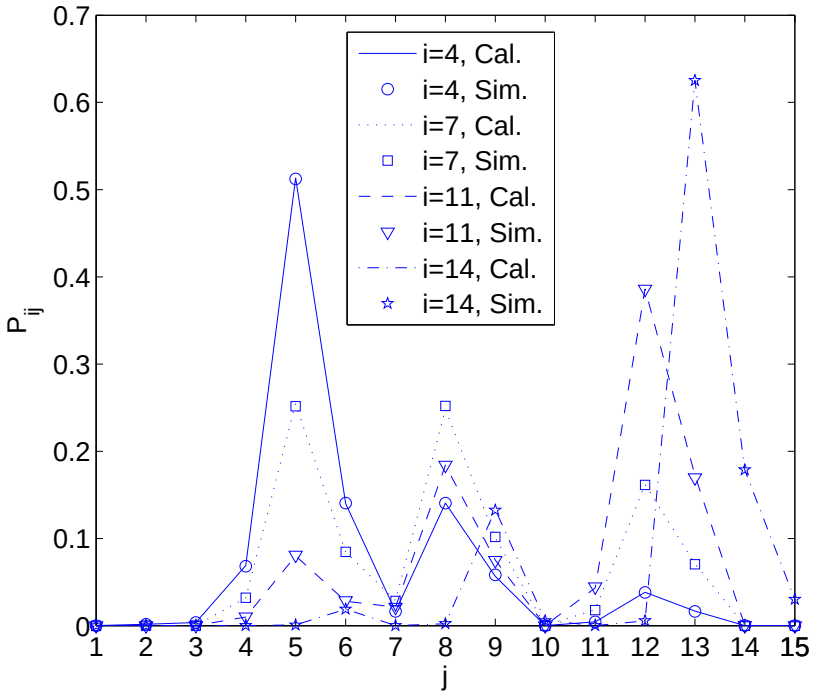

Figure 4.15: Simulated vs. calculated transition probabilities from state i to state j, with $i = 4, 7, 11$, and 14. Mobility level, $f_D\tau = 0.1325$.

This is equivalent to (4.16). Note that $P(i, j)$ and $P(i)$ are the steady state probabilities. The boundary values of the integrals a, b, ..., h, may depend on λ_i or $\widehat{\lambda}_i$. For example, P_{11} involves integrating over the regions $0 < \lambda_2 < \lambda_1 < 0.3310$ and $0 < \widehat{\lambda}_2 < \widehat{\lambda}_1 < 0.3310$. In all cases, calculation of a, b, ..., h is straightforward and is omitted here. Hence, by numerical integration of (4.35) we can calculate the probabilities for all transitions. Selected results are shown in Fig. 4.15. The simulations were carried out using $f_D\tau = 0.1325$ and 2×10^6 samples in total. Clearly, the calculations agree well with the simulations. For larger systems, such an approach may become prohibitive due to the need for a large number of integrations. However, for applications where only a few eigenvalues are of interest, the numerical calculations are quite rapid and stable to compute. The transition probabilities in (4.35) can be used to assess the temporal behavior of the system, as shown in the following sections.

4.3.1 MSER and ASD

In [126], the simultaneous LCR for multiple eigenmodes was approximated by crudely assuming that the eigenmodes are multiple independent processes as in [127][2] . This approach gauges how often multiple eigenmodes enter the outage state simultaneously. In other words, the system is partitioned into two states only: *all below the thresholds* and *otherwise*. Thus, the method in [126] only allows us to determine how often state 1 (outage for all eigenmodes) occurs while all other possible states are not examinable. Fortunately, with the joint PDF, (4.13), derived earlier in this chapter, we can perform a more exact analysis of the joint temporal behavior of the eigenmodes with better accuracy and applicability. In particular, it enables the evaluation of modulation state entering rates, denoted MSER_i, which is defined as the number of times per second that the channel enters a particular state i from any other state. Based on the adaptive system described in this section, it is simple to show that the MSER_i can be written as

$$\mathrm{MSER}_i = \sum_{i \neq j} \frac{P(j)}{\tau} \times P_{ji} = \frac{\sum_{i \neq j} P(i,j)}{\tau}. \tag{4.36}$$

A comparison between calculated and simulated MSER_i values is shown in Fig. 4.16. It is clear that certain states are much more likely to be entered than others.

To determine how long the channel stays in the state i, the ASD needs to be evaluated. This is trivial to calculate since

$$\mathrm{ASD}_i = \frac{P(i)}{\mathrm{MSER}_i}. \tag{4.37}$$

Our results are shown in Fig. 4.17. The MSER and ASD are key parameters for setting the feedback/adaptation rate.

[2]Note that such an assumption does not reflect reality as the eigenmode processes are in fact dependent.

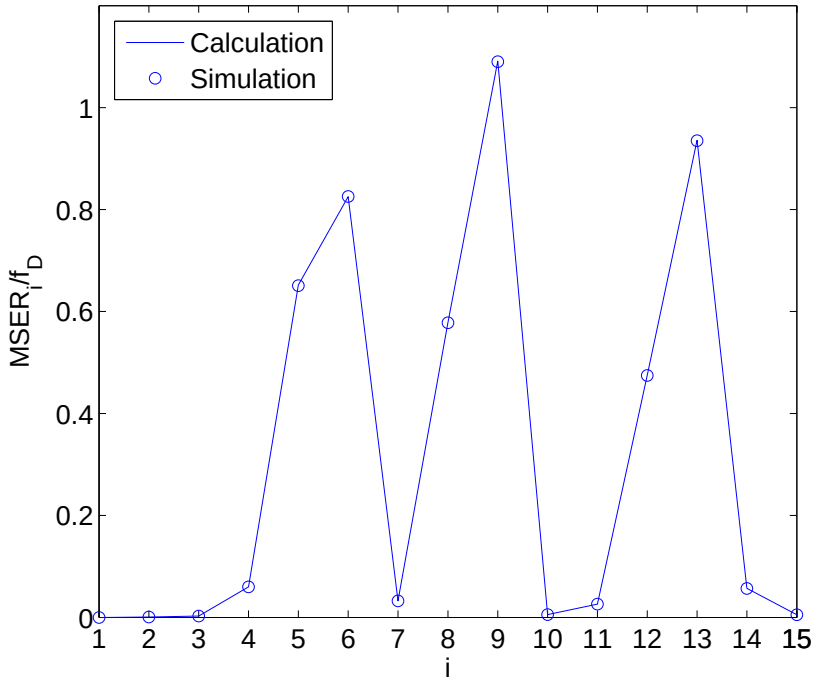

Figure 4.16: Simulated vs. calculated modulation state entering rates.

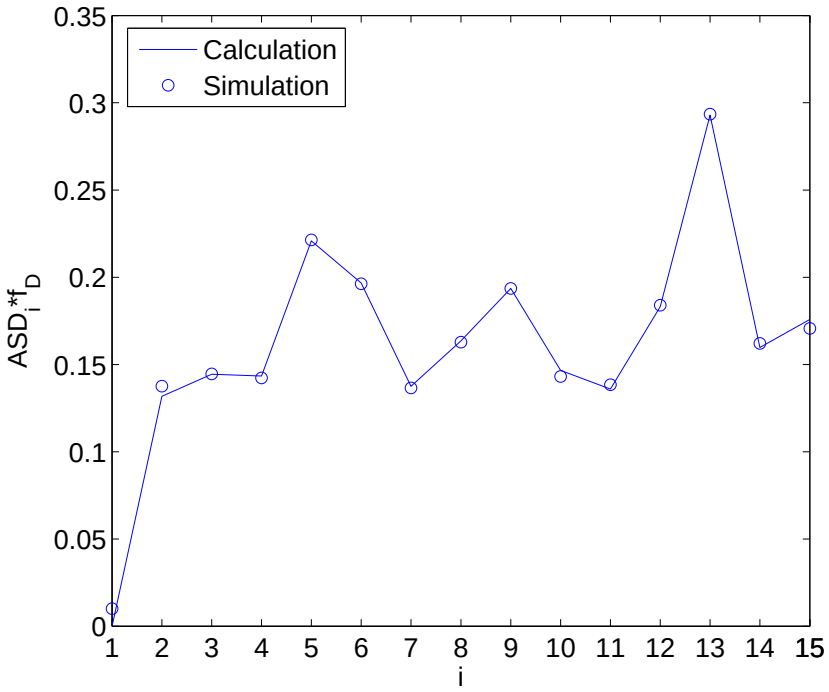

Figure 4.17: Simulated vs. calculated average stay durations.

4.3.2 Impact of Feedback Delay

Using the FSMC model, we now investigate the impact of mobility on the probability of modulation state selection error (MSSE) for state i, denoted $P_{\text{MSSE},i}$. This is the probability that an inappropriate modulation state is chosen because the channel has changed from state i to another state during the feedback interval τ. This probability can easily be written as:

$$P_{\text{MSSE},i} = 1 - P_{ii}\,. \tag{4.38}$$

The idea is the same as in (4.25). We have generated $P_{\text{MSSE},i}$ for two different mobility levels: $f_D\tau = 0.0663$ (moderate mobility) and $f_D\tau = 0.1325$ (high mobility). The results plotted in Fig. 4.18 show that such moderate mobility levels can have a significant impact on modulation selection. The probabilities of choosing an inappropriate modulation state are surprisingly high. The adaptive system is particularly sensitive to time-variation when the eigenmodes occupy certain states (e.g., when $i = 1, 2, 3, 4, 7$, and 10). We observe that when the system is in state 1 (outage for both eigenmodes), it is almost guaranteed that the channel will switch to another state during the feedback period. Fortunately, from the transition probability calculations, we see that the chance of entering state 1 in the first place is very slim.

4.4 Summary

This chapter considers the feasibility of using a first-order FSMC to model adaptive MIMO systems. The models have been applied to characterize the impact of feedback delay in terms of adaptation errors. The metrics that have been investigated include capacity, condition number and the joint eigenvalue behavior. Our investigation has provided further insight into the time-varying characteristics of MIMO channels.

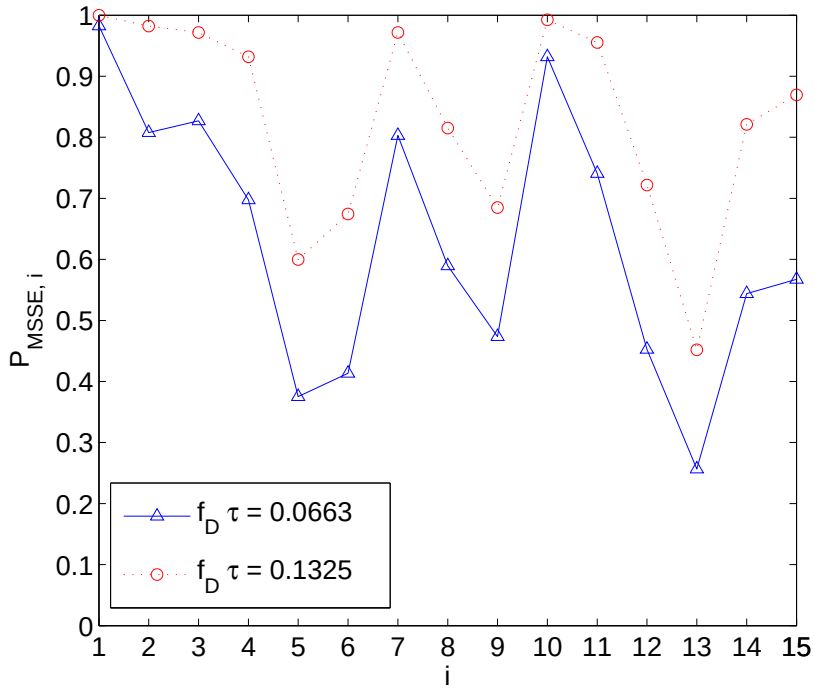

Figure 4.18: The probabilities of MSSE for two mobility levels: $f_D\tau = 0.0663$ and $f_D\tau = 0.1325$.

In the context of MIMO systems research, we often need to model changes in the channel due to temporal or frequency variation and imperfect estimation. This can often be modeled by a Gaussian perturbation. The joint PDF for the eigenvalues of the original and the perturbed channel has been derived at the beginning of this chapter. This joint PDF is then applied as an important tool in FSMC constructions for several MIMO channel metrics.

For rate-feedback systems, we have constructed a FSMC model for the MIMO channel capacity. In order to determine the transition probabilities from one rate-state to another during the feedback period, both conditional probability and LCR methods are invoked. This allows an analytical evaluation of PORAE, and reasonably high levels of incorrect rate selection are observed for moderate feedback delays.

We have also used a FSMC to model the MIMO channel condition number. This is motivated by dual-mode antenna selection, which quantizes the condition number into two states: multiplexing ($\mathcal{S}_1$) and diversity ($\mathcal{S}_2$). Based on an accurate gamma approximation, we have also attempted both the conditional probability method and the LCR method to compute the transition probabilities. Both methods provide good accuracy. Furthermore, the model is applied to study the impact of feedback delay on the adaptation errors. The effects of increasing N_r, f_D and D are also examined.

Finally, our joint PDF has been employed to compute the transition probabilities between modulation states in a MIMO-SVD system. The system is modeled as a FSMC with each state represented by a vector of multiple eigenvalues. From the resultant FSMC, we have analytically computed the MSER and ASD. Results show that system mobility can dramatically affect the adaptive modulation selection performance due to the time-correlated Rayleigh channel changing rapidly in certain states.

Chapter 5

Impacts of Feedback Delay on MIMO-SVD Transceivers

In the preceding chapters, the existence of decoupled scalar channels (eigenmodes) has been shown and discussed. This has inspired the use of singular value decomposition (SVD)-based MIMO transceiver architectures [26, 55]. Since multiple independent data streams can be transmitted simultaneously through these uncoupled eigenmodes, the overall data rate can be improved significantly. The error performance of such a system has been analyzed in [128] under idealized conditions. Also, [129] has characterized the performance of the MIMO-SVD system when it is applied in cellular networks.

As discussed earlier, a MIMO-SVD transceiver requires the transmitter to obtain channel state information (CSI) from the receiver with the aid of a feedback link. In practice, neither end of the link acquires perfect CSI. There are two main impairments to the CSI accuracy: channel estimation error and feedback time delay [130]. In general, with imperfect CSI, the steering matrices (or weight matrices) at both ends are not able to completely decouple the eigenmodes. In this situation, the SVD transmission will experience additional self-interference [131]. The mean capacity of such systems was approximated in [132] assuming an extremely large or small channel estimation error, but the effect of feedback delay was not considered. The influence of imperfect channel

knowledge on the probability of error has been studied in [133] by means of simulation. In [134], a thorough analysis of this issue was undertaken, but it was assumed that the interference is spread evenly over all eigenmodes. By assuming that self-interference power is Gaussian, an accurate prediction of BER in MIMO-SVD systems has been reported in [135].

The goal of this chapter is to explicitly characterize the instantaneous loss in signal power and the introduction of interference due to the mismatch between the true and estimated steering matrices. For the sake of simplicity, we concentrate on the effects of feedback delay by assuming that the receiver tracks the channel perfectly (that is, channel estimation error is excluded, as in [136]). However, the analysis can be extended to cases with channel estimation error using the same principle, at the expense of more cumbersome calculations.

We analytically derive the instantaneous signal and interference power for eigenmode transmission with feedback delay in this chapter. Hence, we can approximate the instantaneous signal to interference noise ratio (SINR). Based on these expressions, two novel metrics which we describe as an *interference factor* and a *relative loss factor*, are identified and proposed. With these novel metrics, the sensitivity to time-variations of the steering matrices can be gauged by observing the eigenvalues of the instantaneous channel correlation matrix.

5.1 MIMO-SVD Systems with Feedback Delay

The operation of a MIMO-SVD transceiver has been explained in Section 2.3.2 in detail. As a result, by using the SVD, the input-output relationship of a

MIMO system can be written as

$$\boldsymbol{Y'} = \Sigma \boldsymbol{X'} + \boldsymbol{n'}. \tag{5.1}$$

To study the effect of feedback delay in such systems, the length of feedback delay is defined to be τ. We also assume that the temporal behavior of the channel coefficients is governed by the Jakes process with an auto-correlation function (ACF) $\rho(\tau) = J_0(2\pi f_D \tau)$. Hence, $\rho(\tau)$ is the ACF at lag τ which controls the change in the channel during the feedback delay. Note that the results in this chapter can be extended to arbitrary types of ACF. We assume that perfect CSI is available at the receiver, while outdated channel information, delayed by τ, is possessed by the transmitter. Thus, with the addition of a time index, (5.1) becomes

$$\widehat{\boldsymbol{Y}}(t) = \Sigma(t)\boldsymbol{V}^{\dagger}(t)\boldsymbol{V}(t-\tau)\,\boldsymbol{X}(t) + \widetilde{\boldsymbol{n}}(t). \tag{5.2}$$

Clearly, the system cannot exactly diagonalize the channel due to the mismatch between $\boldsymbol{V}(t)$ and $\boldsymbol{V}(t-\tau)$. Hence the diagonal Σ in (5.1) is replaced by $\Sigma(t)\boldsymbol{V}^{\dagger}(t)\boldsymbol{V}(t-\tau)$. In Section 5.2.3 we will show that this has the effect of reducing the signal power and creating self-interference.

5.2 Signal and Interference Power Characterizations

In the last section, the effects of feedback delay on MIMO-SVD systems were explained. There are two main effects: the loss of signal power and the introduction of interference in the eigenmode transmissions. The goal of this section is to analytically approximate the instantaneous power of both components in any particular eigenmode transmission. To do this, it is necessary to use some results on Brownian matrices [98]. We develop these now.

5.2.1 Bru's Theorem

Consider a matrix $\boldsymbol{B}$, the entries of which are i.i.d. real Brownian motions. Bru [98] has derived a stochastic differential equation (SDE) for the elements of the eigenvectors of $\boldsymbol{B}^T(t)\boldsymbol{B}(t)$. Defining $\widetilde{\boldsymbol{V}}(t) = [\widetilde{v}_{ij}(t)]$ as the matrix of eigenvectors with $\widetilde{v}_{ij}(t)$ being the i^{th} element of the j^{th} eigenvector of $\boldsymbol{B}^T(t)\boldsymbol{B}(t)$, we have [98]:

$$d\widetilde{v}_{ij}(t) = \sum_{k\neq j} \widetilde{v}_{ik}(t)\sqrt{\frac{w_k(t)+w_j(t)}{[w_k(t)-w_j(t)]^2}}\, d\widetilde{B}_{kj}(t) - \frac{1}{2}\,\widetilde{v}_{ij}(t)\sum_{k\neq j}\frac{w_k(t)+w_j(t)}{[w_k(t)-w_j(t)]^2}\, dt, \tag{5.3}$$

where $\widetilde{B}_{kj}(t)$ are independent Brownian motions and $w_i(t)$ are the eigenvalues of $\boldsymbol{B}^T(t)\boldsymbol{B}(t)$.

5.2.2 A Modified SDE

In this paper, we are interested in the matrix $\boldsymbol{V}(t)$ containing the eigenvectors of $\boldsymbol{H}^{\dagger}(t)\boldsymbol{H}(t)$. The elements of $\boldsymbol{H}(t)$ are complex Gaussians with unit variances, so the SDE (5.3) must be modified to accommodate our requirements. According to [99, 137], the drift (the term containing dt) in the SDE for Wishart matrix eigenvalues is doubled for the complex Wishart case. This is also applicable to the eigenvector SDE, so the factor of $\frac{1}{2}$ in (5.3) is removed. Following the same arguments as in Chapter 3, the Brownian entries in $\boldsymbol{B}(t)$ have to be standardized. We replace w_i with $2t\lambda_i$, and look at the particular time point $t = \tau\,[J_0(2\pi f_D\tau)^{-2} - 1]^{-1}$, which in turn gives $\tau/t \approx 2\pi^2 {f_D}^2\tau^2$. After some algebra, the Euler approximation to the modified SDE is given by

$$\Delta v_{ij}(t) = \sqrt{2}\pi f_D\tau\sum_{k\neq j} v_{ik}(t-\tau)\sqrt{\frac{\lambda_k(t-\tau)+\lambda_j(t-\tau)}{[\lambda_k(t-\tau)-\lambda_j(t-\tau)]^2}}\, Z_{kj} - \pi^2 {f_D}^2\tau^2 v_{ij}(t-\tau)\sum_{k\neq j}\frac{\lambda_k(t-\tau)+\lambda_j(t-\tau)}{[\lambda_k(t-\tau)-\lambda_j(t-\tau)]^2}, \tag{5.4}$$

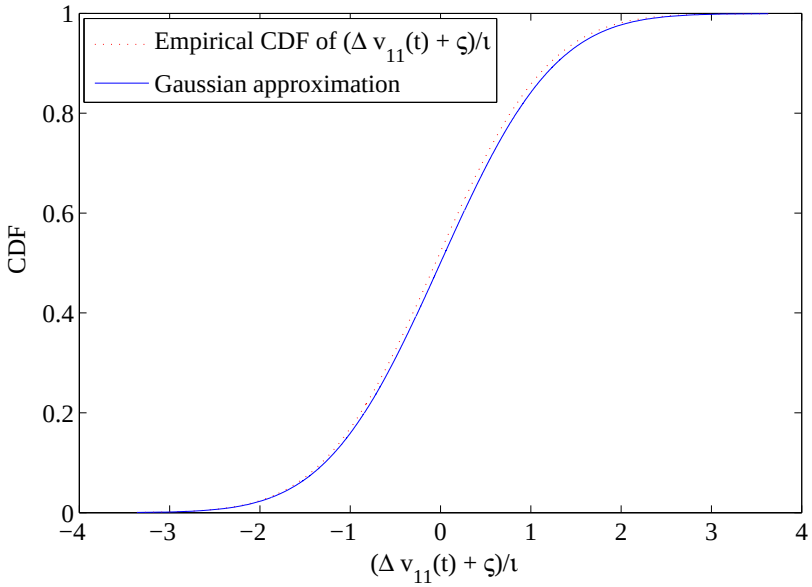

Figure 5.1: A numerical verification of the SDE.

where $\Delta v_{ij}(t) = v_{ij}(t) - v_{ij}(t-\tau)$. Note that $v_{ij}(t)$ represents the j^{th} entry of the i^{th} row of $\boldsymbol{V}$(t), and $\lambda_i(t)$ are the eigenvalues of $\boldsymbol{H}^{\dagger}(t)\boldsymbol{H}(t)$. Furthermore, Z_{kj} is a family of complex Gaussian random variables with zero mean and unit variance, independent of each other and of the $\lambda_i(t)$ processes.

The eigenvector process has been assumed to be continuous in [98], but due to the non-uniqueness of eigenvectors, continuity of the eigenvector process is not guaranteed during computation. Hence, to deal with this issue, we always rotate the first element of the eigenvectors to a common reference axis (the positive real-axis is employed for convenience), to ensure the continuity. In order to confirm the validity of (5.4), we write (5.4) in the form of $\Delta v_{ij}(t) = \iota Z_{kj} - \varsigma$. Then, we inspect the empirical distribution of $(\Delta v_{ij}(t) + \varsigma)/\iota$, which should be approximately Gaussian with zero mean and unit magnitude variance. The results in Fig. 5.1 were obtained from the SDE for $dv_{11}(t)$ in a (2,2) system. As can be seen, the simulated values of $(\Delta v_{ij}(t) + \varsigma)/\iota$ match the Gaussian extremely well. Similar results were obtained for the other eigenvector elements $v_{12}(t)$, $v_{21}(t)$ and $v_{22}(t)$ in the (2,2) case and also for larger systems.

5.2.3 Derivation of the SINR

In this section, we show how the SDE can be applied to derive the SINR in the presence of feedback delay. If (5.4) is re-written in matrix notation, we have

$$\Delta \boldsymbol{V} = \boldsymbol{V}(t) - \boldsymbol{V}(t-\tau) \approx \boldsymbol{V}(t-\tau)\boldsymbol{A}(t-\tau). \tag{5.5}$$

In equation (5.5), some terms have time index t and some have index $t-\tau$. In order to simplify notation, in the rest of the chapter we denote the eigenvalues at time t by $\widehat{\lambda}_i$ and at time $t-\tau$ by λ_i. The elements a_{ij} of $\boldsymbol{A}(t-\tau)$ are given by

$$a_{ij} = \begin{cases} -\pi^2 {f_D}^2 \tau^2 \sum_{k \neq j} \frac{\lambda_k + \lambda_j}{(\lambda_k - \lambda_j)^2}, \; i = j \\ \\ \sqrt{2}\pi f_D \tau \sqrt{\frac{\lambda_k + \lambda_j}{(\lambda_k - \lambda_j)^2}} Z_{kj}, \quad i \neq j. \end{cases}$$

Rewriting (5.5), we have $\boldsymbol{V}(t) = \boldsymbol{V}(t-\tau) + \Delta \boldsymbol{V}$. Thus,

$$\boldsymbol{V}^{\dagger}(t) \approx [\boldsymbol{I} + \boldsymbol{A}(t-\tau)]^{\dagger} \boldsymbol{V}(t-\tau)^{\dagger} \tag{5.6}$$

where $\boldsymbol{I}$ is the identity matrix. Equation (5.6) can be substituted into (5.2), so the overall system equation becomes

$$\begin{aligned} \widehat{\boldsymbol{Y}}(t) &\approx \Sigma(t)[\boldsymbol{I} + \boldsymbol{A}(t-\tau)]^{\dagger} \boldsymbol{V}(t-\tau)^{\dagger} \boldsymbol{V}(t-\tau)\boldsymbol{X}(t) + \boldsymbol{n'}(t) \\ &= \Sigma(t)[\boldsymbol{I} + \boldsymbol{A}^{\dagger}(t-\tau)]\boldsymbol{X}(t) + \boldsymbol{n'}(t). \end{aligned} \tag{5.7}$$

Therefore, it is easy to show that the received signal on the i^{th} eigenmode is given by

$$\widehat{y}_i(t) \approx \sqrt{\widehat{\lambda}_i}\,[(1 + a_{ii}^*)\, x_i(t) + \sum_{j \neq i} a_{ji}^* x_j(t)] + \widetilde{n}_i(t). \tag{5.8}$$

As the signal and interference components are now explicitly identified in (5.8), their power can be derived. In order to simplify the expressions, we assume that all data, x_i, have $\mathrm{E}|x_i|^2 = 1$. In this situation, the instantaneous desired

signal and interference powers, S_i and I_i respectively, are given by

$$\begin{aligned} S_i &\approx \widehat{\lambda}_i \mathrm{E}(|1 + a_{ii}^*|^2) \\ &= \widehat{\lambda}_i \mathrm{E}(1 + a_{ii} + a_{ii}^* + |a_{ii}|^2) \\ &\approx \widehat{\lambda}_i \left[1 - 2\pi^2 {f_D}^2 \tau^2 \sum_{k \neq i} \frac{\lambda_k + \lambda_i}{(\lambda_k - \lambda_i)^2} \right] \end{aligned} \tag{5.9}$$

and

$$\begin{aligned} I_i &\approx \widehat{\lambda}_i \mathrm{E}\left[\sum_{j \neq i} |a_{ji}|^2 \right] \\ &= 2\pi^2 {f_D}^2 \tau^2 \widehat{\lambda}_i \sum_{j \neq i} \frac{\lambda_j + \lambda_i}{(\lambda_j - \lambda_i)^2}, \end{aligned} \tag{5.10}$$

where we have averaged over the signal and noise but conditioned on the channel matrix $\boldsymbol{H}$ at time $t-\tau$ and at time t. Note that we have ignored $|a_{ii}|^2$ in (5.9) because it involves τ^4 and τ is assumed to be small enough to guarantee that $|a_{ii}| << 1$. In scenarios where the eigenvalues are close together the size of $|a_{ii}|$ will increase and smaller values of τ may need to be assumed. However, simulations indicate that this effect does not cause a problem. Hence, the instantaneous SINR is given by

$$SINR_i \approx \frac{\widehat{\lambda}_i \left[1 - 2\pi^2 {f_D}^2 \tau^2 \sum_{k \neq i} \frac{\lambda_k + \lambda_i}{(\lambda_k - \lambda_i)^2} \right]}{N_0 + 2\pi^2 {f_D}^2 \tau^2 \widehat{\lambda}_i \sum_{j \neq i} \frac{\lambda_j + \lambda_i}{(\lambda_j - \lambda_i)^2}}. \tag{5.11}$$

Note that the loss in signal power is exactly the same as the induced interference and both are proportional to $(f_D \tau)^2$.

To verify these expressions, a set of simulations has been performed. We set a feedback delay of 0.1ms and compared our analytical results, from (5.9) to (5.11), against simulation data for the signal power, interference power and SINR. Excellent agreement was found in all cases, and the SINR comparison is shown in Fig. 5.2 for $SINR_1$ in a (2,2) system. In Fig. 5.2 we simulated 20 independent channel matrices at times $t-\tau$ and t. This yields 20 independent SINR values using (5.11). These analytical SINR values were then verified

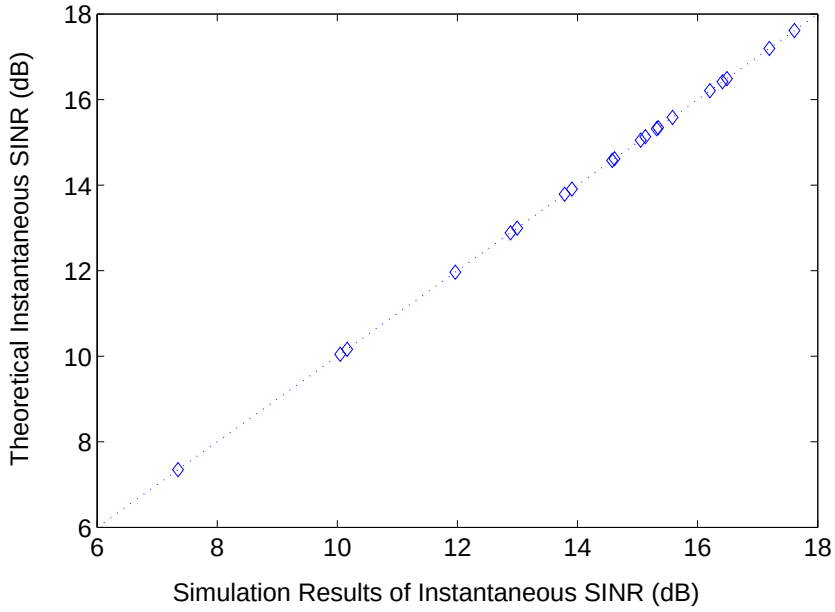

Figure 5.2: A comparison between the analytical SINR result and simulated results.

by simulation in the following way. Fixing the channels at time $t - \tau$ we then generate 1,000 values of the channel at time t using independent Jakes processes and calculate the average SINR by simulation for each of the 20 cases.

5.2.4 The Case with $m = 2$

Some useful conclusions can be drawn from an inspection of the case with $m = 2$. The signal power loss on the first eigenmode is the same as the interference on the first eigenmode and is equal to $I_1 = 2\pi^2 f_D^2 \tau^2 \widehat{\lambda}_1 (\lambda_1 + \lambda_2)(\lambda_1 - \lambda_2)^{-2}$. On the second eigenmode, we have the the signal power loss $I_2 = 2\pi^2 f_D^2 \tau^2 \widehat{\lambda}_2 (\lambda_1 + \lambda_2)(\lambda_1 - \lambda_2)^{-2}$. Since $\widehat{\lambda}_1 > \widehat{\lambda}_2$, we have $I_1 > I_2$, and typical eigenmode traces over time show many occasions when $\widehat{\lambda}_1 >> \widehat{\lambda}_2$, leading to $I_1 >> I_2$. Although the absolute loss in signal power is greater for the first eigenmode, the relative loss is identical, since $I_1/\widehat{\lambda}_1 = I_2/\widehat{\lambda}_2$. The assumption in [134] that signal

power loss in one eigenmode is spread equally over all the other eigenmodes as interference is not valid here. However, the work in [134] focussed on a more complex scenario where such an approximation might be more reasonable. The effect of interference on the different eigenmodes is considered in more detail later.

5.2.5 Sensitivity Characterization

The instantaneous SINR contains a power loss factor and an interference factor which are shown to be equal. This common factor is proportional to the square of the feedback delay. The proportionality constant is independent of the feedback delay, and its behavior is dependent on the radio channel.

From the results in the previous section, we have observed the following. If f_D and τ are assumed to be constant, both the loss in signal power and the magnitude of the interference power are proportional to the value of

$$Q_i = \widehat{\lambda}_i \sum_{k \neq i} \frac{\lambda_k + \lambda_i}{(\lambda_k - \lambda_i)^2}. \tag{5.12}$$

In other words, the SINR on the i^{th} eigenmode degrades more severely with larger values of Q_i. This parameter can be identified as an *interference factor*. Note the expression for Q_i involves eigenvalues at two different time instants. To avoid this complication, we can use the relative power loss, $I_i/\widehat{\lambda}_i$, to determine the system sensitivity to feedback delay. In (5.9) and (5.10), if f_D and τ are both assumed to be constants, it is easy to see that relative power loss in the i^{th} eigenmode $(\widehat{\lambda}_i)$ due to feedback delay is proportional to the factor

$$G_i = \sum_{k \neq i} \frac{\lambda_k + \lambda_i}{(\lambda_k - \lambda_i)^2} \tag{5.13}$$

which is entirely expressed in terms of eigenvalues at one time instant. While Q_i assesses the magnitude of the interference directly, G_i gives the relative power loss due to feedback delay. Therefore, the *relative loss factor* (5.13),

can be used as an alternative measure of the sensitivity to feedback delay with a simpler expression.

From both (5.12) and (5.13), we can infer that one of the worst scenarios is when two eigenvalues are close to each other. In particular, the proportionality constant contains terms which are inversely proportional to the difference between eigenvalues. Therefore, at times when this difference is small, there is a corresponding increase in the power loss and the interference. This can be explained using the notion of a *repelling force*, which has been mathematically interpreted from the drift term of the eigenvalue SDE [137]. The denominator of the drift term in the SDE demonstrates the phenomenon that eigenvalues tend to repel and move away from each other if they are close together. The whole eigen-structure experiences dramatic change at that time. Thus, rapid changes in the eigenvectors caused by repelling eigenvalues may result in large differences between the true and outdated steering matrices. Therefore, the loss in signal power and the induced interference power are particularly significant when eigenvalues are close to each other. Similar observations have been made in [113, 138, 139, 140], where it was noted that a small variation in the channel can result in major shifts in the steering matrices, especially when two singular values (and therefore eigenvalues) are of a similar magnitude.

The occurrence of large G_i values can be predicted from an inspection of the joint density function of the eigenvalues given in (2.15). The mean of G_i exists since its denominator cancels with the numerator of $f(\lambda_1, \ldots, \lambda_m)$. The variance of G_i, however, is infinite since it involves $\mathrm{E}(G_i^2)$ and the resulting integral has terms of the form $(\lambda_k - \lambda_i)^{-2}$ leading to a divergent integral. Hence, G_i (and Q_i) has a long tailed distribution and very large values will occur occasionally. As a result, the second order statistics of G_i, such as the ACF and LCR, do not exist. This statement also holds for Q_i for similar reasons.

As discussed in Section 5.2.4, the relative loss on the two eigenmodes is

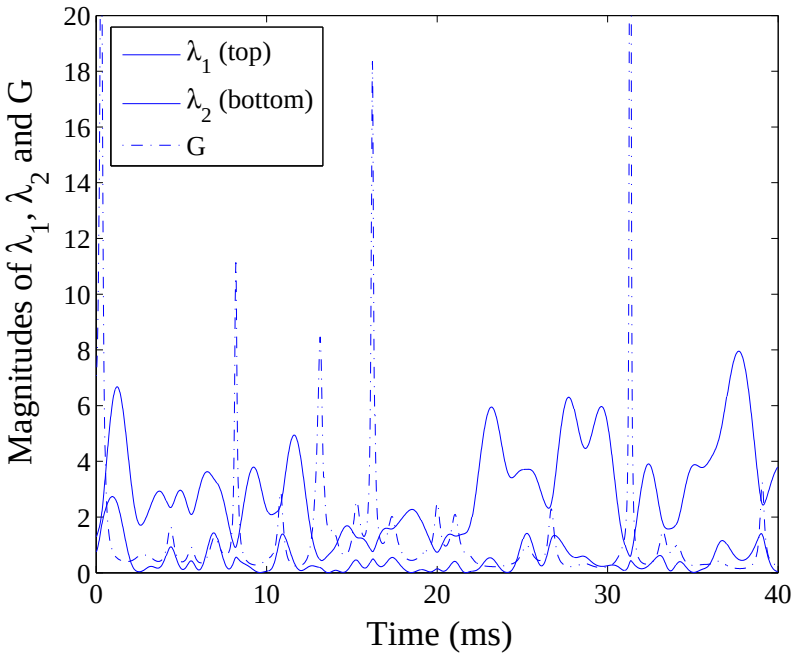

Figure 5.3: A comparison between the instantaneous eigenvalues and the G value in a (2,2) system.

identical for MIMO systems with $m = 2$. Hence we have $G_1 = G_2$. Figure 5.3 shows λ_1, λ_2 and G for a (2,2) system, where $G_1 = G_2 = G$. Clearly seen are the "repelling forces" where $\lambda_1 \approx \lambda_2$ results in a large G value and a divergence of λ values shortly afterwards. Also, note that the largest G peaks are caused by $\lambda_1 + \lambda_2 >> 0$ and $\lambda_1 - \lambda_2 \approx 0$. Hence, in high capacity scenarios where λ_1 and λ_2 are both large and similar in value, there can be very high sensitivity to feedback delay. Additionally, the long tailed nature of G is clear, with a majority of small to moderate values and occasional very large peaks.

For MIMO systems with larger dimensions ($m > 2$), however, the values of both Q and G on every individual eigenmode are different. Figure 5.4 shows Q_1 and Q_4 over time for a (4,4) system, and there is a considerable difference in the interference levels for the largest and smallest eigenmode, with the largest eigenmode experiencing much higher interference. Figure 5.5 shows the percentage power lost to interference (I_i) relative to the original

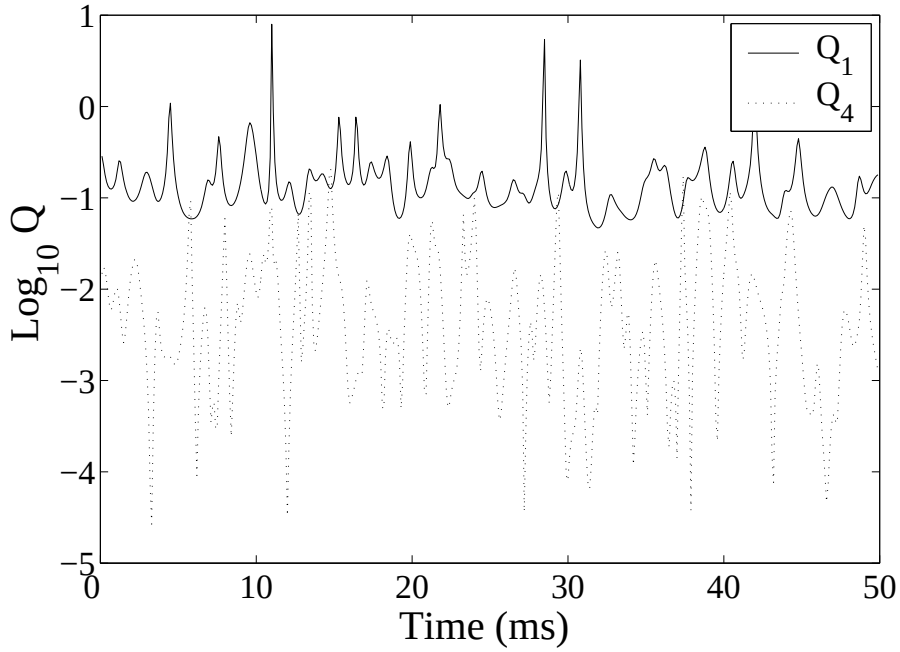

Figure 5.4: An instantaneous comparison between Q_1 and Q_4 in a (4,4) system.

signal power ($\widehat{\lambda_1}$ and $\widehat{\lambda_4}$) in a (4,4) system. The difference in percentage power losses (which is G, assuming normalized $f_D\tau$) between different eigenmodes is less clear, with the smaller eigenmode experiencing more periods of heavy relative interference.

5.3 Simulation Results on BER

In order to illustrate the influence of Q, we have carried out simulations of the strongest eigenmode of several MIMO systems, and examined the relationship between the value of Q and the instantaneous error performance with equal-power BPSK and a feedback delay of 0.1ms. Furthermore, we assume the mobile unit is moving with a speed of 5km/hr and the system carrier frequency is 5.725GHz (HyperLan 2 standard), which gives a Doppler frequency of 26.5Hz. Considering the coherence time corresponding to the Doppler frequency of 26.5Hz, the feedback delay of 0.1ms is very small and will have very little impact on the quality of the channel estimates. However, as discussed

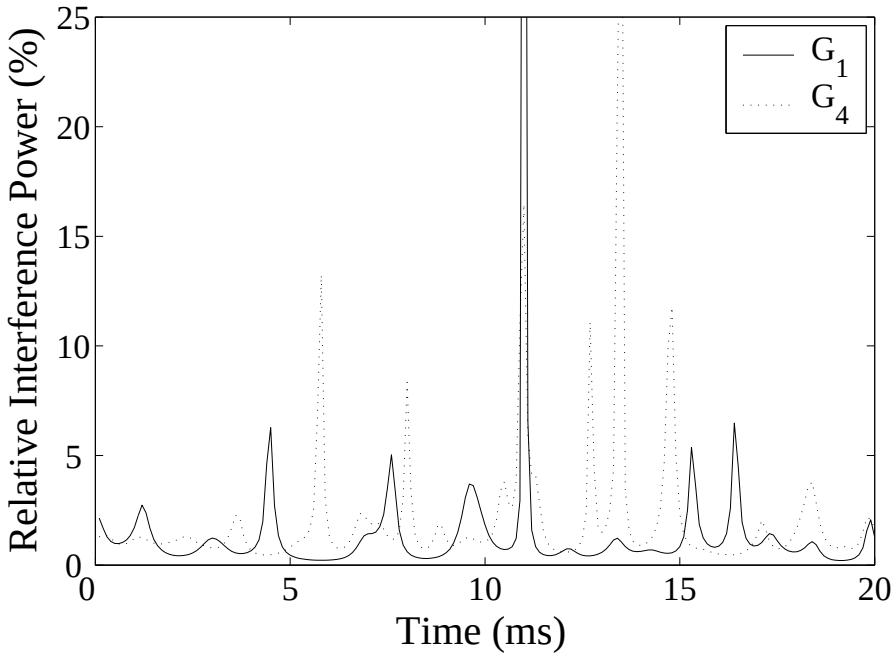

Figure 5.5: The relative power loss (G_i) of the strongest and weakest eigenmodes in a (4,4) system.

earlier, even for small feedback delay, the SINR degrades whenever two or more eigenvalues are nearly the same. The results for (2,2), (2,4) and (4,4) systems are shown in Figs. 5.6, 5.7 and 5.8 respectively. The lower curve is the value of Q and the top curves are the instantaneous BER curves (solid line - with feedback delay, dashed line - perfect CSI). Note that conditioned on λ_1, λ_2, $\ldots$, λ_m, the interference-plus-noise component in (5.8) is Gaussian due to the Z_{kj} terms. Hence, we have a signal in AWGN with SINR given by (5.11), and the corresponding instantaneous error probability is simply $\mathbf{\Phi}(-\sqrt{SINR_i})$ for BPSK. Note that $\mathbf{\Phi}(\cdot)$ is the cumulative distribution function of a standard Gaussian variable.

From Figs. 5.6 - 5.8 we observe that the effect of feedback delay on λ_1 increases as the system size increases. This can be seen from the gap between the BER curves for perfect CSI and delayed CSI. It is clear that the (2,2) system is more impervious to feedback delay than (2,4) and (4,4) systems. Inspection of Figs. 5.6 - 5.8 also shows the relationship between BER and Q.

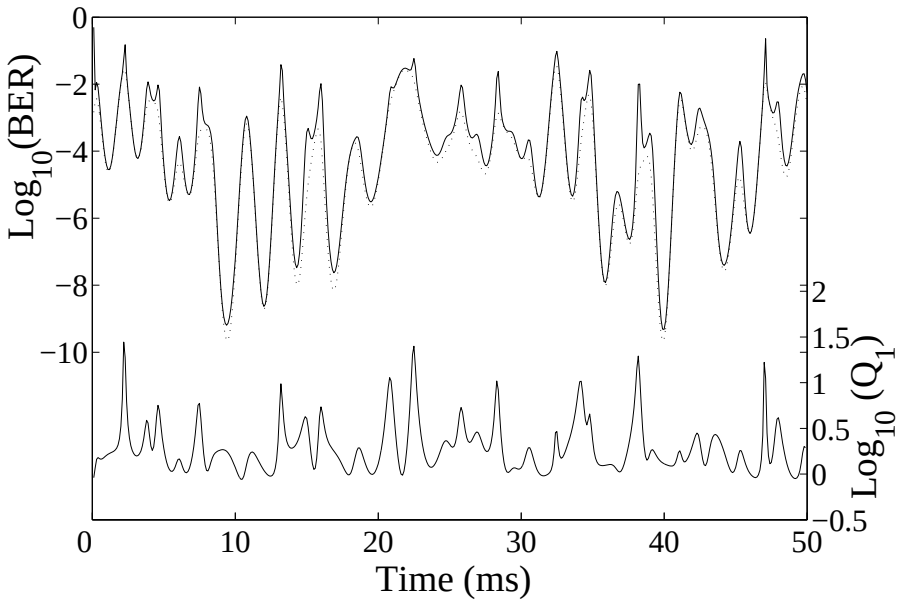

Figure 5.6: A comparison between instantaneous error performance with and without feedback delay in a (2,2) system. Also shown is the interference factor Q_1.

When the BER for delayed CSI peaks at a high value, with a large gap to the perfect CSI case, there is a corresponding peak in the Q_1 value. Furthermore, the average Q_1 value increases from (2,2) to (4,4) systems, and this drives the BER curves further apart. This can also be observed from the analytical result, (5.10), since large system sizes have more terms in the interference factor. Finally in Fig. 5.9 we take a global look at error performance, averaging over the λ values to get average BER results for $\lambda_1, \lambda_2, \lambda_3$ and λ_4 in a (4,4) system. Note that the time delay leads to a floor in BER performance which is most noticeable for λ_1.

5.4 Summary

In this chapter, we have derived novel analytical expressions for the instantaneous signal power, self-interference power and hence the SINR of MIMO eigenmode transmission with feedback delay. These results have been verified

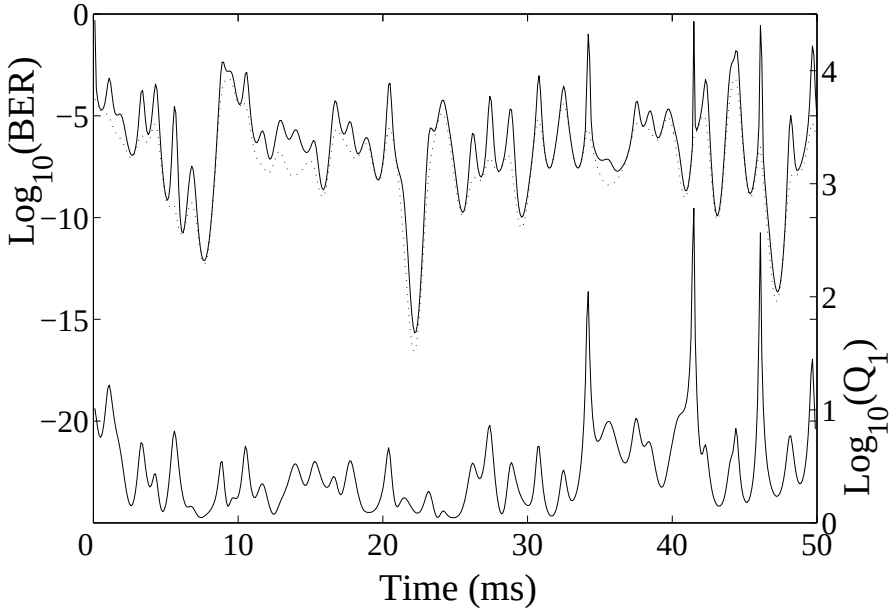

Figure 5.7: A comparison between instantaneous error performance with and without feedback delay in a (2,4) system. Also shown is the interference factor Q_1.

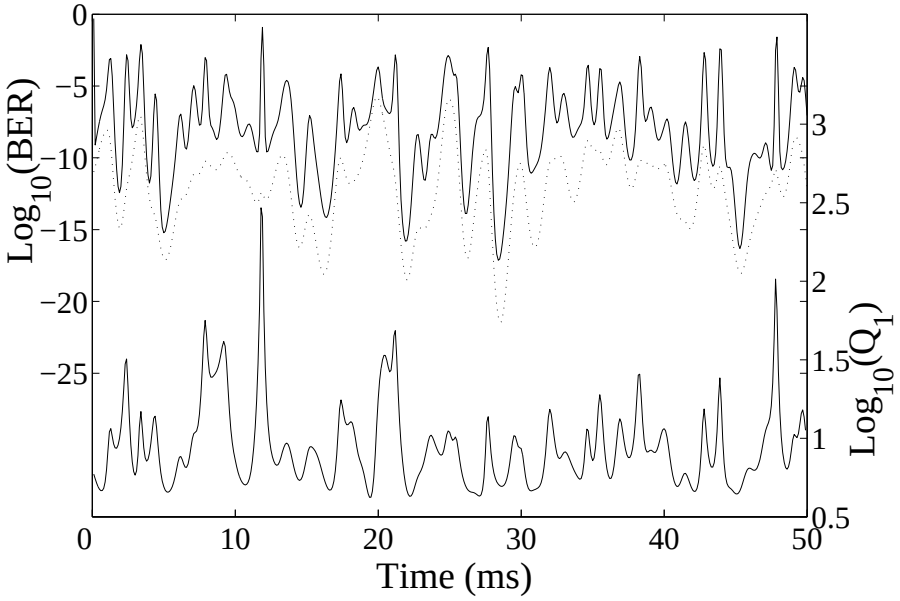

Figure 5.8: A comparison between instantaneous error performance with and without feedback delay in a (4,4) system. Also shown is the interference factor Q_1.

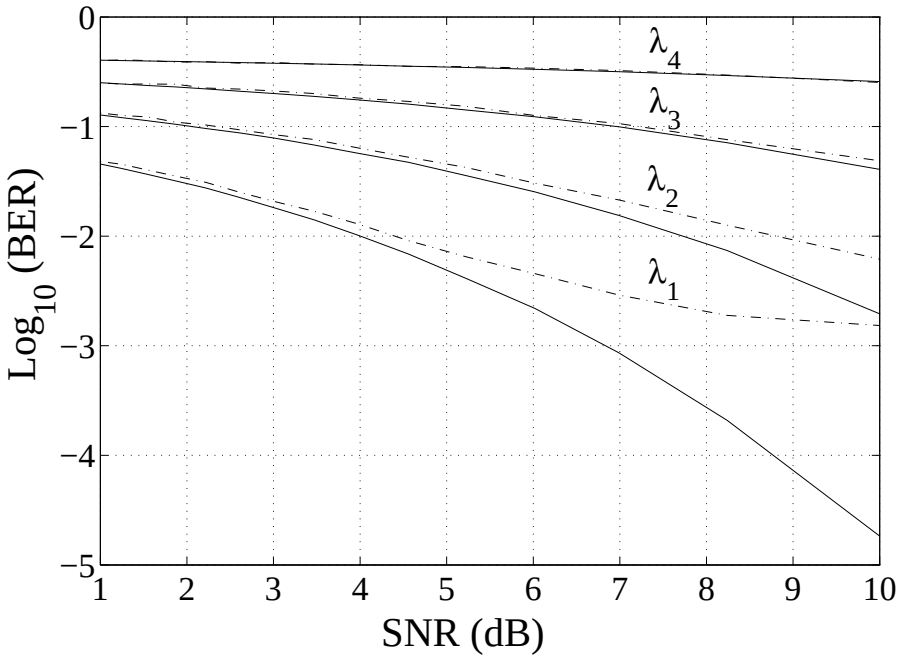

Figure 5.9: The average error probability curve for a (4,4) system. Solid lines and dashed lines represent the behavior without and with feedback delay respectively.

through simulations. From these expressions, it can be shown that the loss in signal power is identical to the induced interference. The instantaneous interference power has been shown to be a Gaussian variable, hence the impact of interference power on the channel can be described as an extra additive Gaussian noise term.

Also, this interference power is proportional to a single number which can be determined using the channel eigenvalues. Thus, we propose this parameter, Q, as a novel channel metric that can be employed to gauge the performance sensitivity to feedback delay. Note that the value of Q depend on eigenvalues at two different time instants. Alternatively, G indicates the relative power loss due to feedback delay, and is nicely expressed in terms of the eigenvalues at one time instant.

Thus, we have identified the effects of feedback delay in terms of a "background effect" proportional to the squared delay which is multiplied by a channel factor which measures the sensitivity of the channel to the delay. This leads to the interesting conclusion that any feedback delay, however small, can result in a degraded SINR if the channel is in a "sensitive" state. It is worth noting that a MIMO system with large similar eigenvalues lead to high capacity and in such situations, with adaptive SVD, the use of the link would be maximized by employing large constellations. Unfortunately, the metrics Q and G imply that this scenario is also the one with the highest interference. Hence, caution may be necessary in switching to higher level schemes.

Using the analytical results we can see an increase in sensitivity to delay as the system size increases and large differences between absolute interference levels in the different eigenmodes. However, the relative interference on the eigenmodes tends to be quite similar. Also, the interference is a long tailed variable which can produce large values at times of high capacity when the link would ideally be operating at high rates.

Chapter 6

OFDM Channel Variation in the Frequency Domain

We have concentrated on the time variations of a narrow band channel in Chapters 3 - 5. In channels with a small coherence bandwidth, however, a multi-carrier air-interface is often used to alleviate time-dispersion and hence mitigate the impacts of frequency selectivity. As shown in Table 1.1, orthogonal frequency division multiplexing (OFDM) is the dominant air-interface in many standards for next generation wireless communication systems. Hence, this technique has been considered in depth in recent decades.

In OFDM systems, the broad bandwidth is split into multiple frequency bins, and independent data streams are transmitted on these parallel links simultaneously. The OFDM signals are modulated via inverse discrete Fourier transforms (IDFT). As a result, the carrier frequency of each sub-channel is a harmonic of the baseband and hence signal orthogonality can be achieved. Each of the subcarriers can be treated as a narrow-band, flat-fading channel. In MIMO-OFDM, the channel response of each subcarrier is a complex matrix $\boldsymbol{H}$ with random entries as in (2.2).

This chapter aims to provide insights into the behavior of OFDM systems. In particular, we are interested in the channel variation over frequency in both SISO and MIMO schemes. Akin to the work in previous chapters, the

investigation of channel fluctuation in the frequency domain is motivated by the use of adaptive schemes that adjust signalling parameters in accordance with the prevailing link quality. The study is divided into two categories, as described below.

Firstly, assume that the link quality is quantized into multiple states and that each state corresponds to a specific modulation mode. Here, we are interested in the distribution of the total number of subcarriers using a certain mode within the entire OFDM block. In this context, a Gaussian approximation based on the central limit theorem (CLT) is proposed. We compute the mean and variance of the distribution analytically to fit this approximation. The results are applied to a few different scenarios in both SISO and MIMO cases.

Secondly, extending the work in Chapter 3, we look at the channel gain fluctuations over frequency. By invoking a similar analysis, the LCR in the frequency domain (denoted LCR_f) can be derived, which also leads to the equivalent of AFD in the frequency domain: the average fade bandwidth (AFB). Such a measure indicates how many successive subcarriers are in deep fades on average. Our scope examines both SISO channel gains and the largest eigenmode in MIMO systems.

6.1 Preliminaries

OFDM originated from the concept of multi-carrier modulation (MCM), which converts an input data streams into several symbol streams with much lower rates which are transmitted simultaneously on multiple subcarriers.

Denote the total bandwidth of an OFDM block by $\mathcal{B}$ Hz, which is divided into M subcarriers. Thus, the frequency spacing between adjacent subcarriers is

$$\triangle f = \frac{\mathcal{B}}{M}. \tag{6.1}$$

It is apparent that a larger value of $\triangle f$ results in a lower correlation between two neighboring subcarriers. In addition, the frequency selectivity is also influenced by the delay spread, τ_d, which is the root mean square (RMS) value of the delays of the multipath components. The correlation structure between the channel responses at two different frequencies can be modeled by a single-tap filter (4.4) as

$$\boldsymbol{H}_{f+\triangle f} = \rho_f \boldsymbol{H}_f + \sqrt{1-\rho_f^2}\boldsymbol{\Xi} \tag{6.2}$$

where $\boldsymbol{\Xi}$ is a complex Gaussian matrix with the same dimensions and distribution as $\boldsymbol{H}_f$. Note that we use a matrix notation for the channel response here to cover both SISO and MIMO cases. $\boldsymbol{H}$ is simply a 1×1 complex scalar in the SISO case.

Assuming Jakes fading, the auto-correlation coefficient in the frequency domain, ρ_f, is a complex value. It can be written as [39]

$$\rho_f = \frac{1 - j2\pi\tau_d\triangle f}{1 + 4(\pi\tau_d\triangle f)^2} \tag{6.3}$$

where $j = \sqrt{-1}$. It is awkward to work with a complex correlation coefficient. Fortunately, as the entries of $\boldsymbol{H}$ are circular symmetric complex Gaussians, the angular rotation in the channel entries caused by the complex correlation coefficient does not affect the statistics of the channel gain. Hence, we can simply replace ρ_f by $|\rho_f|$ in (6.2), and therefore the parameter

$$|\rho_f| = \sqrt{\frac{1}{1 + (2\pi\tau_d\triangle f)^2}} \tag{6.4}$$

plays a more important role in our work here.

In this chapter, we carry out our experimental work under the assumption of a HYPERLAN II standard, some basic parameters of which are tabulated in Table 6.1 [141]. The physical layer parameters of many other standards can be found in [142].

Note that the guard interval is a time gap inserted between two successive symbols in transmission. A cyclic prefix of the signal is used in these gaps,

Parameters	Values
Number of subcarriers (M)	64
Total bandwidth ($\mathcal{B}$)	20 MHz
Frequency spacing ($\triangle f$)	3.125 kHz
Guard Interval	800 ns
Modulation	BPSK, QPSK, 16-QAM and 64-QAM

Table 6.1: Physical layer parameters for the HYPERLAN II standard

which helps to avoid interference from other subcarriers and signal distortion caused by the transient response.

6.2 A Gaussian Approximation for OFDM Block-Based Channel Metrics

In adaptive OFDM systems, the signalling parameters or the mode of the subcarriers are adjusted to adapt to the time-varying radio environment [143]. As discussed in Section 2.4, the parameters or the modes are selected based on the states of certain channel quality metrics.

In some cases, the sum of the parameter values in every subcarrier over one OFDM realization can be employed as a metric to characterize an aspect of the system. For example, in a rate-adaptive OFDM system, the number of bits assigned to each of the subcarriers is adaptively chosen in accordance with the link quality of that particular subcarrier. Hence, the total number of bits transmitted in one OFDM block is simply the sum of the number of bits employed on each subcarrier. Such a metric gives the instantaneous system throughput. Another possible application arises from OFDM schemes based on binary mode transmission. For example, some OFDM systems suspend the subcarriers with poor link quality to improve the overall reliability. If one scores the subcarriers in an OFDM block with the parameter '1' (for transmission) and '0' (for outage), then the sum of scores is the total number of

subcarriers that are used in that particular realization. The statistical distribution of these metrics can provide useful insights into the behavior of adaptive OFDM systems.

We now formulate the problem in a more concrete manner. Consider an arbitrary scalar quality metric, $p(f)$, which is a random process in frequency. Assume that there is a set of N possible values of an arbitrary signalling parameter:

$$\varpi \in \{\varphi_0, \varphi_1, \varphi_2, \ldots, \varphi_{N-1}\}.$$

The values of ϖ are assigned to the subcarriers in correspondence with the N states of the link quality metric:

$$p(f) \in \{\mathcal{S}_0, \mathcal{S}_1, \mathcal{S}_2, \ldots, \mathcal{S}_{N-1}\}.$$

Hence, we are interested in the distribution of

$$\Lambda = \sum_{k=1}^{M} \varpi_k \tag{6.5}$$

where ϖ_k represents the signalling parameter value assigned to the k^{th} subcarrier in an OFDM block with M subcarriers. Figure 6.1 shows L OFDM realizations where the link quality of each subcarrier is determined by a single threshold level T, so there are two states of signalling mode. On the other hand, an OFDM block where the link quality is partitioned into four states, is depicted in Fig. 6.2.

From (6.5), we can see that Λ is simply a sum of M random variables. If ϖ_k are independent random variables, it is straightforward to apply the central limit theorem (CLT), especially if M is sufficiently large, and hence obtain a Gaussian approximation for Λ. Unfortunately, in OFDM systems, the channel responses of adjacent subcarriers are usually highly correlated. Furthermore, the strength of the correlation is high enough to make the problem one of *long range dependence* (also known as *strong correlation*) as discussed in [144],

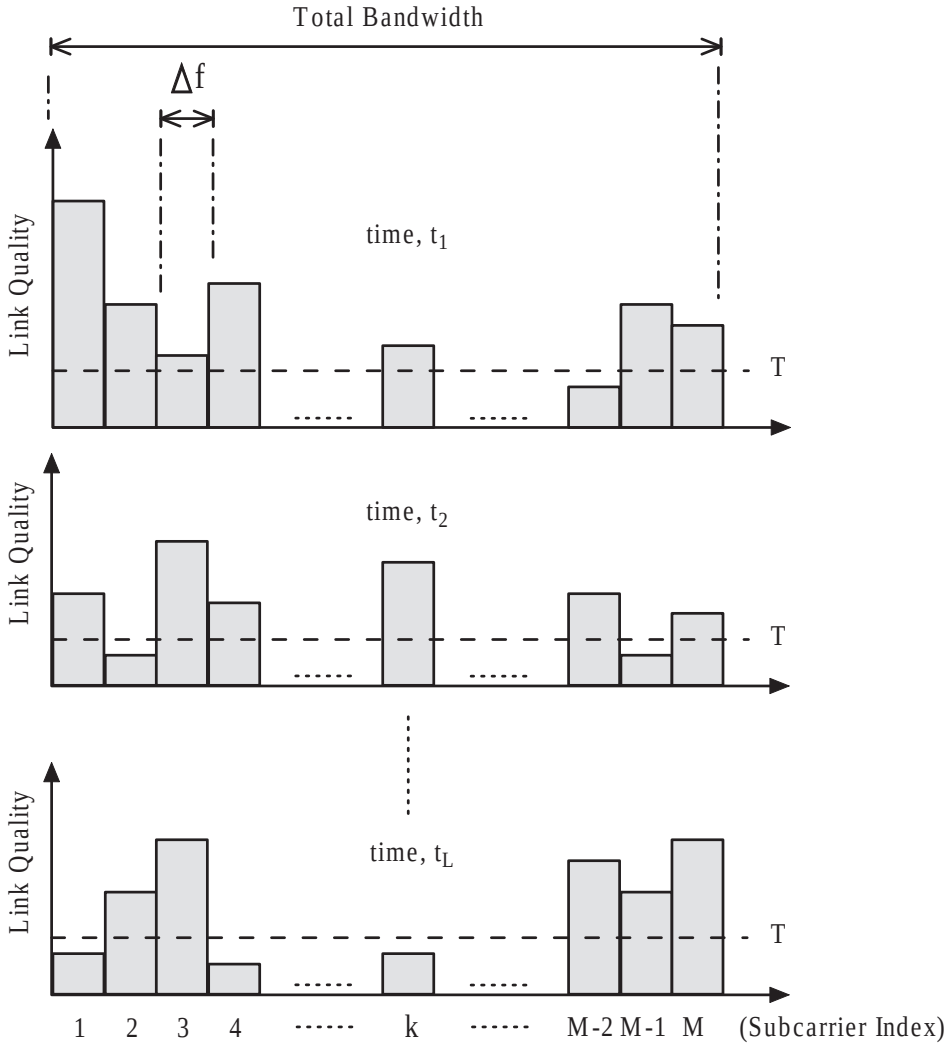

Figure 6.1: An illustration of adaptive OFDM systems with two states.

which prevents the application of classic CLT results. Nevertheless, for the same channel model, the distribution of the symbol error rates in an OFDM block has been examined in [144] based on a version of the CLT which handles such strongly correlated scenarios [145]. Following the same argument, we can conjecture that Λ can also be approximated by a Gaussian random variable. Based on this hypothesis, the scope of this section is focussed on the analytical derivation of the corresponding mean and variance of Λ. We then verify that the Gaussian distribution offers an accurate approximation by fitting the CDF

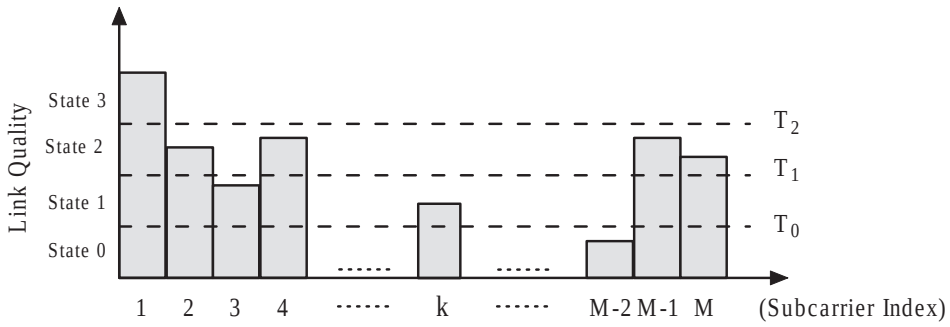

Figure 6.2: An illustration of adaptive OFDM systems with more than two states.

with the analytically computed mean and variance.

In this section, we will commence with a presentation of a unified method to compute the mean and variance of Λ. Then the method is applied to three different cases as numerical examples.

6.2.1 Calculation of Mean and Variance

If the quality metric, $p(f)$, is a stationary process and its statistical properties (marginal distributions and correlation structures) are known, both the mean and variance of Λ can be computed analytically. From (6.5), the mean of Λ is given by

$$\mathrm{E}[\Lambda] = M\,\mathrm{E}[\varpi_k] = M \sum_{i=0}^{N-1} \varphi_i \,\mathrm{Prob}(p_k \in \mathcal{S}_i) \tag{6.6}$$

where p_k represents $p(f_k)$, the value of the quality metric in the k^{th} subcarrier. The probabilities in (6.6) can be obtained from the distribution function of $p(f)$.

Since Λ is the sum of a sequence of correlated random variables $\varpi_1, \ldots, \varpi_M$, the variance of Λ can be written as

$$\begin{aligned}\mathrm{Var}[\Lambda] &= \sum_{k=1}^{M} \mathrm{Var}[\varpi_k] + 2 \sum_{k=1;k<j}^{M} \mathrm{Cov}[\varpi_k, \varpi_j] \\ &= M\,\mathrm{Var}[\varpi_k] + 2 \sum_{k=1}^{M-1} (M-k)\,\mathrm{Cov}[\varpi_1, \varpi_{1+k}] \end{aligned} \tag{6.7}$$

In order to compute Var[Λ] we require

$$\mathrm{Var}[\varpi_k] = \mathrm{E}[\varpi_k^2] - \mathrm{E}[\varpi_k]^2 \tag{6.8}$$

and

$$\mathrm{Cov}[\varpi_1, \varpi_{1+k}] = \mathrm{E}[\varpi_1 \varpi_{1+k}] - \mathrm{E}[\varpi_1]\mathrm{E}[\varpi_{1+k}] \tag{6.9}$$

The expected value, E[ϖ_k], is given in (6.6) and the second moment is simply expressed as

$$\mathrm{E}[\varpi_k^2] = \sum_{i=0}^{N-1} \varphi_i^2\,\mathrm{Prob}(p_k \in \mathcal{S}_i). \tag{6.10}$$

Hence, we only require the cross product moment

$$\mathrm{E}[\varpi_1 \varpi_{1+k}] = \sum_{i=0}^{N-1} \sum_{j=0}^{N-1} \varphi_i\,\varphi_j\,\mathrm{Prob}(\varpi_1 \in \mathcal{S}_i, \varpi_{1+k} \in \mathcal{S}_j). \tag{6.11}$$

The joint probability in (6.11) can be evaluated using the joint density of p_1 and p_{1+k}. Finally, we substitute (6.10) and (6.11) into (6.7), in order to compute Var[Λ] analytically.

6.2.2 Numerical Examples

As we postulated that Λ is approximately Gaussian, we can now evaluate the accuracy of this approximation by using the mean and variance derived above. We consider the following three cases, where Λ represents:

1. the number of subcarriers that are in outage/transmission state in one SISO-OFDM realization;

2. the number of subcarriers using diversity/multiplexing as the transmission strategy in adaptive MIMO-OFDM systems;

3. the total data rate per SISO-OFDM realization in adaptive modulation schemes.

For the sake of convenience, the Λ metrics in the three cases above are written as Λ_1, Λ_2 and Λ_3 respectively. In all examples, unless otherwise specified, we have generated $L = 10,000$ OFDM realizations for simulation, and the switching thresholds are determined using the same method as in Chapter 4, assuming the SNR and the target BER are 18 dB and 1×10^{-3} respectively. Other simulation parameters for the OFDM system are summarized in Table 6.1. As a rule of thumb, the guard interval is usually two to four times larger than the expected delay spread (τ_d) [146]. Hence, we use 250 ns as the value of τ_d in the simulation model in this section, unless otherwise specified.

Clearly, the first two cases (Λ_1 and Λ_2) correspond to a "dual-state" system (Fig. 6.1), while the last case is a "multi-state" (Fig. 6.2) scenario. In the first two cases, we are interested in the number of subcarriers per OFDM realization using a certain binary transmission mode. Hence, we can write

$$\varpi \in [\varphi_0, \varphi_1] = [0, 1]$$

In adaptive OFDM systems, some subcarriers may be too weak to support transmission and hence are excluded [143]. We describe such channels as being in "outage" (as in Chapter 4). The other usable subcarriers using BPSK or a higher order modulation are referred to as being in "transmission" mode. The statistical distribution of the number of subcarriers with outage/transmission states is examined. Intuitively, the suitable link quality metric in this case, is the channel power gain of the subcarriers, denoted $|h_k|^2$, where k is the subcarrier index. When $|h_k|^2$ drops below a certain threshold level, the desired error performance in that subcarrier cannot be achieved, and its state

becomes outage. Assuming a Rayleigh fading SISO channel, the power gain of each subcarrier is distributed as an exponential random process in frequency. Thus, we can use the method presented in Section 6.2.1 to obtain the mean and variance of Λ_1. In order to compute the joint probability as required, the bivariate exponential distribution (4.15) could be used, with ρ replaced by $|\rho_f|$. Alternatively, the probability can also be obtained using a bivariate Rayleigh distribution. We have exploited the infinite power series representation for a bivariate Rayleigh distribution given in [147] to work out these joint probabilities. To verify our analysis, we fit a Gaussian CDF using the calculated mean and variance of Λ_1 (for both outage and transmission), and then compare this approximate CDF with the empirical CDF obtained via simulation. Figure 6.3 exhibits the accuracy of the Gaussian approximation, for the number of subcarriers in both outage and transmission states.

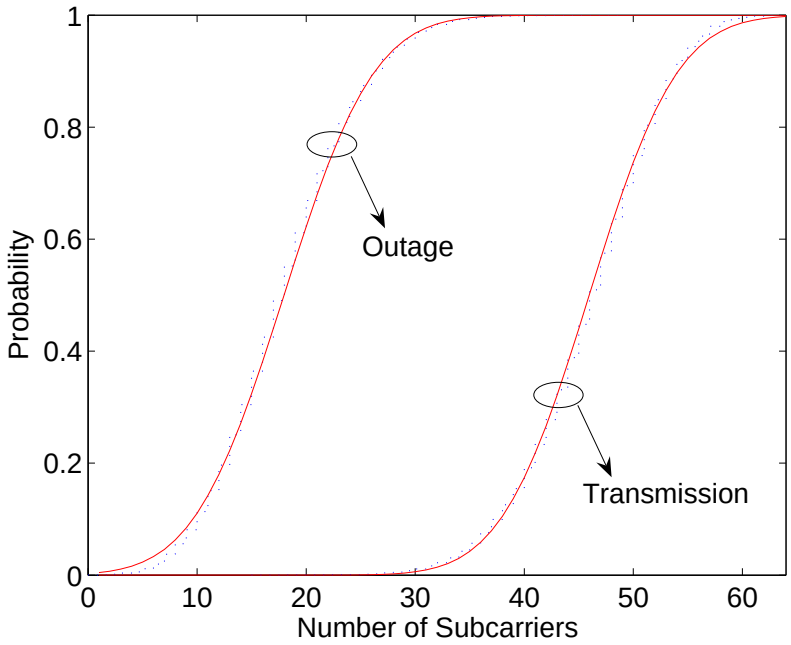

Figure 6.3: A comparison between the simulated CDF of Λ_1 (dots) and a Gaussian approximation (line) using the calculated mean and variance.

The dual-mode antenna selection scheme discussed in Chapter 4 is also applicable in MIMO-OFDM systems. Such a scheme switches between spatial multiplexing and diversity based on the channel condition number. As the condition number is a random process across frequency, the distribution of the number of subcarriers choosing spatial multiplexing or diversity (Λ_2) is studied. A similar problem has been considered in [82] through field measurements in various propagation environments. The procedure is similar to that described above for Λ_1. However, instead of using univariate and bivariate exponential distributions, univariate and bivariate gamma distributions (4.28) are required, as we have seen that the log-condition number, K, is very accurately approximated by a gamma process in Chapter 3.

Here we are interested in the effects of different data rates (per subcarrier), D, on Λ_2. Using the same simulation parameters as in Section 4.2.3, we choose $D = 4$ and $D = 8$. Recall that D is fixed regardless of whether diversity or spatial multiplexing is chosen, and the threshold level, T, is also determined by D. The distributions of Λ_2 in both cases are plotted in Figs. 6.4 and 6.5, along with the Gaussian approximation, which shows excellent accuracy. From the results, it is clear that the diversity scheme dominates for lower data rates (see Fig. 6.4), while at higher data rates, spatial multiplexing is much more common (see Fig. 6.5).

Finally, when adaptive modulation is applied to SISO-OFDM systems, the data rates are allocated in accordance with the prevailing gains of the subcarriers. Consider a numerical example, where there are five signalling options: outage, BPSK, QPSK, 16-QAM and 64-QAM. We are interested in the total number of bits sent per OFDM realization (Λ_3). Hence, in this case we have

$$\varpi \in [\varphi_0, \varphi_1, \varphi_2, \varphi_3, \varphi_4] = [0, 1, 2, 4, 6].$$

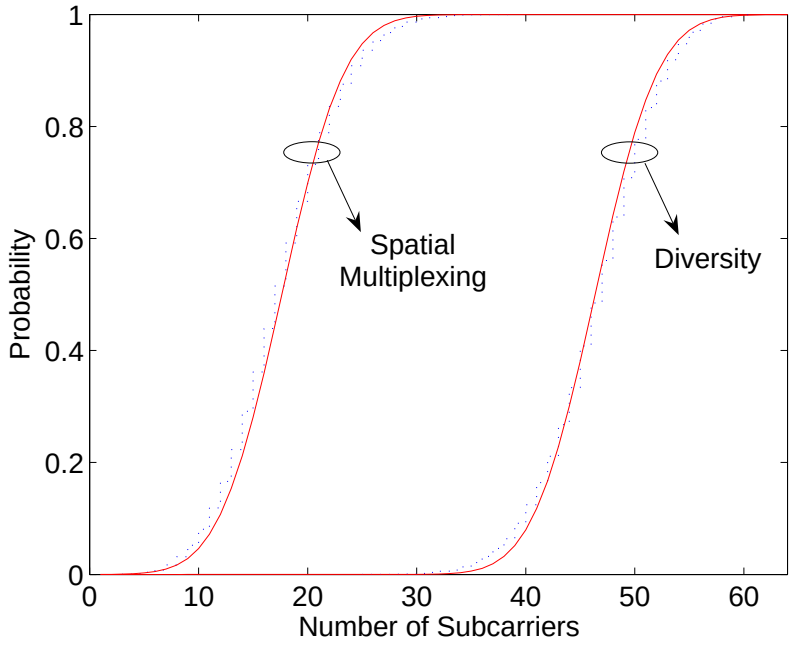

Figure 6.4: A comparison between the simulated CDF of Λ_2 (dots) in a (2,4) system and a Gaussian approximation (line) using the calculated mean and variance. The total data rate $D = 4$ bits per signalling interval.

Since a SISO system is considered here, univariate and bivariate exponential distributions are utilized to obtain the required mean and variance following the procedure given in Section 6.2.1. The resulting comparison between simulations and the Gaussian approximation is shown in Fig. 6.6.

We can see that Gaussian approximations are reasonably accurate in all cases. It can be anticipated that such an approximation will be even better in OFDM systems with more subcarriers, such as digital TV standards where $M = 2048$ [142].

6.3 LCR and AFB in the Frequency Domain

In Chapter 3, we considered the LCR and AFD of various MIMO metrics in the time-domain assuming a narrow-band channel. Here we are interested in how the channel gain fluctuates over the bandwidth of the OFDM system. To

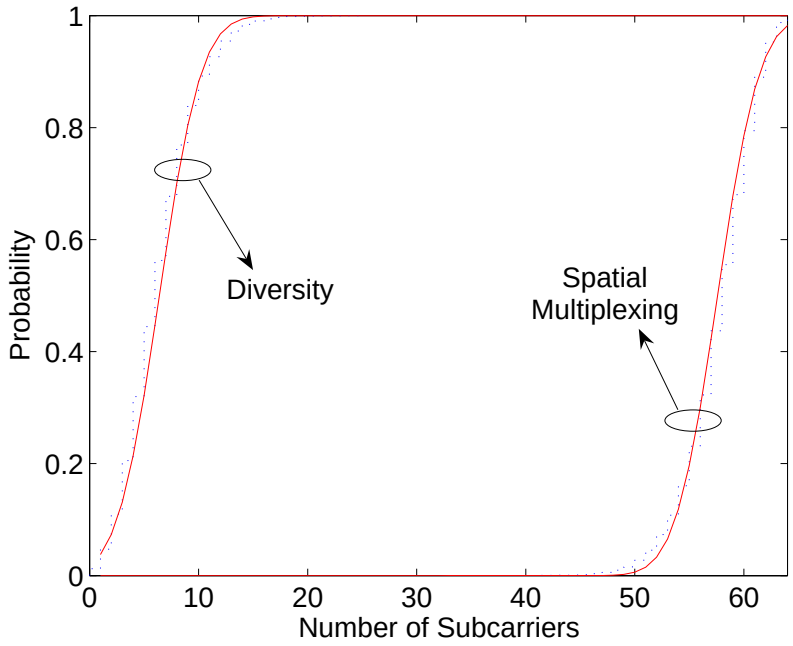

Figure 6.5: A comparison between the simulated CDF of Λ_2 (dots) in a (2,4) system and a Gaussian approximation (line) using the calculated mean and variance. The total data rate $D = 8$ bits per signalling interval.

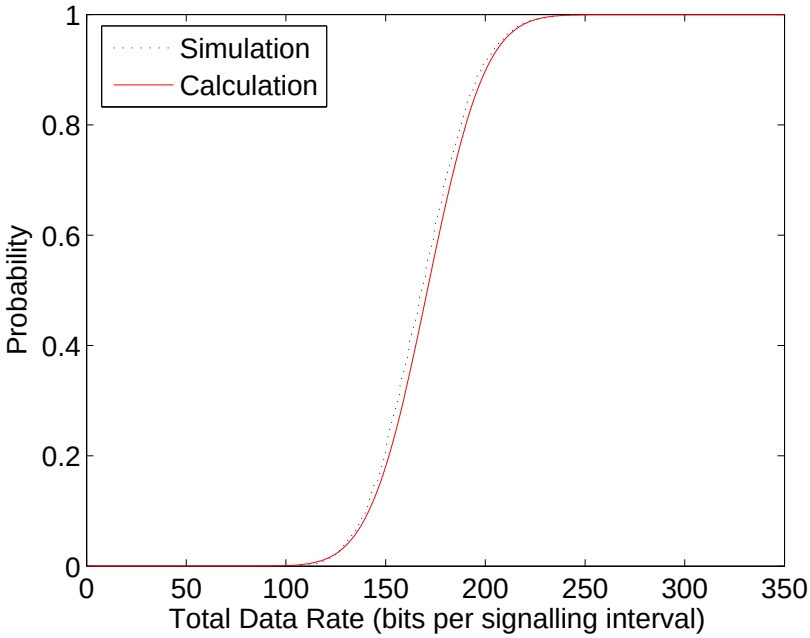

Figure 6.6: A comparison between simulated CDF of Λ_3 (dots) and a Gaussian approximation (line) using the calculated mean and variance.

be specific, we aim to derive analytical expressions for the LCR and AFB in the frequency domain (written as LCR_f and AFB_f, respectively) for the SISO subcarrier gain, the MIMO link gain and the MIMO eigenmode gain.

This work can be thought of as an extension of Chapter 3. As shown in Chapter 3, the LCR of any random process in time, $p(t)$, can be employed to compute its AFD if the statistical distribution of $p(t)$ is also known. Analogously, the average fading bandwidth (AFB) of an arbitrary random process in frequency, $p(f)$, can be evaluated from its LCR in the frequency domain (denoted $\text{LCR}_{f,p}(T)$). All of our analysis is carried out under the assumption of an i.i.d. Rayleigh channel. The potential practical applications of our results are also discussed.

6.3.1 Subcarrier Link Gain in OFDM

It is well known that the link gain of a SISO Rayleigh fading channel, $|h|^2$, is a complex chi-squared (χ^2) process with one degree-of-freedom, as the gain is the sum of squares of two i.i.d. Gaussian components (the real and imaginary parts in (2.3)). Hence, following [95], the corresponding LCR for the process in the frequency domain is given by

$$\text{LCR}_{f,|h|^2}(T) = \sqrt{\frac{-\ddot{\rho}_f(0)\,T}{\pi}}\,\exp(-T) \tag{6.12}$$

where $\ddot{\rho}_f(0)$ is the second derivative of the ACF, $\rho_f(\triangle f)$, at $\triangle f = 0$. As stated in Section 6.1, instead of using ρ_f (which has a complex value), we can equivalently use $|\rho_f|$, given in (6.4). In order to determine $\ddot{\rho}_f(0)$, the correlation function is expanded into a polynomial in Δf (valid for small Δf) as

$$\rho_f(\Delta f) \approx 1 + j\,2\pi\,\tau_d\,\Delta f - \frac{(2\pi\,\tau_d\,\Delta f)^2}{2}\,. \tag{6.13}$$

Hence, the curvature of $\rho_f(\Delta f)$ at $\Delta f = 0$ can be obtained trivially by doubling the coefficient of the $(\Delta f)^2$ term in (6.13), yielding

$$\ddot{\rho}_f(0) = -4\,\pi^2\,\tau_d^2\,. \tag{6.14}$$

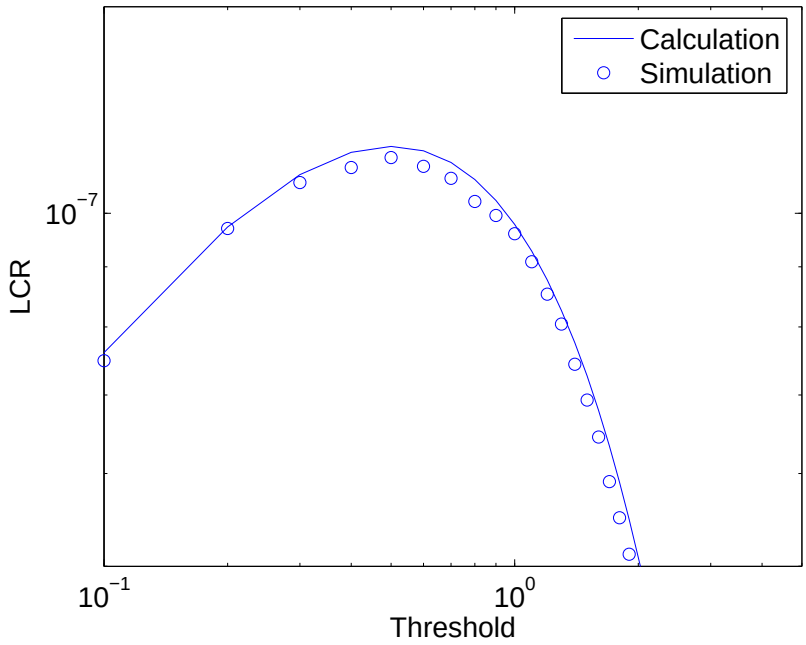

Figure 6.7: A comparison between the simulated LCR_f of $|h|^2$ and our formula. ($\mathcal{B} = 20$MHz, $M = 64$, and $\tau_d = 100$ns)

A very simple, closed-form LCR formula for $|h|^2$ in the frequency domain can therefore be obtained by substituting (6.14) into (6.12). This gives:

$$\mathrm{LCR}_{f,|h|^2}(T) = 2\,\tau_d\,\sqrt{\pi\,T}\,\exp(-T)\,. \tag{6.15}$$

Clearly, LCR_f is proportional to τ_d, which agrees with the work in [148]. Furthermore, the same argument can be used to obtain LCR_f for the total power gain of a MIMO link, simply by substituting (6.14) into (3.8). The resulting formula is given by:

$$\mathrm{LCR}_{f,\gamma}(T) = \frac{2\sqrt{\pi}\tau_d\,T^{N_rN_t-1/2}\exp(-T)}{\Gamma(N_rN_t)}\,. \tag{6.16}$$

Using the simulation parameters given in Table 6.1 with $\tau_d = 100$ns, we have compared simulated LCR values with the calculations given in (6.15) and (6.16). The results are plotted in Figs. 6.7 and 6.8.

Additionally, the AFB can be computed using the well-known relationship

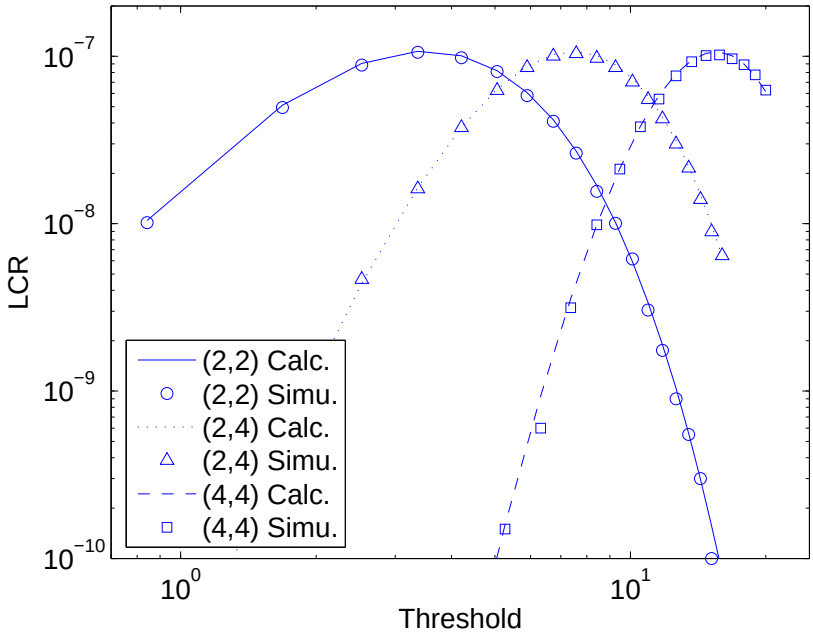

Figure 6.8: A comparison between the simulated LCR_f of γ and our formula. ($\mathcal{B} = 20$MHz, $M = 64$, and $\tau_d = 100$ns)

between the LCR and AFB:

$$\mathrm{AFB}_\gamma(T) = \frac{\mathrm{Prob}(\gamma < T)}{\mathrm{LCR}_{f,\gamma}(T)}. \tag{6.17}$$

Note that (6.17) also holds for $|h|^2$ as it is simply a special case of γ.

In Fig. 6.9, it can be seen that the simulated AFB saturates above a certain threshold level T. This is because the simulation results are generated from OFDM blocks with finite bandwidth, and the largest fade bandwidth we can possibly observe in the simulation is therefore constrained to $\mathcal{B} = M\Delta f$ Hz. In contrast, the analysis yields the AFB for a continuous frequency process over an unbounded range. Hence, we might expect good agreement for fades of small bandwidth which might occur inside an OFDM block. For large bandwidth fades the simulation results will fall below the analytical results as the simulations can be truncated by the finite bandwidth of the block. Fortunately, we are most interested in AFB values such that the channel gain is in a fade.

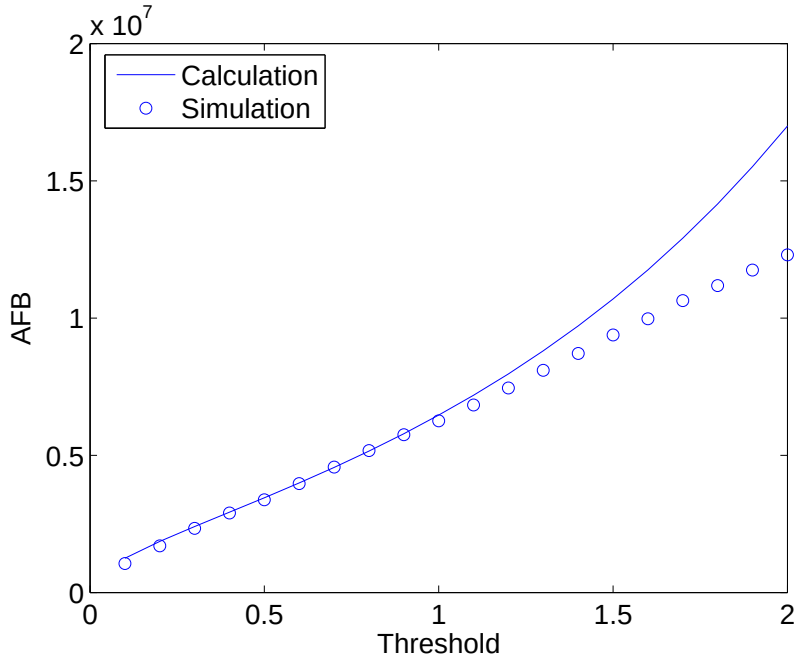

Figure 6.9: A comparison between the simulated and calculated AFB for $|h|^2$. ($\mathcal{B} = 20$MHz, $M = 64$, and $\tau_d = 100$ns)

The formulas (6.15) and (6.16) are derived assuming that the subcarrier gain is a continuous process in frequency. The simulations, however, consider a discrete process over the M frequencies, $f_1, f_2, \ldots, f_M$. For small τ_d values such as 100ns used in Figs. $6.7 -$ 6.9, this difference is not important, as the process is very smooth ($|\rho_f(\Delta f)| \approx 0.99$) and the continuous approximation is very accurate. Increasing the value of $\Delta f\, \tau_d$ results in a lower $\rho_f(\Delta f)$, and the process tends to become more discrete. This leads to reduced accuracy in the formulas (6.15) and (6.16), as well as the resultant AFB computations.

To ameliorate this problem, we can alternatively evaluate the LCR from the the joint density of a subcarrier gain and the gain of its adjacent neighbor. For example, the LCR for a SISO-OFDM system with $\tau_d = 250$ns ($|\rho_f(\Delta f)| \approx 0.8$) can be alternatively calculated using

$$\mathrm{LCR}_{f,|h|^2} = \frac{\mathrm{Prob}(|h|^2(f) > T, |h|^2(f + \triangle f) < T)}{\triangle f}. \tag{6.18}$$

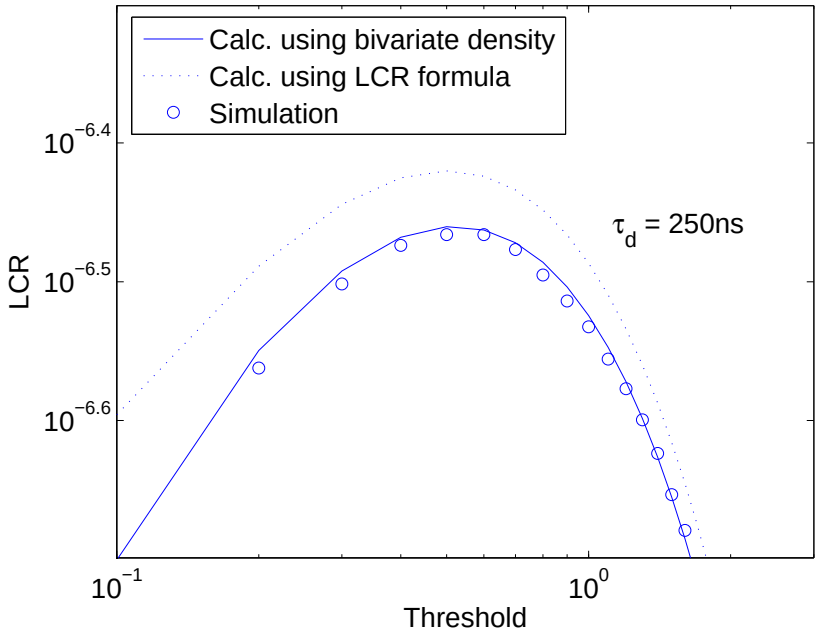

Figure 6.10: Comparison between simulation and alternative formulas for LCR_f of SISO-OFDM channel with lower correlation ($M = 64$ and $\tau_d = 250$ns).

Results from (6.18) are compared with simulations in Fig. 6.10. The calculations using the initial formula (6.15) are also plotted in the same figure for further comparison. The discrete version is clearly more accurate. Note that the continuous LCR is higher than the discrete version, since in continuous frequency there can be level crossings between the discrete points resulting in a higher value.

6.3.2 Subcarrier Eigenmode Gain in MIMO-OFDM

Assuming that full CSI is available at both transmitter and receiver, the SVD can be performed to realize the m eigenmodes in each of the subcarriers, where m is the minimum number of antennas at either terminal. For example, Figure 6.11 shows the three eigenmodes in an OFDM block with 64 subcarriers for a (3,3) MIMO-OFDM system.

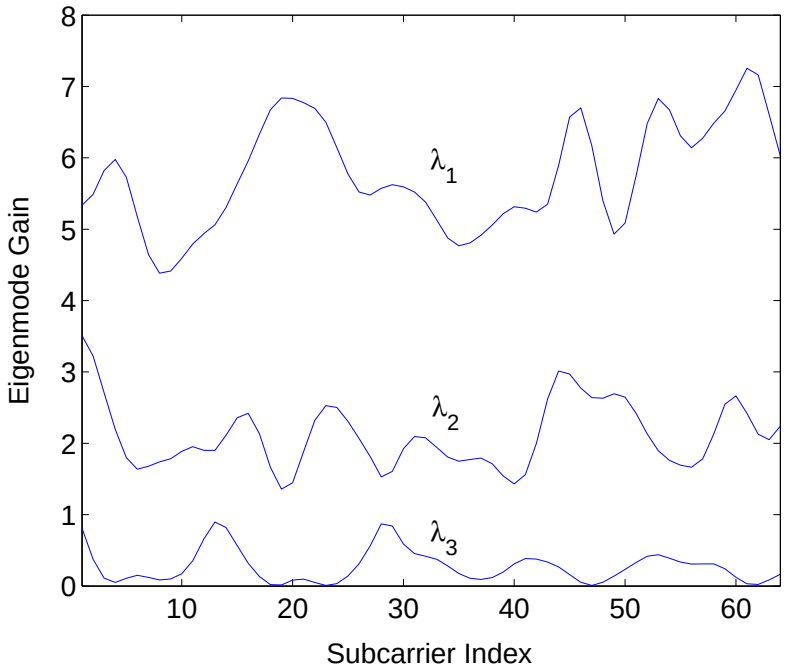

Figure 6.11: The three eigenmode gains across 64 subcarriers in a (3,3) MIMO-OFDM system. ($\mathcal{B} = 20$MHz and $\tau_d = 100$ns)

In many MIMO-OFDM systems, only the largest eigenmode is used for transmission [149]. Hence, the objective here is to investigate how the maximum eigenvalues and hence the subcarrier SNR values evolve with frequency in a MIMO OFDM channel. In particular, a very simple method for LCR computation has been given in Section 3.4, and the application of this technique is extended here to derive the LCR and AFB for MIMO eigenmodes in the frequency domain.

As shown in Section 3.4, the eigenvalues as well as the singular values, $s = \sqrt{\lambda}$, can be accurately approximated by gamma processes. As a result, the LCR for the eigenvalue process can be approximated using

$$\mathrm{LCR}_{f,\lambda}(T) = \frac{1}{2\,\Gamma(r)} \sqrt{\frac{2|\ddot{R}_s(0)|}{\pi}} \left(\theta\sqrt{T}\right)^{r-0.5} \exp\left(-\theta\sqrt{T}\right) \tag{6.19}$$

where $r = \mathrm{E}[s]^2/\mathrm{Var}[s]$ and $\theta = \mathrm{E}[s]/\mathrm{Var}[s]$ are the shape and scale factors of the gamma variable that approximates the singular value process. Note that

these parameters depend solely on the first two moments of the singular value process, and hence can be acquired from the distribution of the eigenvalues. More details on computing E[s] and Var[s] can be found in [58]. Also, following the same argument as in Section 3.4, $\ddot{R}_s(0)$ is the curvature of the correlation function of the singular value s, which can be deduced from (3.34) to be

$$\ddot{R}_s(0) = \frac{-\ddot{\rho}_f(0)\,\theta^2}{2\,r}\,. \tag{6.20}$$

Hence, from (6.14) it is trivial to see that

$$\ddot{R}_s(0) = \frac{2\pi^2\,\tau_d^2\,\theta^2}{r}\,. \tag{6.21}$$

Substituting (6.21) into (6.19) we have the closed-form LCR formula

$$\mathrm{LCR}_{f,\lambda}(T) = \sqrt{\frac{\pi}{r}}\,\frac{\tau_d\,\theta}{\Gamma(r)}\,\left(\theta\,\sqrt{T}\right)^{r-0.5}\exp\left(-\theta\,\sqrt{T}\right)\,. \tag{6.22}$$

From (6.22), we can conclude that the LCR for the eigenmode in the frequency domain is also proportional to τ_d. This formula simply requires the first two moments (for r, θ) of the corresponding singular value process, both of which can be acquired from the Wishart distribution [56, 58].

As shown in Figs. 6.12 and 6.13, the LCR formula (6.22) exhibit excellent accuracy for the largest eigenmode in both (2,2) and (2,4) systems. Note that although we are particularly interested in the largest eigenmode as many proposed schemes only use λ_1 for transmission [149], our formula is valid for any eigenmode of interest. In Fig. 6.14, we have plotted the LCR_f for both λ_1 and λ_3 in a (3,3) system. The peak LCR of λ_3 is much higher than λ_1. This is plausible as it has been stated in [150] that the larger eigenmodes have substantially higher frequency selectivity than the small eigenmodes.

Moreover, the AFB for the eigenmode gain is easily computed using

$$\mathrm{AFB}_\lambda(T) = \frac{\mathrm{Prob}(\lambda < T)}{\mathrm{LCR}_{f,\lambda}(T)} \tag{6.23}$$

where $\mathrm{Prob}(\lambda < T)$ can be calculated using either its gamma approximation or the exact marginal density of the eigenvalue [58]. We plot the AFB for the

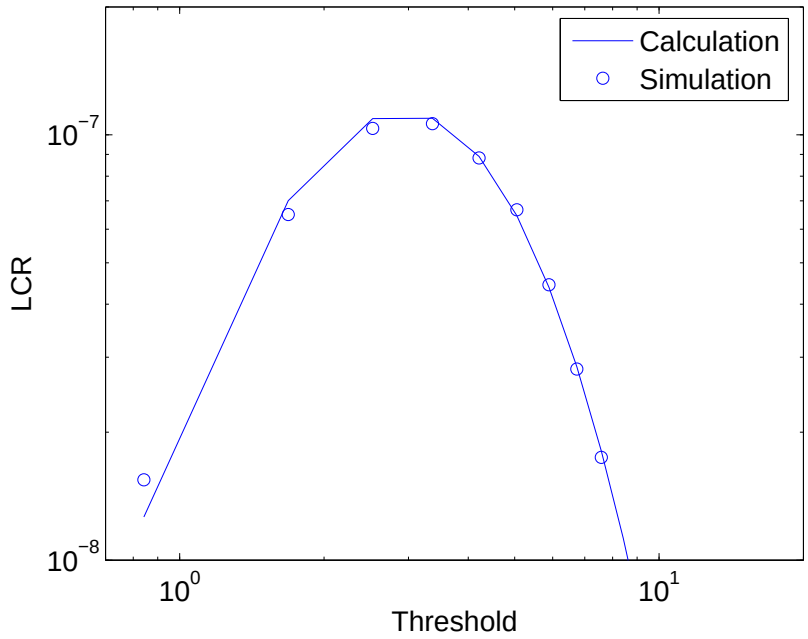

Figure 6.12: The LCR for λ_1 in a (2,2) MIMO-OFDM system in the frequency domain. ($\mathcal{B} = 20$MHz, $M = 64$, and $\tau_d = 100$ns)

eigenmode gains of (2,2) and (2,4) systems in Figs. 6.15 and 6.16. As observed in Section 6.3.1, the simulated AFB saturates above a certain threshold. Once again this is caused by the limited bandwidth of the OFDM block compared to the infinite bandwidth assumed by the analysis.

6.3.3 Potential Practical Applications

Equipped with a knowledge of the channel variation in the frequency domain, many of the major mechanisms and parameters of an adaptive OFDM system, such as the channel estimation method, feedback overhead and power/bit allocation algorithms, can be designed in a more judicious manner. For example, in lieu of adjusting the transmission mode on a subcarrier by subcarrier basis (the feedback overhead of which is intuitively a heavy burden for the system [36]) in adaptive OFDM schemes, many researchers have suggested aggregating consecutive subcarriers with similar gains into groups or clusters called

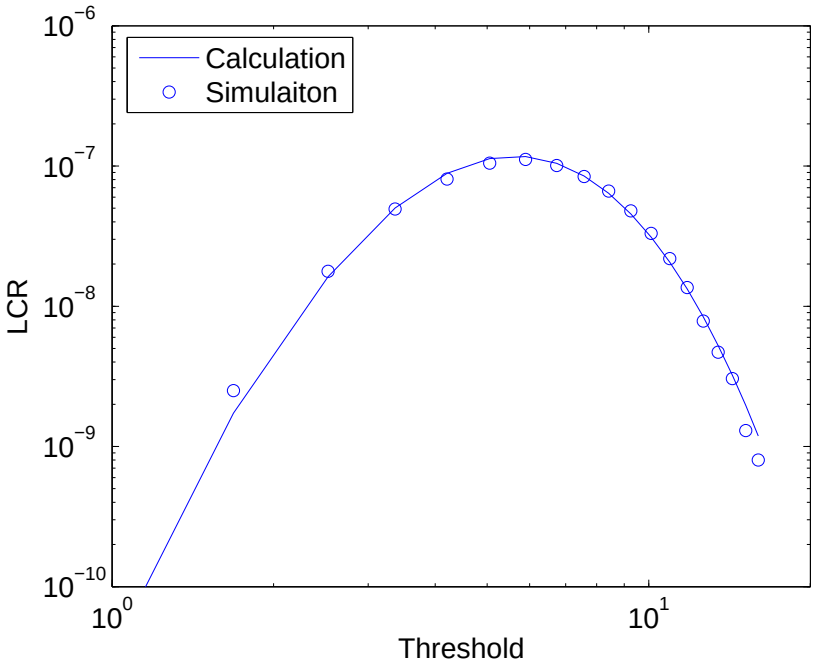

Figure 6.13: The LCR for λ_1 in a (2,4) MIMO-OFDM system in the frequency domain. ($\mathcal{B} = 20$MHz, $M = 64$, and $\tau_d = 100$ns)

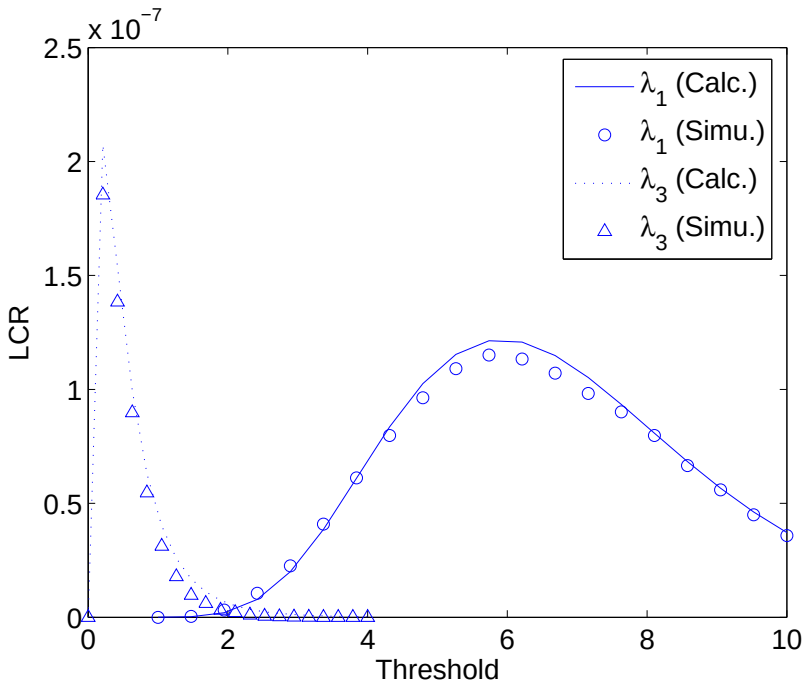

Figure 6.14: The LCR for λ_1 and λ_3 in a (3,3) MIMO-OFDM system in the frequency domain. ($\mathcal{B} = 20$MHz, $M = 64$, and $\tau_d = 100$ns)

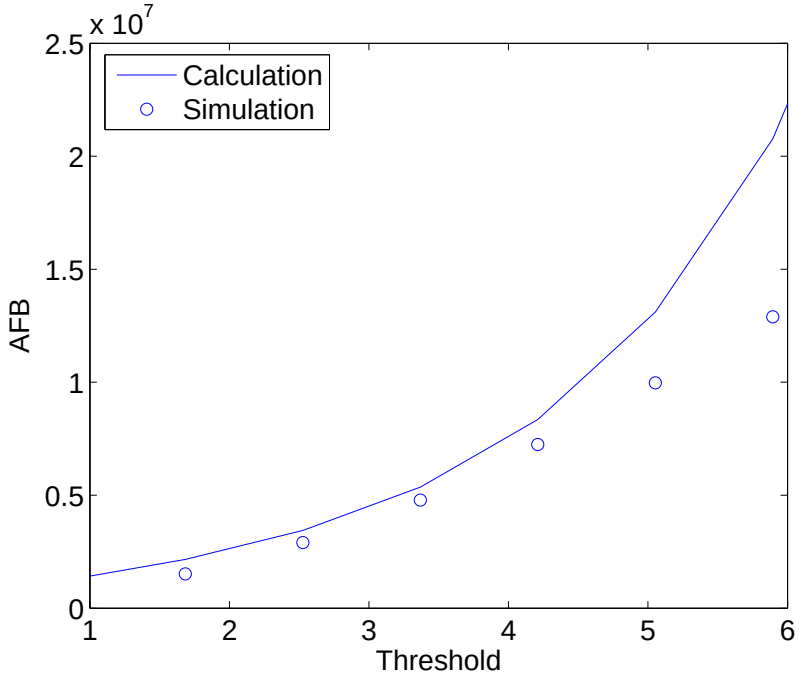

Figure 6.15: The AFB for λ_1 in a (2,2) MIMO-OFDM system in the frequency domain. ($\mathcal{B} = 20$MHz, $M = 64$, and $\tau_d = 100$ns)

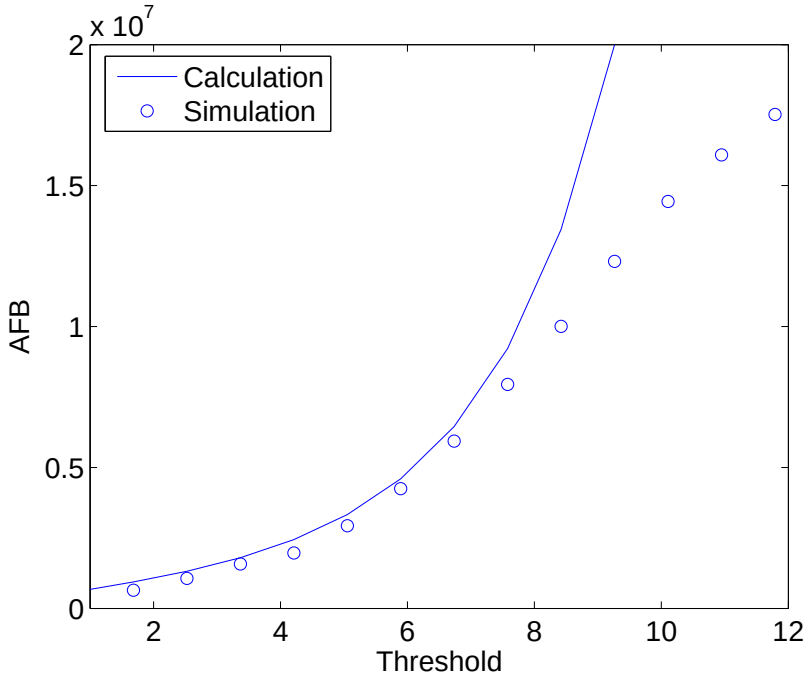

Figure 6.16: The AFB for λ_1 in a (2,4) MIMO-OFDM system in the frequency domain. ($\mathcal{B} = 20$MHz, $M = 64$, and $\tau_d = 100$ns)

"sub-bands" (see e.g. [151, 152]). Such a strategy can significantly decrease the resources required for the feedback, and thus lead to a more efficient operation of the system despite the resulting performance loss. Assuming that the adaptive system is switching between "transmission" and "outage", the LCR in the frequency domain and the AFB gauge the appropriate number of subcarriers that can be grouped in interpolation-based channel estimators [153] as well as the suitable size for the sub-bands. For systems that switch among more than two transmission modes, the mode entering rate (MER) and average stay bandwidth (ASB) are of more interest. Further investigation of the MER and ASB are, however, beyond the scope of this thesis.

6.4 Summary

Some techniques for adaptive OFDM system characterization are provided in this chapter, which commenced with a brief discussion of adaptive OFDM systems and channel models. The channel variation in the frequency domain was then examined from two perspectives.

Firstly, based on a central limit theorem, Gaussian distributions are proposed to approximate the distribution of the number of subcarriers using a certain transmission mode (signalling/outage and diversity/multiplexing), as well as the total data rate per signalling interval in an OFDM system with adaptive modulation. In particular, the mean and variance are computed analytically and used to fit a Gaussian CDF for comparison with simulation data. In all cases, good agreements can be observed in the simulation results.

Secondly, we extended the level crossing analysis in Chapter 3 to the frequency domain. Simple closed-form formulas for the LCR_f of the total power gains and individual eigenmode gains of SISO/MIMO-OFDM channels are derived. Furthermore, the AFB can be computed trivially from LCR_f. The potential applications of these results are also discussed.

Chapter 7

Conclusions and Future Work

In this final chapter, we summarize the main findings and conclusions that have been presented in the thesis. Also, some open problems are pointed out, giving possible research directions for the future.

7.1 Conclusions

A wireless communication architecture with multiple antenna elements at both transmitter and receiver, known as a MIMO system, is a promising approach to achieve high channel capacity for next generation wireless technologies. However, the time-varying nature of the fading channel is a major challenge in wireless communication systems design. In spite of its practical importance, research in this area is relatively rare in the literature. Adaptive transmission is a crucial example where the time-variation of the MIMO channels is of interest. Such schemes require the transmitter to possess information regarding the current channel status via a feedback link, in order to further improve the system performance. The feedback mechanism can be designed more appropriately if the dynamic behavior of the channel is known. In Chapter 1, we briefly describe the potential benefits of MIMO systems, as well as the main motivation of this research project.

The eigen-structures of MIMO channels play a critical role in both the design and analysis of MIMO systems, and can be analyzed via the SVD. To be specific, the eigenvalues and eigenvectors of the MIMO channel correlation matrix can be used to represent the spatial link gains and the steering weights for beam-forming schemes respectively. The second half of Chapter 2 elaborates various channel metrics that are associated with the eigenvalues. The instantaneous channel quality can be assessed from these metrics.

All of the eigenvalue-dependent metrics that have been discussed, can be employed as the switching criterion of certain adaptive schemes. Thus, how these metrics evolve with time is of great interest. Closed-form formulas for the LCR and AFD of the total power gain, individual eigenmode gain, channel capacity and condition numbers in i.i.d Rayleigh fading MIMO channels, are derived in Chapter 3. By exploiting the fact that these metrics can be approximated by either gamma or Gaussian distributions, the main focus of the research work becomes the derivation of the ACF curvature of the processes. The results show that the smaller eigenvalues have higher peak LCR and hence experience more severe fluctuation in all systems. This implies that transmission on the smaller eigenmodes may need more frequent feedback. Most of the analysis is carried out under the assumption of Jakes fading, which caters for the scenario where the AoA is uniformly distributed over $[-\pi, \pi]$. However, the analytical method is valid for any fading model for which the channel ACF has a second derivative at zero. For example, for the total power gain and for the individual eigenmode gains, simple formulas for the LCR have also been developed with different types of ACF, including mobile-to-mobile channels and fading with a Laplacian PAS. In contrast to Jakes fading, the smaller angular spread of a Laplacian PAS leads to a lower peak in the LCR of the eigenmodes. Conversely, the MM channel results in even higher fluctuations of the eigenmodes than Jakes fading. All analytical results agree with computer simulations.

In Chapter 4, the temporal behavior of channel metrics are investigated using Markov models. In order to evaluate the behavior of eigenvalues at two time instants, the joint density of the eigenvalues of two correlated complex Wishart matrices is derived. The derivation is based on some results on Brownian diffusion processes, which leads to a more general and versatile result with a simpler derivation than previous work. For the special case where $N_t = N_r = 1$, the joint density simplifies to the bivariate exponential distribution. We have considered Markov modeling for channel capacity and condition number. Their transition probabilities can be computed based on the bivariate Gaussian and bivariate gamma approximations respectively. Alternatively, assuming that the channel is varying slowly enough, the transition probabilities can be approximated by using the LCR results found in Chapter 3. From the results, we observed that feedback delay can have a significant impact on adaptation performance in all adaptive schemes that we have considered. In dual-mode antenna selection schemes, the transition probability from multiplexing preferred channels to diversity preferred channels decreases when an antenna is added at the receiver. The transition probability from a diversity preferred channel to a multiplexing preferred channel has the opposite pattern. Also, in terms of the overall adaptation error, the dual-mode antenna selection scheme behaves better when the data rate (and hence the threshold level) is reasonably high. An investigation has also been carried out to examine the joint behavior of multiple eigenvalues, which provides insights into the characteristics of the MIMO systems that merge SVD and adaptive modulation.

For the SVD transceiver architecture, feedback delay causes a mismatch between steering matrices. Specifically, the steering matrix used at the transmitter becomes outdated due to feedback delay, so the system cannot diagonalize the channel perfectly and and signal loss and self-interference occur. An analysis has been undertaken in Chapter 5 to characterize the resultant

SINR in such a scenario, based on a modified stochastic differential equation (SDE) of the eigenvector elements. The analysis shows that the loss in signal power is a Gaussian variable and is approximately identical to the induced interference. In addition, this power is higher when two or more eigenvalues are of the similar magnitude. We can therefore identify some novel channel metrics that gauge the system sensitivity to the feedback delay.

Finally, we considered channel variation in the frequency domain in Chapter 6. This is mainly motivated by the popular air-interface known as OFDM, which is widely used to alleviate frequency-selectivity and mitigate intersymbol-interference. We examine some statistical properties of OFDM (in both SISO and MIMO) systems that adapt the transmission parameters in accordance with the prevailing channel quality. In certain cases, the sum of parameter values over one OFDM realization can be used to assess the channel behavior. Based on a central limit theorem, we showed that such a sum is approximately Gaussian. In order to verify this hypothesis, the mean and variance are calculated analytically to compute the Gaussian CDF. We considered three numerical examples, including the total number of suspended subcarriers, the total number of subcarriers using multiplexing/diversity in MIMO-OFDM, and the total data rate per OFDM realization. In addition, by extending the work in previous chapters, the LCR of both the total link gain and the eigenmode gain in the frequency domain are derived. This also leads to the evaluation of AFB, which may have practical applications in the development of sub-band grouping algorithms and channel estimation mechanisms.

7.2 Suggested Future Work

In this thesis, the channel variations in MIMO systems have been studied in a few different respects. Nevertheless, there still remain many open issues that require further exploration. Some of these open problems are enumerated

below.

Throughout this thesis, we have concentrated on i.i.d Rayleigh channels, which are more suitable for urban or indoor environments. In practice, however, a LOS path may be present and in such scenarios a Ricean fading model may be preferable. Additionally, our assumption of i.i.d. channel entries may not be realistic, since spatial correlation is usually unavoidable when the antenna spacing and/or the angular spread of the incoming rays are small. For these scenarios, the dynamic behavior of the eigenmodes and other metrics remains unknown. For example, analytical expressions for the eigenmode LCR and AFD in Ricean and/or spatial correlation scenarios are not available. These are important issues in the context of MIMO channel modeling. In particular, it is known that channels with a LOS path and/or spatial correlation may experience rank-deficiency, and we anticipate that the condition number would behave very differently as compared to the i.i.d Rayleigh case.

Regarding the channel condition number, the analysis is limited to asymmetrical MIMO systems. It has been shown that the first moment of the condition number in a symmetrical system is infinite. Hence, the LCR and AFD in continuous time do not exist. However, if one treats the condition number as a discrete process in time instead of a continuous process, it may be possible to develop analytical methods for computing LCR, AFD, and transition probabilities.

The mathematical derivations in this thesis are largely based on the exploitation of various SDEs and the corresponding Euler approximation. Specifically, a SDE for the eigenvector elements is employed to characterize the impact of feedback delay on SVD schemes. This approach is only valid when the time displacement, τ, is extremely small. Thus, for situations with large feedback delay or severe channel estimation error, the approach may become invalid. Further studies are needed to address this issue.

We have examined the distribution of the metric Λ, which is the sum of

transmission parameter values (in each subcarrier) over the whole bandwidth. Typical examples of Λ include the total number of subcarriers using certain transmission modes, or the data rate per realization. However, Λ is also a function of time. Thus, to investigate how Λ evolves with time is another important issue for adaptive system design. There are other areas of the OFDM work which could be extended. The results on AFB give information on the number of successive subcarriers that are in a deep fade. In adaptive OFDM systems with multiple modulation levels, the average stay bandwidth (ASB) is also of interest. The ASB gives the mean number of successive subcarriers in a particular state $\mathcal{S}_i$. Theoretically, the ASB can be computed as:

$$\mathrm{AFB}(\mathcal{S}_i) = \frac{\mathrm{Prob}(p \in \mathcal{S}_i)}{\mathrm{LCR}_{f,p}(T_i) + \mathrm{LCR}_{f,p}(T_{i+1})}$$

Moreover, we have only considered the largest eigenmode in MIMO-OFDM systems. For systems that use multiple eigenmodes for transmission (for example, in [75, 154] and many other publications), the joint behavior of the eigenvalues across the frequency domain should be explored.

The last, and probably the most important issue, is how the results in this thesis can be applied in practical systems. We have provided a number of techniques that can be used to evaluate the dynamic characteristics of MIMO channels. The development of improved schemes exploiting the knowledge of the channel variation is one of the major potential research directions in the future.

Bibliography

[1] A. F. Naguib, N. Seshadri, and A. R. Calderbank, "Increasing data rate over wireless channels," *IEEE Signal Processing Mag.*, pp. 76–92, May 2000.

[2] W. Mohr and W. Konhauser, "Access network evolution beyond third generation mobile communications," *IEEE Commun. Mag.*, pp. 122–133, Dec. 2000.

[3] L. M. Correia and R. Prasad, "An overview of wireless broadband communications," *IEEE Commun. Mag.*, pp. 28–33, Jan. 1997.

[4] T. M. Cover and J. A. Thomas, *Elements of Information Theory*, 2nd ed. Wiley-Interscience, 2006.

[5] A. J. Paulraj and C. B. Papadias, "Space-time processing for wireless communications," *IEEE Signal Processing Mag.*, pp. 49–82, Nov. 1997.

[6] A. Lozano, F. R. Farrokhi, and R. A. Valenzuela, "Lifting the limits on high-speed wireless data access using antenna arrays," *IEEE Commun. Mag.*, pp. 156–162, Sept. 2001.

[7] S. D. Blostein and H. Leibs, "Multiple antennas systems: Their role and impact in future wireless access," *IEEE Commun. Mag.*, pp. 94–101, July 2003.

[8] D. Gesbert, M. Shafi, D.-S. Shiu, P. Smith, and A. Naguib, "From theory to practice: An overview of MIMO time-space coded wireless systems," *IEEE J. Select. Areas Commun.*, vol. 21, pp. 281–302, Apr. 2003.

[9] A. J. Paulraj, D. A. Gore, R. U. Nabar, and H. Bolcskei, "An overview of MIMO communications - a key to gigabit wireless," *Proc. IEEE*, vol. 92, no. 2, pp. 198–218, Feb. 2004.

[10] "Introduction to MIMO systems," Application Note 1MA102, Rohde and Schwarz, June 2006.

[11] G. L. Stuber, J. R. Barry, S. W. McLaughlin, Y. Li, M. A. Ingram, and T. G. Pratt, "Broadband MIMO-OFDM wireless communications," *Proc. IEEE*, vol. 92, no. 2, pp. 271–294, Feb. 2004.

[12] I. Berenguer and Z. Wang, "Space-time coding and signal processing for MIMO communications," *J. Comput. Sci. Tech.*, vol. 18, no. 6, pp. 689–702, 2003.

[13] G. L. Stuber, *Principles of Mobile Communications*, 2nd ed. Norwell, MA: Kluwer, 2002.

[14] T. S. Rappaport, *Wireless Communications: Principles and Practice*, 2nd ed. Upper Saddle River, NJ: Prentice-Hall, Inc., 2002.

[15] V. Tarokh, N. Seshadri, and A. R. Calderbank, "Space-Time codes for high data rate wireless communication: Performance criterion and code construction," *IEEE Trans. Inform. Theory*, vol. 44, pp. 744–765, Mar. 1998.

[16] S. M. Alamouti, "A simple transmit diversity technique for wireless communications," *IEEE J. Select. Areas Commun.*, vol. 16, pp. 1451–1458, Oct. 1998.

[17] V. Tarokh, H. Jafarkhani, and A. R. Calderbank, "Space-time block codes from orthogonal designs," *IEEE Trans. Inform. Theory*, vol. 45, pp. 1456–1467, July 1999.

[18] B. Vucetic and J. Yuan, *Space-Time Coding*. Chichester, England: John Wiley and Sons, 2003.

[19] G. J. Foschini, "Layered space-time architecture for wireless communication in a fading environment when using multi-element antennas," *Bell Labs. Tech. J.*, vol. 1, no. 2, pp. 41–59, 1996.

[20] J. H. Sung and J. R. Barry, "Space-time processing with channel knowledge at the transmitter," in *Proc. EUROCON.*, vol. 1, Bratislava, Slovak Republic, July 2001, pp. 26–29.

[21] L. Zheng and D. N. C. Tse, "Diversity and multiplexing: A fundamental tradeoff in multiple-antenna channels," *IEEE Trans. Inform. Theory*, vol. 49, pp. 1073–1096, May 2003.

[22] J. P. Kermoal, L. Schumacher, K. I. Pedersen, P. E. Mogensen, and F. Frederiksen, "A stochastic MIMO radio channel model with experimental validation," *IEEE J. Select. Areas Commun.*, vol. 20, no. 6, pp. 1211–1227, 2002.

[23] G. Lebrun, Y. Tan, and M. Faulkner, "MIMO transmission over a time-varying channel using SVD," in *Proc. IEEE GLOBECOM*, vol. 1, Taipei, Taiwan, 2002, pp. 414–418.

[24] H. Sampath, P. Stoica, and A. Paulraj, "Generalized linear precoder and decoder design for MIMO channels using the weighted MMSE criterion," *IEEE Trans. Commun.*, vol. 49, pp. 2198–2206, Dec. 2001.

[25] A. Scaglione, P. Stoica, S. barbarossa, G. B. Giannakis, and H. Sampath, "optimal designs for space-time linear precoders and decoders," *IEEE Trans. Signal Processing*, vol. 50, pp. 1051–1064, May 2002.

[26] G. Lebrun, J. Gao, and M. Faulkner, "MIMO transmission over a time-varying channel using SVD," *IEEE Trans. Wireless Commun.*, vol. 4, pp. 757–764, Mar. 2005.

[27] X. Zhang and B. Ottersten, "Power allocation and bit loading for spatial multiplexing in MIMO systems," in *Proc. IEEE ICASSP*, vol. 5, Hong Kong, China, 2003, pp. 53–56.

[28] Z. Zhou, B. Vucetic, M. Dohler, and Y. Li, "MIMO systems with adaptive modulation," *IEEE Trans. Veh. Technol.*, vol. 54, pp. 1828–1842, Sept. 2005.

[29] C. Michalke, M. Stege, F. Schafer, and G. Fettweis, "Efficient tracking of eigenspaces and its application to eigenbeamforming," in *Proc. IEEE PIMRC*, Beijing, China, Sept. 2003, pp. 2847–2851.

[30] Y. Tan, G. Lebrun, and M. Faulkner, "An adaptive channel SVD tracking strategy in time-varying TDD system," in *Proc. IEEE VTC Spring.*, Jeju Island, Korea, Apr. 2003, pp. 769–773.

[31] J. C. Roh and B. D. Rao, "An efficient feedback method for MIMO systems with slowly time-varying channels," in *Proc. IEEE WCNC*, Atlanta, GA, USA, 2004, pp. 760–764.

[32] S. T. Chung, A. Lozano, and H. C. Huang, "Approaching eigenmodes BLAST channel capacity using V-BLAST with rate and power feedback," in *Proc. IEEE VTC Fall*, vol. 2, Atlantic City, NJ, USA, Oct. 2001, pp. 915–919.

[33] T. Dahl, N. Christophersen, and D. Gesbert, "Blind MIMO eigenmode transmission based on the algebraic power method," *IEEE Trans. Signal Processing*, vol. 52, pp. 2424–2431, Sept. 2004.

[34] D. P. Palomar, J. M. Cioffi, and M. A. Lagunas, "Uniform power allocation in MIMO channels: A game-theoretic approach," *IEEE Trans. Inform. Theory*, vol. 49, pp. 1707–1727, July 2003.

[35] C.-S. Maa, Y.-C. Wang, and J.-T. Chen, "Structure-based water-filling algorithm in multipath MIMO channels," in *Proc. IEEE ICASSP*, vol. 2, Montreal, Canada, May 2004, pp. 317–320.

[36] S. Catreux, V. Erceg, D. Gesbert, and R. W. Heath, "Adaptive modulation and MIMO coding for broadband wireless data networks," *IEEE Commun. Mag.*, vol. 40, no. 6, pp. 108–115, June 2002.

[37] V. Pohl, P. H. Nguyen, V. Jungnickel, and C. von Helmolt, "How often channel estimation is needed in MIMO systems," in *Proc. IEEE GLOBECOM.*, San Francisco, CA, USA, Dec. 1-5, 2003, pp. 814–818.

[38] A. Grant, "Rayleigh fading multi-antenna channels," *EURASIP J. Appl. Sig. Processing*, no. 3, pp. 316–329, 2002.

[39] W. C. Jakes, *Microwave Mobile Communications*. Piscataway, NJ: IEEE Press Classic Reissue, 1995.

[40] N. Sharma, L. H. Ozarow, and A. G. Kogiantis, "MIMO channel statistics in the presence of non-uniform angle spread," *IEEE Commun. Lett.*, vol. 8, no. 7, pp. 428–430, 2004.

[41] A. S. Akki, "Statistical properties of mobile-to-mobile land communication channels," *IEEE Trans. Veh. Technol.*, vol. 43, pp. 826–831, Nov. 1994.

[42] F. R. Farrokhi, G. J. Foschini, A. Lozano, and R. A. Valenzuela, "Link-optimal space-time processing with multiple transmit and receive antennas," *IEEE Commun. Lett.*, vol. 5, pp. 85–87, Mar. 2001.

[43] M. Stoytchev and H. Safar, "Statistics of MIMO radio channel in indoor environments," in *Proc. IEEE VTC Fall*, vol. 3, Atlantic City, NJ, USA, Oct. 2001, pp. 1804–1808.

[44] G. Lebrun, M. Faulkner, M. Shafi, and P. J. Smith, "MIMO Ricean channel capacity," in *Proc. IEEE ICC*, Paris, France, May 2004, pp. 2939–2943.

[45] D.-S. Shiu, G. J. Foschini, M. J. Gans, and J. M. Kahn, "Fading correlation and its effect on the capacity of multielement antenna systems," *IEEE Trans. Commun.*, vol. 48, pp. 502–513, Mar. 2000.

[46] D. Chizhik, F. Rashid-Farrokhi, J. Ling, and A. Lozano, "Effect of antenna separation on the capacity of BLAST in correlated channels," *IEEE Commun. Lett.*, vol. 4, pp. 337–339, Nov. 2000.

[47] K. Yu and B. Ottersten, "Models for MIMO propagation channels: a review," *Wirel. Commun. Mob. Comput.*, vol. 2, pp. 653–666, 2002.

[48] P. J. Smith, S. Roy, and M. Shafi, "Capacity of MIMO systems with semicorrelated flat fading," *IEEE Trans. Inform. Theory*, vol. 49, pp. 2781–2788, Oct. 2003.

[49] M. T. Ivrlac, W. Utschick, and J. A. Nossek, "Fading correlations in wireless MIMO communication systems," *IEEE J. Select. Areas Commun.*, vol. 21, pp. 819–828, June 2003.

[50] D. Gesbert, H. Bolcskei, D. Gore, and A. Paulraj, "MIMO wireless channels: capacity and performance prediction," in *Proc. IEEE GLOBECOM*, vol. 2, San Francisco, CA, USA, Nov. 2000, pp. 1083–1088.

[51] D. Chizhik, G. J. Foschini, M. J. Gans, and R. A. Valenzuela, "Keyholes, correlations, and capacities of multielement transmit and receive antennas," *IEEE Trans. Wireless Commun.*, vol. 1, pp. 361–368, Apr. 2002.

[52] P. Almers, F. Tufvesson, and A. F. Molisch, "Measurement of keyhole effect in a wireless multiple-input multiple-output (MIMO) channel," *IEEE Commun. Lett.*, vol. 7, pp. 373–375, Aug. 2003.

[53] M. A. Jensen and J. W. Wallace, "A review of antennas and propagation for MIMO wireless communications," *IEEE Trans. Antennas Propagat.*, vol. 52, no. 11, pp. 2810–2824, Nov. 2004.

[54] G. G. Raleigh and J. M. Cioffi, "Spatio-temporal coding for wireless communication," *IEEE Trans. Commun.*, vol. 46, pp. 357–366, Mar. 1998.

[55] J. B. Andersen, "Array gain and capacity for known random channels with multiple element arrays at both ends," *IEEE J. Select. Areas Commun.*, vol. 18, pp. 2172–2178, Nov. 2000.

[56] A. Edelman, "Eigenvalues and condition numbers of random matrices," Ph.D. dissertation, Massachusetts Inst. Technol., Cambridge, MA, USA, 1989.

[57] I. E. Telatar, "Capacity of multi-antenna Gaussian channels," *European Trans. on Telecomm. Related Technol.*, vol. 10, pp. 585–595, Nov. 1999.

[58] A. Zanella, M. Chiani, and M. Z. Win, "On the marginal eigenvalues distribution of Wishart matrices," University of Bologna, Bologna, Italy, IEIIT B0-07-06 Tech. Rep., Dec. 2006.

[59] L. Hanzo, C. H. Wong, and M. S. Yee, *Adaptive Wireless Transceivers.* Chichester, England: John Wiley and Sons, 2002.

[60] J. H. Sung and J. R. Barry, "Bit-allocation strategies for MIMO fading channels with channel knowledge at transmitter," in *IEEE VTC Spring*, Jeju Island, Korea, Apr. 2003, pp. 813–817.

[61] J. C. Roh and B. D. Rao, "Adaptive modulation for multiple antenna channels," in *Proc. Asilomar Conf. on Sig. Sys. and Comp.*, vol. 1, Pacific Grove, CA, USA, Nov. 2002, pp. 526–530.

[62] B. N. Getu, J. B. Andersen, and J. R. Farserotu, "MIMO systems: optimizing the use of eigenmodes," in *Proc. IEEE PIMRC*, Beijing, China, 2003, pp. 1129–1133.

[63] G. Jongren, M. Skoglund, and B. Ottersten, "Combining beamforming and orthogonal space-time block coding," *IEEE Trans. Inform. Theory*, vol. 48, pp. 611–627, Mar. 2002.

[64] S. Zhou and G. B. Giannakis, "Optimal transmitter eigen-beamforming and space-time block coding based on channel mean feedback," *IEEE Trans. Signal Processing*, vol. 50, pp. 2599–2613, Oct. 2002.

[65] A. Pascual-Iserte, A. I. Perez-Neira, and M. A. Lagunas, "A maximin approach for robust MIMO design: Combining OSTBC and beamforming with minimum transmission power requirements," in *Proc. IEEE ICASSP*, vol. 2, Montreal, Canada, May 2004, pp. 1–4.

[66] P. A. Dighe, R. K. Mallik, and S. S. Jamuar, "Analysis of transmit-receive diversity in Rayleigh fading," *IEEE Trans. Commun.*, vol. 51, pp. 694–703, Apr. 2003.

[67] G. Burel, "Statistial analysis of the smallest singular value in MIMO transmission systems," in *Proc. WSEAS Int. Conf. on Sig. Speech and Img. Processing*, Skiathos, Greece, Sept. 2002.

[68] R. Shimura, T. Ohno, T. Kambayashi, and I. Sasase, "Transmit phase control to increase the minimum eigenvalue of channel correlation matrix in the E-SDM/OFDM system," in *Proc. IEEE VTC Fall*, Los Angeles, CA, USA, Sept. 2004, pp. 2024–2028.

[69] R. W. Heath, S. Sandhu, and A. Paulraj, "Antenna selection for spatial multiplexing systems with linear receivers," *IEEE Commun. Lett.*, vol. 5, pp. 142–144, Apr. 2001.

[70] T. Haustein, C. von Helmolt, E. Jorswieck, V. Jungnickel, and V. Pohl, "Performance of MIMO systems with channel inversion," in *Proc. IEEE VTC Spring.*, Birmingham, AL, USA, May 2002, pp. 35–39.

[71] C. B. Peel, B. M. Hochwald, and A. L. Swindlehurst, "A vector-perturbation technique for near-capacity multiantenna multiuser communication - part I: channel inversion and regularization," *IEEE Trans. Commun.*, vol. 53, pp. 195–202, Jan. 2005.

[72] S. Sandhu and A. Paulraj, "Space-time block codes: A capacity perspective," *IEEE Commun. Lett.*, vol. 4, pp. 384–386, Dec. 2000.

[73] T. Shu and Z. Niu, "A near-optimal antenna selection in MIMO system by using maximum total eigenmode gains," in *Proc. IEEE GLOBECOM*, San Francisco, CA, USA, Dec. 1-5, 2003, pp. 297–301.

[74] B. M. Hochwald, T. L. Marzetta, and V. Tarokh, "Multiple-antenna channel hardening and its implications for rate feedback and scheduling," *IEEE Trans. Inform. Theory*, vol. 50, pp. 1893–1909, Sept. 2004.

[75] K. Miyashita, T. Nishimura, T. Ohgane, Y. Ogawa, Y. Takatori, and K. Cho, "High data-rate transmission with eigenbeam-space division multiplexing (E-SDM) in a MIMO channel," in *Proc. IEEE VTC Fall*, Vancouver, BC, Canada, Sep. 24-29, 2002, pp. 1302–1306.

[76] D. W. Bliss, K. W. Forsythe, A. O. Hero, and A. F. Yegulalp, "Environmental issues for MIMO capacity," *IEEE Trans. Signal Processing*, vol. 50, pp. 2128–2142, Sept. 2002.

[77] D. Tse and P. Viswanath, *Fundamentals of Wireless Communication*. New York: Cambridge University Press, 2005.

[78] P. Almers, F. Tufvesson, O. Edfors, and A. F. Molisch, "Measured capacity gain using water-filling in frequency selective MIMO channels," in *Proc. IEEE PIMRC*, Lisbon, Portugal, Sep. 15-18, 2002, pp. 1347–1351.

[79] R. W. Heath and D. J. Love, "Multimode antenna selection for spatial multiplexing systems with linear receivers," *IEEE Trans. Signal Processing*, vol. 53, pp. 3042–3056, Aug. 2005.

[80] S. Shim, J.-S. Choi, C. Lee, and D.-H. Youn, "Rank adaptive transmission to improve the detection performance of the BLAST in spatially correlated MIMO channel," in *Proc. IEEE VTC Fall*, Vancouver, BC, Canada, Sep. 24-29, 2002, pp. 195–198.

[81] R. W. Heath and A. J. Paulraj, "Switching between diversity and multiplexing in MIMO systems," *IEEE Trans. Commun.*, vol. 53, pp. 962–968, June 2005.

[82] N. Kita, W. Yamada, A. Sato, D. Mori, and S. Uwano, "Measurement of Demmel condition number for 2x2 MIMO-OFDM broadband channels," in *Proc. IEEE VTC Spring*, Milan, Italy, May 17-19, 2004, pp. 294–298.

[83] J. D. Parsons, *The Mobile Radio Propagation Channel*, 2nd ed. Chichester, England: John Wiley and Sons, 2000.

[84] D. P. McNamara, M. A. Beach, and P. N. Fletcher, "Experimental investigation of the temporal variation of MIMO channels," in *Proc. IEEE VTC Fall*, Atlantic City, NJ, USA, Oct. 7-11, 2001, pp. 1063–1067.

[85] J. W. Wallace, A. Gummalla, M. A. Jensen, and H. Lee, "Experimental characterization of the outdoor MIMO wireless channel temporal variation," *IEEE Trans. Veh. Technol.*, vol. 56, pp. 1041–1049, May 2007.

[86] A. Giorgetti, M. Chiani, M. Shafi, and P. J. Smith, "Level crossing rates and MIMO capacity fades: Impacts of spatial/temporal channel correlation," in *Proc. IEEE ICC*, Anchorage, AK, USA, May 11-15, 2003, pp. 3046–3050.

[87] B. O. Hogstad and M. Patzold, "Capacity studies of MIMO channel models based on the geometrical one-ring scattering model," in *Proc. IEEE PIMRC*, Barcelona, Spain, Sep. 5-8, 2004, pp. 1613–1617.

[88] A. Abdi, C. Gao, and A. M. Haimovich, "Level crossing rate and average fade duration in MIMO mobile fading channels," in *Proc. IEEE VTC Fall*, Orlando, FL, USA, Oct. 2003, pp. 3164–3168.

[89] P. Ivanis and D. Drajic, "Average level crossing rate and fading duration in correlated MIMO subchannels," in *Proc. 7th Int'l. Conf. on Telecommun. in Modern Satellite, Cable and Broadcasting Services*, Serbia and Montenegro, Sept. 28-30, 2005, pp. 89–92.

[90] P. J. Smith and M. Shafi, "An approximate capacity distribution for MIMO systems," *IEEE Trans. Commun.*, vol. 52, pp. 887–890, June 2004.

[91] R. Barakat, "Level-crossing statistics of aperture-integrated isotropic speckle," *J. Opt. Soc. Amer.*, vol. 5, pp. 1244–1247, 1988.

[92] J. T. Y. Ho and P. J. Smith, "A quick simulation method for fading communications channels using a novel eigenvalue importance sampling technique," in *Proc. IEEE VTC Fall*, Vancouver, BC, Canada, Sep. 24-29, 2002, pp. 449–453.

[93] Y. Karasawa, "MIMO propagation channel modeling," *IEICE Trans. Commun.*, vol. E88-B, no. 5, pp. 1829–1842, May 2005.

[94] M. Wennstrom, M. Helin, A. Rydberg, and T. Oberg, "On the optimality and performance of transmit and receive space diversity in MIMO channels," in *Proc. IEE Technical Seminar on MIMO systems: From Concept to Implementation*, London, UK, Dec. 12, 2001, pp. 4/1–4/6.

[95] R. A. Silverman, "The fluctuation rate of the chi process," *IRE Trans. Inform. Theory*, vol. 4, no. 1, pp. 30–34, Mar. 1958.

[96] C. D. Charalambous and N. Menemenlis, "Stochastic models for short-term multipath fading channels: chi-square and Ornstein-Uhlenbeck processes," in *Proc. IEEE Conf. on Decision and Control*, Phoenix, AZ, USA, Dec. 1999, pp. 4959–4964.

[97] S. Primak, V. Kontorovic, and V. Lyandres, *Stochastic Methods and Their Applications to Communications: Stochastic Differential Equations Approach*. Chichester, England: John Wiley and Sons, 2004.

[98] M. F. Bru, "Diffusions of perturbed principal component analysis," *J. Multivariate Anal.*, vol. 29, pp. 127–136, 1989.

[99] W. Konig and N. O'Connell, "Eigenvalues of the Laguerre process as non-colliding squared Bessel processes," *Electron. Comm. Probab.*, vol. 6, pp. 107–114, 2001.

[100] K. Sulonen, P. Suvikunnas, J. Kivinen, L. Vuokko, and P. Vainikainen, "Study of different mechanisms providing gain in MIMO systems," in *Proc. IEEE VTC Fall*, Orlando, FL, USA, Oct. 4-9, 2003, pp. 352–356.

[101] E. Jorswieck, G. Wunder, V. Jungnickel, and T. Haustein, "Inverse eigenvalue statistics for Rayleigh and Rician MIMO channels," in *Proc. IEE*

Technical Seminar on MIMO systems: From Concept to Implementation, London, UK, Dec. 12, 2001, pp. 3/1–3/6.

[102] A. M. Tulino, A. Lozano, and S. Verdu, "Bandwidth-power tradeoff of multiple-antenna systems in the low-power regime," *DIMACS Series in Discr. Math. and Theo. Comp. Sci*, vol. 62, pp. 15–42, 2003.

[103] N. L. Johnson, S. Kotz, and N. Balakrishnan, *Continuous Univariate Distributions, 2nd Edition.* New York: John Wiley and Sons, 1994.

[104] M. Katori and H. Tanemura, "Symmetry of matrix-valued stochastic processes and noncolliding diffusion particle systems," *J. Math. Phys.*, vol. 45, pp. 3058–3085, 2004.

[105] H. S. Wang and N. Moayeri, "Finite-state Markov channel - a useful model for radio communication channels," *IEEE Trans. Veh. Technol.*, vol. 44, pp. 163–171, Feb. 1995.

[106] Q. Zhang and S. A. Kassam, "Finite-state Markov models for Rayleigh fading channels," *IEEE Trans. Commun.*, vol. 47, pp. 1688–1692, Nov. 1999.

[107] R. D. Souza, J. Garcia-Frias, and A. M. Haimovich, "Using hidden Markov models to improve performance of space-time codes in MIMO flat fast-fading channels," in *Proc. IEEE VTC Spring*, Milan, Italy, 2004, pp. 1305–1309.

[108] A. E. Ekpenyong and Y.-F. Huang, "Feedback-detection strategies for adaptive modulation systems," *IEEE Trans. Commun.*, vol. 54, pp. 1735–1740, Oct. 2006.

[109] M. R. McKay, P. J. Smith, H. A. Suraweera, and I. B. Collings, "On the capacity distribution of OFDM-based spatial multiplexing: Exact variance and outage approximation," submitted to *IEEE Trans. on Inform. Theory*, 2006.

[110] T. L. Marzetta, "BLAST training: Estimating channel characteristics for high capacity space-time wireless," in *Proc. 37th Ann. Allerton Conf. on Comm. Contr. and Comp.*, Monticello, IL, USA, Sept. 1999.

[111] Q. Sun, D. C. Cox, H. C. Huang, and A. Lozano, "Estimation of continuous flat fading MIMO channels," *IEEE Trans. Wireless Commun.*, vol. 1, pp. 549–553, Oct. 2002.

[112] A. Narula, M. J. Lopez, M. D. Trott, and G. W. Wornell, "Efficient use of side information in multiple-antenna data transmission over fading channels," *IEEE J. Select. Areas Commun.*, vol. 16, pp. 1423–1436, Oct. 1998.

[113] T. J. Willink, "Improving power allocation to MIMO eigenbeams under imperfect channel estimation," *IEEE Commun. Lett.*, vol. 9, pp. 622–624, July 2005.

[114] N. Khaled, G. Leus, C. Desset, and H. DeMan, "A robust joint linear precoder and decoder MMSE design for slowly time-varying MIMO channels," in *Proc. IEEE ICASSP*, vol. 4, Montreal, Canada, 2004, pp. 485–488.

[115] P. J. Smith and L. M. Garth, "Distribution and characteristic functions for correlated complex Wishart matrices," *J. Multivariate Anal.*, vol. 98, no. 4, pp. 661–677, 2007.

[116] A. N. Borodin and P. Salminen, *Handbook of Brownian Motion: Facts and Formulae.* Berlin: Birkhauser, 1996.

[117] S. Lawi, "A characterization of markov processes enjoying the time-inversion property," 2005, submitted to *Probab. Theory Related Fields*, revised Jan. 2006.

[118] G. Ben-Arous and S. Peche, "Universality of local eigenvalue statistics for some sample covariance matrices," *Commun. on Pure Appl. Math.*, vol. 58, pp. 1316–1357, 2005.

[119] R. K. Mallik, "On multivariate Rayleigh and exponential distributions," *IEEE Trans. Inform. Theory*, vol. 49, no. 6, pp. 1499–1515, 2003.

[120] S. Vaihunthan, S. Haykin, and M. Sellathurai, "MIMO channel capacity modeling using Markov models," in *Proc. IEEE VTC Spring*, Stockholm, Sweden, Apr. 2005, pp. 126–130.

[121] A. Forenza, A. Pandharipande, H. Kim, and R. W. Heath, "Adaptive MIMO transmission scheme: exploiting the spatial selectivity of wireless channels," in *Proc. IEEE VTC Spring*, Stockholm, Sweden, Apr. 2005, pp. 3188–3192.

[122] G. E. Oien, H. Holm, and K. J. Hole, "Impact of channel prediction on adaptive coded modulation performance in Rayleigh fading," *IEEE Trans. Veh. Technol.*, vol. 53, pp. 758–769, May 2004.

[123] X. Zhang, J. Tang, H.-H. Chen, S. Ci, and M. Guizani, "Cross-layer based modeling for quality of service guarantees in mobile wireless networks," *IEEE Commun. Mag.*, vol. 44, pp. 100–106, Jan. 2006.

[124] S. T. Chung and A. J. Goldsmith, "Degrees of freedom in adaptive modulation: a unified view," *IEEE Trans. Commun.*, vol. 49, pp. 1561–1571, Sept. 2001.

[125] S. Zhou and G. B. Giannakis, "Adaptive modulation for multiantenna transmissions with channel mean feedback," *IEEE Trans. Wireless Commun.*, vol. 3, pp. 1626–1636, Sept. 2004.

[126] P.-H. Kuo and P. J. Smith, "Temporal behavior of MIMO channel quality metrics," in *Proc. IEEE Int. Conf. on Wireless Networks, Communications and Mobile Computing*, Maui, HI, USA, June 2005, pp. 857–862.

[127] L. Yang and M.-S. Alouini, "Level crossing rate over multiple independent random processes - an extension of the applicability of the Rice formula," in *Proc. IEEE GLOBECOM*, San Francisco, CA, USA, 2003, pp. 1644–1648.

[128] L. M. Garth, P. J. Smith, and M. Shafi, "Exact symbol error probabilities for SVD transmission of BPSK data over fading channels," in *Proc. IEEE ICC*, Seoul, Korea, May 2005, pp. 2271–2276.

[129] P. J. Smith, L. M. Garth, and M. Shafi, "Performance analysis for adaptive MIMO SVD transmission in a cellular system," in *Proc. 7th Australian Communications Theory Workshop*, Perth, Australia, Feb. 2006, pp. 49–54.

[130] D. L. Goeckel, "Adaptive coding for time-varying channels using outdated fading estimates," *IEEE Trans. Commun.*, vol. 47, pp. 844–855, June 1999.

[131] T. Taniguchi, R. Takemoto, N. X. Tran, and Y. Karasawa, "Design of MIMO communication systems robust to eigenvector mismatch problems," in *Proc. IEEE ISSPIT*, Darmstadt, Germany, 2003, pp. 74–77.

[132] V. T. Ermolayev, A. G. Flaksman, I. P. Kovalyov, and I. M. Averin, "Weight error loss in MIMO systems with adaptive transmit and receive beamformers," in *Proc. IEEE Int. Conf. Antenna Theory and Techniques*, Sevasropol, Ukraine, Sept. 2003, pp. 333–336.

[133] A. Cano-Gutierrez, M. Stojanovic, and J. Vidal, "Effect of channel estimation error on the performance of SVD-based MIMO communication systems," in *Proc. IEEE PIMRC*, Barcelona, Spain, 2004, pp. 508–512.

[134] T. S. Ho, K. Sakaguchi, and K. Araki, "Performance analysis of MIMO eigenmode transmission system under realistic channel and system conditions," in *Proc. IEEE VTC Spring*, Milan, Italy, 2004, pp. 708–712.

[135] E. K. S. Au and W. H. Mow, "Accurate BER analysis for singular value decomposition-based MIMO receivers with imperfect channel state information," submitted to *IEEE Trans. Commun.*, Mar. 2006.

[136] E. N. Onggosanusi, A. Gatherer, A. G. Dabak, and S. Hosur, "Performance analysis of closed-loop transmit diversity in the presence of feedback delay," *IEEE Trans. Commun.*, vol. 49, pp. 1618–1630, Sept. 2001.

[137] C. Donati-Martin, Y. Doumerc, H. Matsumoto, and M. Yor, "Some properties of the Wishart processes and a matrix extension of the Hartman-Watson laws," *Publ. Res. Inst. Math. Sci.*, vol. 40, pp. 1385–1412, 2004.

[138] M. N. Rodero, "Receive and transmit strategies for multiple antennas systems," Ph.D. dissertation, Univ. of South Australia, Adelaide, Australia, 2002.

[139] S. Spiteri, G. Lebrun, and M. Faulkner, "Prediction for time-varying SVD systems," in *Proc. IEEE PIMRC*, Barcelona, Spain, 2004, pp. 1608–1612.

[140] G. Lebrun, S. Spiteri, and M. Faulkner, "Channel estimation for an SVD-MIMO system," in *Proc. IEEE ICC*, Paris, France, 2004, pp. 3025–3029.

[141] N. R. Prasad and H. Teunissen, "A state-of-the-art of Hiperlan/2," in *Proc. IEEE VTC Fall*, Amsterdam, Netherland, Sept. 1999, pp. 2661–2665.

[142] S. Hara and R. Prasad, *Multicarrier Techniques for 4G Mobile Communications*. Boston: Artech House, 2003.

[143] T. Keller and L. Hanzo, "Adaptive multicarrier modulation: a convenient framework for time-frequency processing in wireless communications," *Proc. IEEE*, vol. 88, no. 5, pp. 611–640, May 2000.

[144] A. Clark, "On coding for orthogonal frequency division multiplexing," Ph.D. dissertation, Univ. of Canterbury, Christchurch, New Zealand, 2006.

[145] M. A. Arcones, "Limit theorems for nonlinear functionals of a stationary Gaussian sequence of vectors," *The Annals of Probability*, vol. 22, no. 4, pp. 2242–2274, 1994.

[146] V. Chakaravarthy, A. S. Nunez, J. P. Stephens, A. K. Shaw, and M. A. Temple, "TDCS, OFDM, and MC-CDMA: a brief tutorial," *IEEE Commun. Mag.*, vol. 43, no. 9, pp. S11–S16, Sept. 2005.

[147] C. C. Tan and N. C. Beaulieu, "Infinite series representations of the bivariate Rayleigh and Nakagami-m distributions," *IEEE Trans. Commun.*, vol. 45, no. 10, pp. 1159–1161, Oct. 1997.

[148] K. Witrisal, "OFDM air-interface design for multimedia communications," Ph.D. dissertation, Delft Univ. of Technology, Netherland, 2002.

[149] Y.-H. Pan, K. B. Letaief, and Z. Cao, "Dynamic spatial subchannel allocation with adaptive beamforming for MIMO/OFDM systems," *IEEE Trans. Wireless Commun.*, vol. 3, no. 6, pp. 2097–2107, Nov. 2004.

[150] S. Nanda, R. Walton, J. Ketchum, M. Wallace, and S. Howard, "A high-performance MIMO OFDM wireless LAN," *IEEE Commun. Mag.*, vol. 43, no. 2, pp. 101–109, Feb. 2005.

[151] R. Grunheid, E. Bolinth, and H. Rohling, "A blockwise loading algorithm for the adaptive modulation technique in OFDM system," in *Proc. IEEE VTC Fall*, Atlantic City, NJ, USA, Oct. 2001, pp. 948–951.

[152] M. Lei and P. Zhang, "Subband bit and power loading for adaptive OFDM," in *Proc. IEEE VTC Fall*, Orlando, FL, USA, Oct. 2003, pp. 1482–1486.

[153] A. R. S. Bahai, B. R. Saltzberg, and M. Ergen, *Multi-carrier Digital Communications: Theory and Applications of OFDM*, 2nd ed. Boston: Springer, 2004.

[154] M. Codreanu, D. Tujkovic, and M. Latva-Aho, "Adaptive MIMO-OFDM wih low signalling overhead for unbalanced antenna systems," in *Proc. IEEE PIMRC*, Barcelona, Spain, Sept. 2004, pp. 2382–2386.